Transmission of pathogenic α-synuclein to mice

Dissertation

zur Erlangung des Doktorgrades (Dr. rer. nat.)

der

Mathematisch-Naturwissenschaftlichen Fakultät

der

Rheinischen Friedrich-Wilhelms-Universität Bonn

von

Sara Breid

aus Saarbrücken

Bonn 2017

Angefertigt mit Genehmigung der Mathematisch-Naturwissenschaftlichen Fakultät der Rheinischen Friedrich-Wilhelms-Universität Bonn

1 Gutachter: PD Dr. Gültekin Tamgüney

2 Gutachter: Prof. Dr. Jörg Höhfeld

Tag der mündlichen Prüfung: 12.06.17

Erscheinungsjahr: 2017

Erklärung

Hiermit erkläre ich, dass ich die vorliegende Dissertation selbständig und ausschließlich mit Hilfe der angegeben Quellen und Hilfsmittel angefertigt habe. Die aus anderen Quellen direkt oder indirekt übernommenen Daten und Konzepte sind unter Angabe der Quellen kenntlich gemacht. Wörtlich oder sinngemäß übernommenes Gedankengut habe ich als solches kenntlich gemacht.

Ergebnisse dieser Arbeit wurden in Teilen veröffentlicht:

Breid, Sara, et al. "Bioluminescence Imaging of Neuroinflammation in Transgenic Mice After Peripheral Inoculation of Alpha-Synuclein Fibrils." *JoVE (Journal of Visualized Experiments)* 122 (2017): e55503-e55503.

Breid, Sara, et al. "Neuroinvasion of α-synuclein prionoids after intraperitoneal and intraglossal inoculation." *Journal of Virology* 90.20 (2016): 9182-9193.

Ort, Datum

Summary

α-Synuclein is a soluble, cellular protein that in a number of neurodegenerative diseases, including Parkinson's disease, multiple system atrophy, and Lewy body dementia aggregates into pathological protein deposits. Principles how misfolded and aggregated α-synuclein is transmitted within the central nervous system (CNS) causing neurologic disease were found to be similar to those of prions. Misfolded α-synuclein can be transmitted between cells and act as a seed, recruiting native, unfolded α-synuclein to form insoluble aggregates. The mechanisms and the routes through which pathogenic proteins enter the CNS causing progressive disease are still not completely understood. The work in this thesis confirms previous findings indicating that α-synuclein fibrils intracerebrally injected into wild-type mice for α-synuclein can induce neuropathology in interconnected brain regions as similarly observed in sporadic Parkinson's disease. In contrast, α-synuclein fibrils injected into the tongue muscle of wild-type mice for α-synuclein did not neuroinvade the CNS causing α-synuclein pathology. Moreover, the present study is the first to show, that α-synuclein fibrils peripherally injected into the tongue and the peritoneum of mice overexpressing human α-synuclein, can neuroinvade the CNS, cause widespread α-synuclein pathology and induce neurologic symptoms. The induction of neuropathology was accompanied by neuroinflammation as monitored by astrocytic gliosis and microgliosis. In addition, the study presented here indicates that exposure of mice overexpressing human α-synuclein with pathogenic α-synuclein aerosols was not sufficient for α-synuclein prionoids to enter the brain via the olfactory epithelium and induce neuropathology. In summary, these findings corroborate the prionoid character of misfolded α-synuclein using similar routes like prions to neuroinvade brain and spinal cord and induce neurologic disease.

Zusammenfassung

α-Synuclein ist ein lösliches, zelluläres Protein, das in seiner fehlgefalteten Form zu pathologischen Proteinablagerungen aggregiert. Diese Ablagerungen sind charakteristisch für eine Vielzahl von neurodegenerativen Erkrankungen wie Morbus Parkinson, Multisystematrophie und Lewy-Body-Demenz. Es hat sich gezeigt, dass die Mechanismen nach denen sich fehlgefaltetes und aggregiertes α-Synuclein Protein innerhalb des Zentralnervensystems (ZNS) ausbreitet und neurologische Erkrankungen auslöst denen von Prionen sehr ähnlich sind. Fehlgefaltetes α-Synuclein kann zwischen Zellen übertragen werden und nicht gefaltetes, natives α-Synuclein dazu veranlassen unlösliche Aggregate zu bilden. Die Mechanismen und die Wege, durch die pathogene Proteine in das ZNS einwandern und folglich progressive neuronale Erkrankungen auslösen, sind noch nicht vollständig bekannt. Die Ergebnisse dieser Thesis bestätigen vorhergehende Beobachtungen, dass pathogene α-Synuclein Fibrillen, die intrazerebral in Wildtyp-Mäuse injiziert wurden, Neuropathologie in miteinander verbundenen Gehirnregionen hervorrufen, wie es in ähnlicher Weise in Patienten mit sporadischem Morbus Parkinson beobachtet wurde. Die Injektion von fehlgefaltetem α-Synuclein in den Zungenmuskel derselben Mauslinie führte jedoch nicht zur Einwanderung von pathogenem α-Synuclein in das ZNS. Zudem zeigt die vorliegende Arbeit erstmalig, dass α-Synuclein Fibrillen, die peripher in den Zungenmuskel oder in das Peritoneum von Mäusen, die humanes α-Synuclein überexprimieren, injiziert wurden in das ZNS einwandern und neben einer ausgeprägten Neuropathology auch neurologische Symptome auslösen. Mit dem Fortschreiten der Neuropathologie ging auch eine neuronale Entzündung einher, die anhand von astrozytischer Gliose und Mikrogliose nachgewiesen werden konnte. Darüber hinaus zeigt diese Studie, dass pathogene α-Synuclein Aerosole mit denen α-Synuclein überexprimierende Mäuse inhaliert wurden, das olfaktorische Epithel nicht passieren und Neuropathologie auslösen konnten. Diese Erkenntnisse bestätigen, dass fehlgefaltetes α-Synuclein ähnliche Übertragungswege und Mechanismen wie Prionen nutzt, um in Gehirn und Rückenmark einzuwandern und dort eine neurologische Erkrankung auszulösen.

Table of contents

1 Introduction

1.1 The prion protein and prion-like behavior

In several neurodegenerative diseases the assembly of misfolded proteins into highly ordered so-called amyloids is a prevalent principle (Table 1.1). The common structural motif that characterizes amyloids is the cross-β-sheet conformation. Filamentous amyloids are, despite their generic cross-β-sheet conformation, highly polymorphic (Selkoe, 2003). One of the best-characterized amyloids is the prion protein. In prion diseases, the cellular prion protein PrP^{C} undergoes a conformational change into a protease-resistant, β-sheet-rich prion conformation PrP^{Sc}. This infectious prion conformation can act as a seed and promote the conversion of PrP^{C} into its amyloid conformation PrP^{Sc}. This process initiates prion replication, polymerization, and propagation, which is a self-sustained seeding mechanism (Cohen et al., 1994). Notably, not only the stable PrP^{Sc} bears infectivity, also its small protease-sensitive intermediates show similar to higher infection potential (Aguzzi and Lakkaraju, 2016).

Table 1.1 Brain diseases that are characterized by progressive misfolding and aggregation of proteins

Disease	Protein	Pathology	Strains	Transmissible	Bona fide infectivity
Prion diseases	PrP^{Sc}	extracellular plaques, oligomers are outside neurons	yes	yes	yes
Parkinson's disease	α-synuclein	neuronal cytoplasma	maybe	yes	not shown
Alzheimer's disease	amyloid-β	extracellular plaques, tangles in neuronal cytoplasm	yes	yes	not shown
Tauopathies	tau	tangles in neuronal cytoplasm	yes	yes	not shown

Iatrogenic transmission of prions causing Creutzfeldt-Jakob disease (CJD) was reported when children with stunted growth were treated with cadaveric growth hormone. Similarly, bovine spongiform encephalopathy (BSE) in cattle was transmitted to humans

as a variant of CJD (vCJD) after consumption of prion-infected meat and was further transmitted among humans via blood transfusions (Brown et al., 2012; Hewitt et al., 2006; Hill et al., 1997). It is also known that prions are transmissible among sheep causing scrapie or among deer and elk causing chronic wasting disease (CWD) (Tamgüney et al., 2009b; Tamgüney et al., 2012). Although prion diseases remain the only protein-misfolding diseases that are transmissible between individuals, there is growing evidence that there are numerous parallels between the prion protein and other proteins associated with neurodegenerative diseases. These proteins include for example: α-synuclein as the relevant agent of Parkinson's disease, amyloid-β associated with Alzheimer's disease (AD), and the microtubule associated protein tau (MAPT) that is linked with AD and other tauopathies. These amyloidogenic proteins do not seem to be naturally transmitted between individual hosts like common –so called– *bona fide* prions, but resemble prions in many other ways. The term "prion-like" or "prionoid" was suggested to describe some aspects of their biological properties (Table 1.1) (Aguzzi, 2009; Aguzzi and Lakkaraju, 2016; Aguzzi and Rajendran, 2009). The only reference for iatrogenic transmission of amyloidogenic proteins has been suggested for amyloid-β. In this report, the occurrence of amyloid-β pathology and cerebral amyloid angiopathy has been confirmed in CJD patients that were previously treated with infected growth hormone (Jaunmuktane et al., 2015b).

Prions in distinct conformations have divers biochemical and functional properties that cause individual pathologies and clinical manifestation. According to their biochemical and pathophysiological properties, they have been classified into strains (Collinge and Clarke, 2007; Tanaka et al., 2004). Analog to prions, amyloid-β and tau also occur as individual strains that can be transmitted to hosts and cause distinct disease phenotypes (Sanders et al., 2014; Stohr et al., 2014; Watts et al., 2014). Similarly, conformational strains have also been described for disease-associated α-synuclein and hypothesized to cause the heterogeneity of synucleinopathies. (Bousset et al., 2013; Guo et al., 2013; Peelaerts et al., 2015). There is evidence that the bacterial endotoxin lipopolysaccharide (LPS) affects the biochemical and pathogenic properties of recombinant α-synuclein causing distinct pathological phenotypes (Kim et al., 2016). Despite that α-synuclein has some concordant characteristics with the prion protein, there is no current evidence for its iatrogenic transmissibility.

1.1.1. Intercellular transmission of prions

Oral ingestion of prion-infected material seems to be the most relevant route for prions to naturally enter the central nervous system (CNS) under non-experimental conditions (McBride et al., 2001). The alimentary route is interconnected to the enteric nervous system (ENS) that autonomously controls the functionality of the gastrointestinal tract. In rodents it has been shown that after entering the ENS, prions primarily use efferent fibers of the vagus nerve and the splanchnic nerves to neuroinvade brain and spinal cord (Beekes et al., 1998; McBride et al., 2001). Furthermore, prions peripherally injected into muscles like the femoral biceps (hindlimb) or the lingual muscle (tongue) are also able to rapidly infect the CNS (Bartz et al., 2003; Bosque et al., 2002). Similarly, intraperitoneal, intraocular, and intravenous injections have been described as additional peripheral entrance points for prions to neuroinvade the CNS (Bartz et al., 2002; Kimberlin and Walker, 1980, 1986). Among these non-neuronal routes, infection into the tongue muscle was shown to be the most efficient transmission route for prions. Prions injected into the tongue can rapidly neuroinvade the brain stem causing disease after an incubation time of two weeks or be reversely transmitted from the brain to the tongue (Bartz et al., 2003; Mulcahy et al., 2004). Although these peripheral routes are less relevant for naturally transmitted agents, these findings implicate that the peripheral nervous system including the ENS is likely involved in the spread of prion infectivity.

1.2 Synucleinopathies

Neurodegenerative diseases such as Parkinson's disease (PD), multiple system atrophie (MSA) and Lewy body dementia (LBD) that are pathologically characterized by the accumulation of misfolded α-synuclein proteins within the nervous system are referred to as synucleinopathies. PD as the second most common neurodegenerative disease besides Alzheimer's disease is associated with a set of clinical motor symptoms like bradykinesia, resting tremor, rigidity, postural instability and periods of freezing, and non-motor symptoms like olfactory deficits, sleep disorders, and cognitive impairments (Gallagher et al., 2010; Klingelhoefer and Reichmann, 2015). Besides idiopathic PD, which constitutes the prevalent form of PD, familial cases have been described (Pankratz and Foroud, 2004).

The accumulation of misfolded α-synuclein in the CNS of PD patients proceeds gradually and follows a predetermined topographical pattern. According to the stereotypic

progression over time the PD-related α-synuclein pathology has been classified in six developmental stages (Braak et al., 2003a). It has been shown that the course of PD can take years or decades until the disease reaches advanced stages (3rd to 6th) with clinical manifestation. During the proceeded disease stages, accumulation of α-synuclein aggregates induces the loss of dopaminergic neurons in the substantia nigra pars compacta projecting to the striatum. This neuronal loss is cause for the characteristic motor symptoms (Hirsch et al., 1988; Masliah et al., 2000). In many PD cases the pathological features and the loss of dopaminergic neurons are not only restricted to the substantia nigra but have also been found in other parts of the nervous system such as the basal forebrain (nucleus basalis of Meynert) and the brainstem (motor nucleus of the vagus and locus coeruleus) (Spillantini and Goedert, 2000).

1.2.1 Biology of α-synuclein

α-Synuclein is a small acidic 140 amino acid protein that in its native, soluble form is abundant at the presynaptic terminals of neurons. α-Synuclein associates with membranes and binds to synaptic vesicles to maintain their synaptic vesicle pools suggesting its role in neurotransmitter release (Fortin et al., 2004; Jo et al., 2000). Although the majority of native α-synuclein is found within the nervous tissue, the red blood cells have been shown to contain relatively large concentrations of α-synuclein, too (Barbour et al., 2008; Bendor et al., 2013).

The human SNCA gene encoding α-synuclein is located on chromosome 4q21.3-q22 and comprises 111 kb (Fig.1.1). The gene spans a set of seven exons and five of those, exon 2 to exon 6, correspond to its coding region. The amino acid sequence is divided into three parts: an amphipathic region, a non-amyloid β component (NAC) domain and an acidic tail. A cluster of KTKEGV consensus repeats characterizes the N-terminal sequence. A 12-amino acid stretch within the hydrophobic NAC region is a prerequisite for its polymerization into fibrils (Giasson et al., 2001). The entire sequence of α-synuclein is highly conserved between mouse and human and differs only in seven amino acids (Appendix Fig. 5.1) (Maroteaux et al., 1988; Murphy et al., 2000). Gene duplications and triplications as well as six missense mutations A30T, E46K, H50Q, G51D, A53E, and A53T within the human SNCA sequence cause an autosomal-dominant

form of familial PD with an early disease onset (Kruger et al., 1998; Lesage et al., 2013; Polymeropoulos et al., 1997; Singleton et al., 2003; Zarranz et al., 2004).

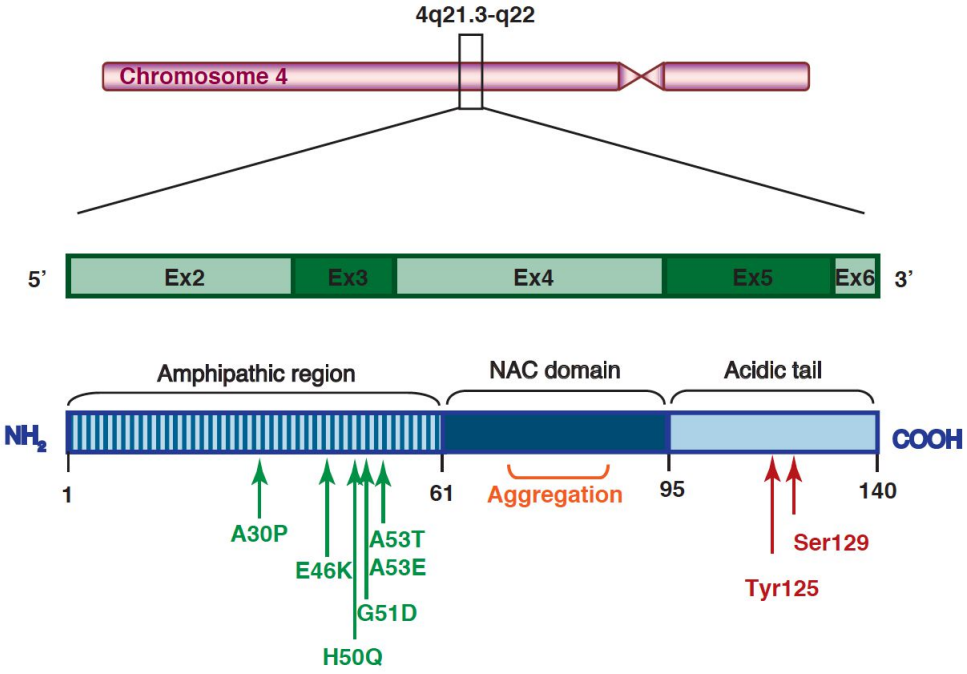

Fig. 1.1 Schematic view of human α-synuclein. Chromosomal localization of the α-synuclein gene (top panel). Coding region of α-synuclein represented by its m-RNA (middle panel). The amino acid sequence of α-synuclein is divided into an amphipathic region, a non-amyloid β component (NAC) domain and an acidic tail. Six missense mutations associated with familial PD and the phosphorylation sites at serine 129 and tyrosine 125 are indicated (bottom panel) (adapted from Venda et al., 2010, with permission from Elsevier).

1.2.2 Aggregation and toxicity of α-synuclein

Under physiological conditions, the α-synuclein protein occurs mostly as unfolded monomer. When it becomes pathological, it forms insoluble, highly ordered conformations with toxic properties. Notably, the native α-synuclein does not only occur as monomer but also as helically folded tetramer that prevents its pathological aggregation (Bartels et al., 2011; Wang et al., 2011). Polymerization of the monomeric α-synuclein into disease-associated fibrillar structures is a multi-step process beginning with the conversion of monomers into dimers that consequently polymerize into various intermediate oligomeric structures e.g. ring-like oligomers (Fig.1.2). Such intermediate forms of α-synuclein are generally termed protofibrils. Misfolded α-synuclein recruits unfolded monomers through conformational templating and induces them to adopt a β-rich conformation. This amyloid conformation can polymerize and in turn seed its

conformation to unfolded proteins by a self-perpetuating seeding mechanism. Finally the oligomers assemble to β-sheet-rich amyloid fibrils forming deposits in the neuronal cytosol called Lewy bodies (LBs). This Polymerization and assembly occurs either within the cytoplasm or is associated with membranes. (Kalia et al., 2013; Lashuel et al., 2013).

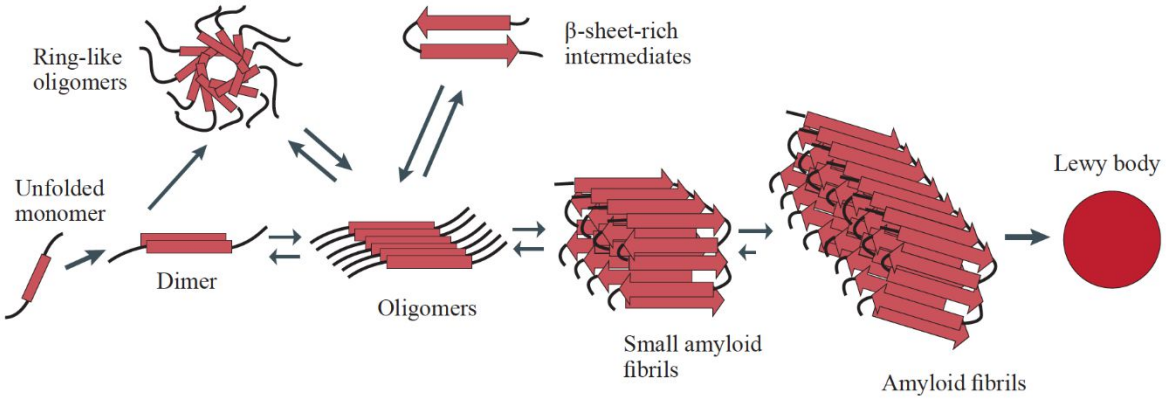

Fig. 1.2 Mechanism of α-synuclein polymerization. Unfolded, monomeric α-synuclein polymerizes stepwise into β-sheet-enriched amyloid fibrils that finally assemble to Lewy bodies (adapted from Lashuel et al., 2013, with permission from Nature Publishing Group).

Various studies support the idea that not only amyloid fibrils bear toxic properties. The intermediate protofibrils and oligomers show a similar or even enhanced cellular virulence. Mutated α-synuclein molecules are less prone to fibrillize when analyzed *in-vitro*. Consequently, the reduced amount of fibrils leads to higher concentrations of oligomeric intermediates, which probably cause the increased toxicity in *in-vivo* models (Conway et al., 2000; Kalia et al., 2013; Karpinar et al., 2009; Winner et al., 2011).

1.2.2.1 Posttranslational modifications

Phosphorylation at serine 129 (Fig. 1.1) has been described as the dominant posttranslational modification of α-synuclein found in synucleinopathy lesions (Anderson et al., 2006; Fujiwara et al., 2002). Therefore it has been assumed, that phosphorylation plays a predominant role during disease progression. Moreover, *in-vitro* experiments indicate that monomeric α-synuclein phosphorylated at serine 129 is more prone to aggregate and polymerize into fibrils. On the contrary, the phosphorylation at tyrosine 125 (Fig. 1.1) diminishes the propensity of α-synuclein to form amyloids (Fig. 1.2) (Venda et al., 2010).

Oxidative stress can cause as well posttranslational modification of α-synuclein. The abundance of reactive oxygen and nitrogen species generates nitrating factors that can alter the protein structure of α-synuclein and influence its pathogenic properties. Particularly, nitrated tyrosine residues were abundantly found in deposits of misfolded α-synuclein when analyzed by immunohistochemical methods (Duda et al., 2000; Giasson et al., 2000; Ischiropoulos and Beckman, 2003).

Furthermore, deposits of misfolded α-synuclein are posttranslationally modified by the attachment of ubiquitin. Even the α-synuclein, phosphorylated at serine 129, is targeted for mono -and diubiquitination and might have implications for disease progression (Spillantini and Goedert, 2000; Tofaris et al., 2003). Not only ubiquitin itself, but also its cytoplasmic binding protein p62 that binds noncovalently to ubiquitin is frequently used as aggregation marker (Kuusisto et al., 2001).

1.2.2.2 Unbalanced cellular homeostasis

Both properly working quality-control and degradation systems are needed to maintain cellular homeostasis. Perturbations affecting protein synthesis, folding and degradation can result in uncontrolled protein aggregation with a subsequent fibril formation and a functional disruption of the cell. In a functioning cell, molecular chaperones control the conformation of proteins and refold misfolded proteins back to their native structure. Misfolded protein conformers can be directly eliminated via the ubiquitin-proteasomal system (UPS) and the autophagy-lysosomal pathway (ALP) (Kalia et al., 2013; Tyedmers et al., 2010). To target proteins for proteasomal degradation at least four ubiquitin conjugates are added to their lysine residues. Only thereafter the targeted protein can be transported to the proteasome. Importantly, only unfolded, soluble proteins can enter the proteasome (Bence et al., 2001; Rubinsztein, 2006). Since proteasome-associated degradation only works for unfolded proteins, the lysosomal pathway represents the default way to deconstruct aggregated proteins. The autophagy-lysosomal pathway can be separated in microautophagy, macroautophagy, and chaperone-mediated autophagy. For lysosomal degradation the proteins are trapped by the autophagosome, a vesicle with a double-membrane that fuses with the lysosome to form an autophagolysosome. The proteinaceous content of the autophagolysosome is finally fractionized by lysosomal hydrolases (Rubinsztein, 2006).

Both clearance mechanisms have been described to be relevant for the degradation of α-synuclein, although aggregated α-synuclein seems to be less prone to degradation (Webb et al., 2003). In contrast to wild-type α-synuclein, the A53T and A30P mutants of α-synuclein (Fig. 1.1) are not efficiently degraded via the lysosomal pathway. Moreover, the proteasomes found in cases of sporadic PD showed an altered structure with an impaired proteolytic activity (Cuervo et al., 2004; McNaught and Jenner, 2001). Proteins that are resistant to degradation, such as α-synuclein in human and animal synucleinopathies were found to colocalize with ubiquitin and its binding protein p62 (sequestosome-1). Therefore both proteins are used as marker targeting pathological aggregated proteins (Ahmed et al., 2012; Komatsu et al., 2007; Kuusisto et al., 2001; Lowe et al., 1988). Impairment of the proteasomal and lysosomal machinery by binding of misfolded α-synuclein might additionally reduce the degradation of other proteins and further contribute to the accumulation of harmful aggregates in the cell.

1.2.2.3 α-Synuclein pathology

One pathological hallmark of surviving neurons in PD is the accumulation of misfolded α-synuclein in form of neuronal deposits in the cytosol termed Lewy bodies (LBs) or in neuronal processes termed Lewy neurites (LNs, Fig. 1.3) (Spillantini et al., 1997).

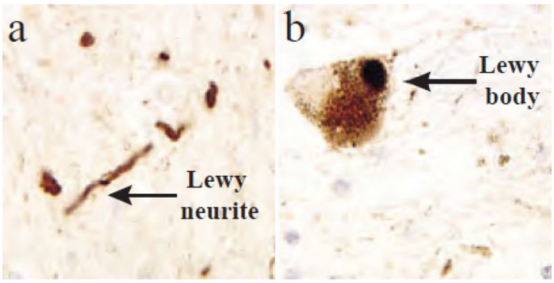

Fig. 1.3 Immunostaining for α-synuclein in the brain of a DLB patient. a) Positive-staining for a Lewy neurite in the substantia nigra. b) Pigmented nerve cell of the substantia nigra shows positive-staining for a Lewy body (adapted from Spillantini et al., 1997, with permission from Nature Publishing Group).

The cytoplasmic inclusions are composed of insoluble, filamentous and granular α-synuclein with a cross-β sheet conformation characteristic for amyloids. In contrast to PD, MSA is characterized predominantly by the deposition of α-synuclein within glial cytoplasmic inclusions (GCI) restricted to oligodentrcytes (Serpell et al., 2000; Spillantini et al., 1998; Spillantini and Goedert, 2000; Spillantini et al., 1997). Besides α-synuclein as the major component of the LBs, further constituents are ubiquitin and neurofilaments,

which are stratified into concentric layers. Triple immunofluorolabeling has shown that ubiquitin builds the LB center surrounded by α-synuclein and neurofilament as the outermost layer (Kanazawa et al., 2008).

1.3 Intercellular transmission of α-synuclein

Extensive neuropathological examinations of human tissue identified that the progression of α-synuclein pathology follows a stereotypic pattern (Braak et al., 2003a). The pathology progression could be determined by the distribution of phosphorylated α-synuclein aggregates over time (Lewy bodies/ Lewy neurites). In this respect the olfactory bulb in the brain and the enteric plexus of the gastrointestinal system were described as initial points from where the disease could start and propagate to distal parts in the cerebrum. The initiation of α-synuclein pathology either in the nasal tracts or the gastrointestinal system was proposed as the "dual hit hypothesis". It suggests that neurotropic pathogens can be transported to the lower brainstem: a) anterogradely along olfactory tracts entering the nasal mucosa or b) retrogradely from the gastrointestinal tract by entering the vagus nerve (Hawkes et al., 2007, 2009). The distribution of α-synuclein aggregates along interconnected neuroanatomical regions indicated that only a certain type of neuron is vulnerable to pathological α-synuclein. These selective vulnerable neurons were identified as long, thin projection neurons that are mainly unmyelinated (Braak and Del Tredici, 2004).

Transmission of misfolded α-synuclein between cells has been suggested after observing the results of neuronal grafting experiments in humans. Embryonic dopaminergic neurons that had been therapeutically grafted into the striata of PD patients had accumulated misfolded α-synuclein after fourteen years. This suggests that misfolded α-synuclein is transferred between cells and induces misfolding by a seeding mechanism (see Fig. 1.2) (Kordower et al., 2008; Li et al., 2008). Inoculation experiments utilizing both α-synuclein overexpressing and wild-type mice indicated that intracerebral injection of pathogenic α-synuclein lead to spread of pathology from the injection site to synaptically interconnected brain regions (Bernis et al., 2015; Luk et al., 2012a; Luk et al., 2012b; Rey et al., 2013; Sacino et al., 2013b; Watts et al., 2013). However, several studies in α-synuclein wild-type mice injected with recombinant α-synuclein fibrils do not show uniform results regarding the disease phenotype and spread of pathology within the CNS

(Luk et al., 2012a; Masuda-Suzukake et al., 2013; Sacino et al., 2013a). Despite the findings that α-synuclein fibrils can cause neuropathology like prions after CNS injection (Lasmezas et al., 1997) it is unclear whether injection via peripheral routes such as the tongue muscle, the peritoneum, or the nasal tracts can result in CNS disease.

1.3.1 Mechanisms for cellular transfer of α-synuclein

After misfolded α-synuclein is internalized into the cytoplasm of neurons, it is further transported along neuronal axons and propagated to neighboring neurons (Desplats et al., 2009; Freundt et al., 2012; Volpicelli-Daley et al., 2011). Different mechanisms mediating the cellular transfer of misfolded proteins between neurons have been proposed. Misfolded and aggregated α-synuclein may be released from a donor cell into the extracellular continuum via a) diffusion or b) membrane-bound vesicles (Fig. 1.4) (Danzer et al., 2012; Emmanouilidou et al., 2011; Emmanouilidou et al., 2010; Guo and Lee, 2014; van Dijk et al., 2014). Proteins that are associated with neurodegenerative diseases like microtubule associated protein tau (MAPT), polyglutamine (PolyQ), superoxide dismutase 1 (SOD1), or prions are potentially internalized into recipient neurons through (1) direct diffusion, (2) endocytosis, (3) receptor-mediated endocytosis, (4) exosome-mediated endocytosis, and (5) nanotube tunneling (Fig. 1.4) (Frost et al., 2009; Gousset et al., 2009; Munch et al., 2011; Ren et al., 2009; Wu et al., 2013). For α-synuclein receptor-mediated endocytosis has been described as a primary pathway to enter recipient cells (Desplats et al., 2009; Guo and Lee, 2014; Hansen et al., 2011; Holmes et al., 2013; Mao et al., 2016). After internalization of misfolded α-synuclein into the cytoplasm of a recipient neuron, endogenous monomers are recruited for fibrillization.

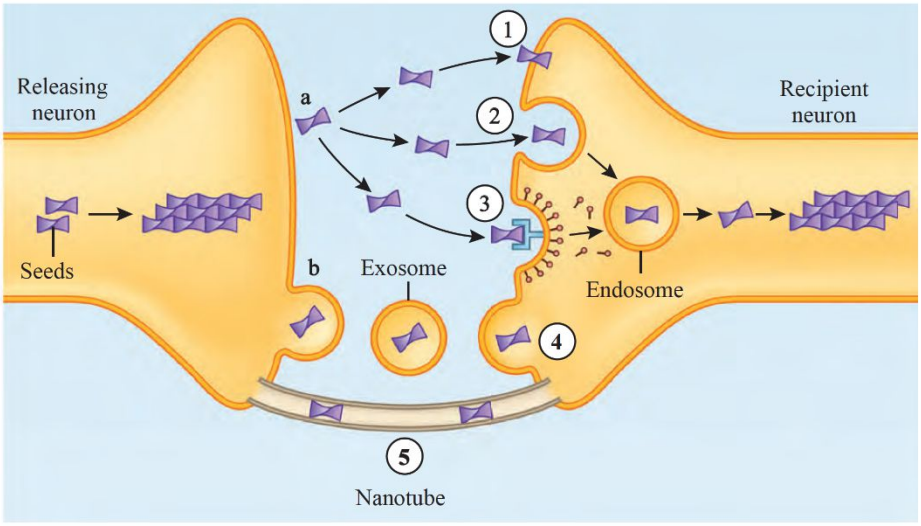

Fig. 1.4 Potential mechanisms of α-synuclein propagation between neighboring neurons. After secretion of α-synuclein from the releasing neuron into the extracellular space, α-synuclein seeds can be internalized from the recipient neuron via five different mechanisms (adapted from Guo and Lee, 2014, with permission from Nature Publishing Group).

1.4 Inflammation in neurodegenerative diseases

Neurodegenerative diseases often have a neuroinflammatory component that is characterized by the activation of astrocytes and microglia (Amor et al., 2014; Wyss-Coray and Mucke, 2002). Particularly, abundance of activated microglia and astrocytes has been demonstrated by histological analysis of the substantia nigra in PD patients (Damier et al., 1993; Imamura et al., 2003).

1.4.1 Microglia

Glial cells including oligodendrocytes, microglia and astrocytes are the non-neuronal cells of the CNS that help to maintain the homeostasis of the neuronal environment (Allen and Barres, 2009). Microglia are the resident macrophages and innate immune cells of the brain that constantly monitor the neuronal microenvironment to detect any injury or pathogenic incidence. In case of any tissue damage or infection, the microglia migrate to the place of injury and change their morphology. Activated microglia release pro-inflammatory cytokines and chemokines that recruit additional immunregulatory cells for the adaptive immune response. The activation of the adaptive immunity is receptor-mediated and controls diverse signaling transduction pathways. The latter regulate the expression of proteins covering a wide range of functions to stem the cause of disturbance (Glass et al., 2010; McGeer and McGeer, 2008; Rivest, 2009). The high turnover of

reactive oxygen species and proinflammatory cytokines like: tumor necrosis factor α (TNF-α), interleukin-1 β (IL-1 β) and interleukin-6 (IL-6) can cause toxicity and possibly neurodegeneration. There is growing evidence that the abundance of misfolded α-synuclein is able to activate microglia resulting in microgliosis and consequently promotes neuronal damage and disease progression (Theodore et al., 2008; Zhang et al., 2005).

1.4.2 Astrocytes

Astrocytes as cellular organizers control the neuronal metabolism, cell-to-cell communication, and are additionally involved in repair mechanisms. Similarly to microglia, activated astrocytes become hypertrophic, change their morphology and express a set of regulatory genes resulting in reactive astrocytic gliosis. After severe tissue damage, astrocytes proliferate and are involved in the formation of glial scars (Maragakis and Rothstein, 2006; Sofroniew, 2009). α-Synuclein released from neurons can be internalized by astrocytes and aggregate as glial inclusions that evoke a neuroinflammatory response (Lee et al., 2010). Astrocytes stand in close relationship to microglia, communicating via the exchange of pro- and anti-inflammatory signals. One important hallmark of reactive astrocytes is the robust upregulation of the glial fibrillary acidic protein (GFAP), which can be detected by immunohistochemical staining. Upregulation of GFAP, predominantly expressed in the CNS, has been demonstrated to indicate neuroinflammation and neuronal injury and increases with its severity. Based on these findings, a transgenic reporter mouse model was established. This model expresses the luciferase gene under control of the GFAP promoter to monitor neuroinflammation in a non-invasive way (Zhu et al., 2004).

1.5 Animal models to study synucleinopathies

1.5.1 Intoxication mouse models

To study the etiology of human synucleinopathies in more detail, animal models that recapitulate the main pathophysiological features of the disease are indispensable. One of the first intoxication models used 1-methyl-4-phenyl-1,2,3,6-tetrahydropyridine (MPTP) as treatment for animals to mimic several of the characteristic symptoms of PD. The intoxication changes the mitochondrial metabolism that lead to an increased turnover of

reactive oxygen species enhancing the propensity of α-synuclein to aggregate and form pathogenic fibrils. Although MPTP treatment in rodents induces important signs of disease-like loss of dopaminergic neurons and a diminished performance in motor-performance tests, the central sign of human α-synuclein pathology, formation of LBs is still lacking (Beal, 2001; Maries et al., 2003; Meredith et al., 2002). Administration of the pesticide rotenone can evoke similar PD-associated pathophysiological signs, with α-synuclein inclusions that structurally resemble LBs more closely than in the MPTP model (Betarbet et al., 2000). Although the neurotoxic models can mimic key features of PD-associated neurodegeneration, these models are limited since they do not recapitulate the progressive nature of disease or non-motor symptoms that are characteristic for synucleinopathies (Dawson et al., 2002).

1.5.2 Transgenic mouse models

The normal cellular function of α-synuclein has been investigated in knockout mice deficient for α-synuclein. Mice with a complete knockout of α-synuclein were viable, did not show morphological abnormalities, but showed changes in the metabolism of dopamine indicating a role for α-synuclein as negative regulator in dopamine neurotransmission (Abeliovich et al., 2000). On the other hand, mice overexpressing human wild-type α-synuclein in neurons under control of the platelet-derived growth factor-β (PDGF- β) promoter develop α-synuclein inclusions, lose striatal dopaminergic terminals and show diminished motor performance (Masliah et al., 2000). Mutations of α-synuclein that cause familial PD have been used to establish further transgenic mouse models. For instance, overexpression of the A30P or A53T mutation under control of the promoter for tyrosine hydroxylase (TH) or the prion protein (PrP) promoter have been used to study pathophysiological features. Targeting the nigrostriatal pathway by use of the TH promoter indicated that overexpression of α-synuclein within dopaminergic neurons is not sufficient to cause LB pathology and neurodegeneration (Matsuoka et al., 2001). Using the promoter for PrP, which is naturally expressed in neurons led to a more pronounced disease phenotype with loss of dopaminergic neurons, behavioral deficits and clear formation of α-synuclein inclusions that were accompanied by signs of neuroinflammation (Giasson et al., 2002; Lee et al., 2002).

1.6 The role of the nose in neurodegenerative diseases

There is some evidence that environmental factors like toxins and chemicals that enter the nasal tracts of humans or rodents could cause or contribute to neurodegeneration (Calderon-Garciduenas et al., 2008; Levesque et al., 2011). The olfactory bulb was described as the first brain region where pathological lesions appear in idiopathic PD. Its dysfunction is accompanied by hyposmia and anosmia as one of the first non-motor symptoms during disease progression (Braak et al., 2003a; Braak et al., 2003b; Weintraub et al., 2008). These findings support the "olfactory vector hypothesis", which assumes that environmental agents might be able to reach the brain by passing the olfactory epithelium and could accelerate or even initiate the progression of pathology (Doty, 2008; Prediger et al., 2012). Airborne particles might enter the olfactory epithelium and become absorbed from the non-myelinated nerve endings of the olfactory cilia that are located in the olfactory mucosa (Fig. 1.5). The olfactory cilia proceeding into sensory receptor neurons that pass through the cribriform plate to reach the olfactory bulb.

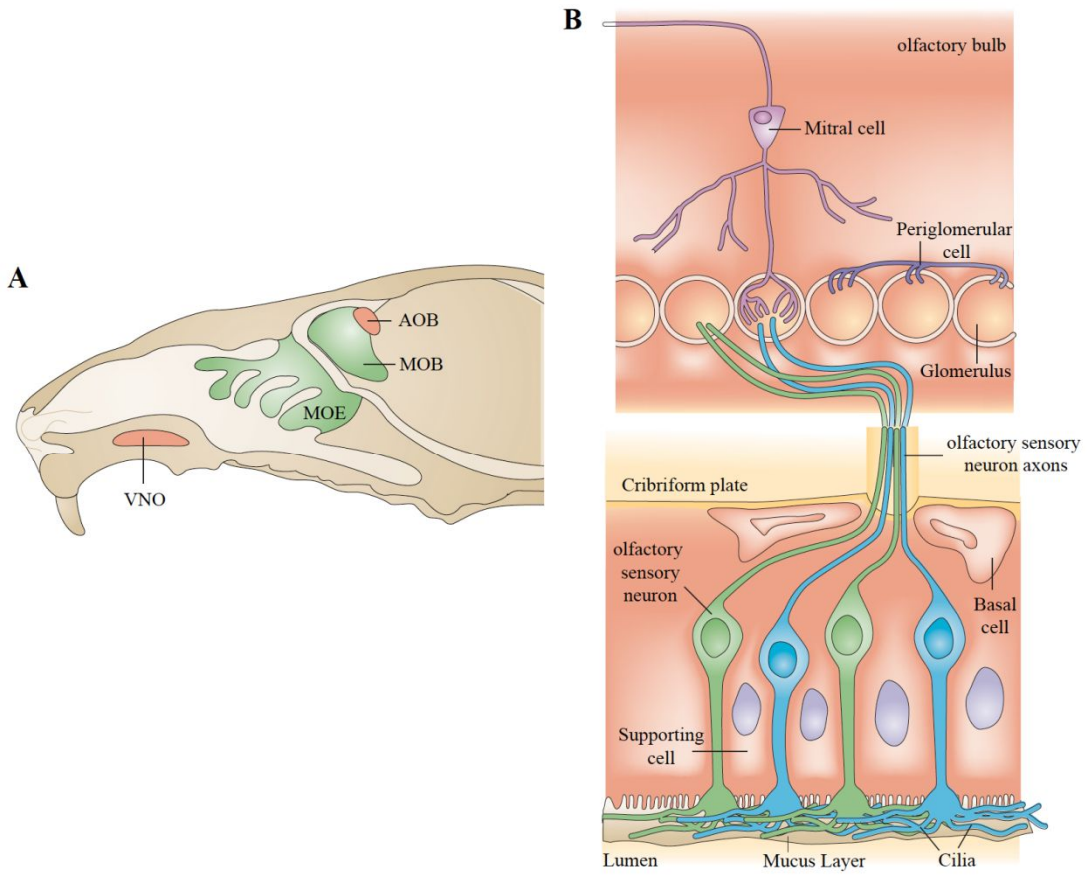

Fig. 1.5 The olfactory system in rodents. A) Schematic view through a rodent head, indicating the vomeronasal organ (VNO), the main olfactory epithelium (MOE), the main olfactory bulb (MOB) and the accessory olfactory bulb (AOB). B) Schematic view through the MOE and its peripheral interconnections to the olfactory bulb (adapted Mombaerts, 2004,with permission from Nature Publishing Group).

In CJD patients PrP^{Sc} accumulates in the olfactory cilia and basal cells in the olfactory mucosa. This shows that these cells are susceptible to prion replication (Zanusso et al., 2003). The nasal cavity as route for prion infection has been confirmed by the extranasal inoculation of hamsters with transmissible mink encephalopathy (TME) prions that accumulated in the nasal-associate lymphoid tissue (Kincaid and Bartz, 2007). In addition, the direct intracerebral injection of TME prions into the olfactory bulb could confirm prion replication in neurons of the olfactory bulb, in olfactory receptor neurons (ORNs) and vomeronasal receptor neurons (VRNs) (Bessen et al., 2010). Accordingly, when transgenic Tg(cerPrP) mice expressing cervid PrP^{C} were exposed to CWD-derived aerosols, they efficiently entered the olfactory epithelium and caused disease (Denkers et al., 2010). Since aerosols are naturally generated solid or liquid particles dispersed in the air, like dust or air pollutants, further studies concerning their infectivity in neurodegeneration is of great interest (Stitz and Aguzzi, 2011).

1.7 Objectives

The general objective of this work is to understand whether disease-associated α-synuclein can neuroinvade the CNS and initiate progressive disease via similar mechanisms and peripheral routes as shown for prions. By using a reporter mouse model for GFAP, the progressive α-synuclein pathology can be correlated to neuroinflammation.

In this respect this thesis pursues the following specific objectives:

1) To evaluate the virulence pattern of neuropathology induced by intracerebral and intraglossal injection of recombinant mouse α-synuclein fibrils
2) To investigate whether a mouse model overexpressing the A53T mutant of α-synuclein is susceptible to develop neuropathology after peripheral injection of recombinant human α-synuclein fibrils via the tongue or the peritoneum
3) To test the ability of aerosols derived from MSA brain homogenate to enter the brain via nasal passages and induce neuropathology

2 Materials and Methods

2.1 Animals

Inoculation experiments were performed in hemizygous Tg(*Gfap*-luc$^{+/-}$) mice and hemizygous bigenic Tg(M83$^{+/-}$:*Gfap*-luc$^{+/-}$) mice at an age of six-to-eight weeks. Tg(Gfap-luc$^{+/-}$) mice express firefly luciferase under control of a murine *Gfap* (Glial fibrillary acidic protein) promoter on a FVB background (Fig. 2.1). The *Gfap*-controlled expression of the firefly luciferase allows monitoring of astroglial activation, which correlates with neuroinflammation and neuronal damage (Zhu et al., 2004). Tg(M83$^{+/-}$:*Gfap*-luc$^{+/-}$) mice were bred by intercrossing homozygous Tg(*Gfap*-luc$^{+/+}$) mice together with homozygous Tg(M83$^{+/+}$) mice (according the Jackson Laboratory also termed as B6;C3-Tg(*Prnp*-SNCA*A53T)83Vle/J mice), which highly express the A53T mutant of human α-synuclein on a C57/BL6 background from the prion protein promoter (Giasson et al., 2002). All mice were housed under standard conditions with a 12 h light/dark cycle and free access to food and water. Animal care and experiments were performed according to protocols approved by the animal protection committee of the North Rhine-Westphalia State Environment Agency (LANUV).

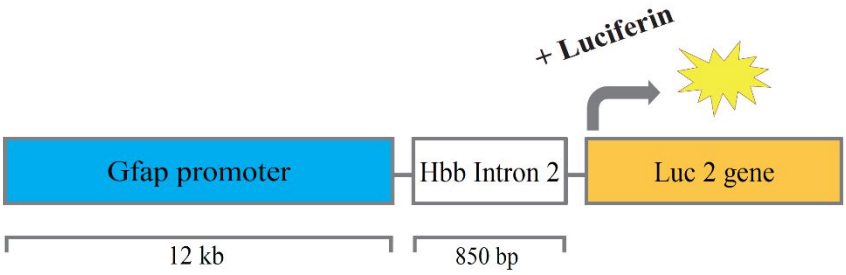

Fig. 2.1 Schematic view of the firefly luciferase reporter gene construct. The luciferase gene 2 (Luc2) is driven from a *Gfap* promoter and has a hemoglobin beta intron 2 (Hbb) as an adapter. Activation of the *Gfap* promoter initiates expression of luciferase, which catalyzes the oxidative decarboxylation of its substrate luciferin into oxyluciferin wherby a bioluminescence signal is emitted.

2.1.1 Genotyping

Presence of the firefly luciferase transgene in the offspring of the Tg(Gfap-luc$^{+/-}$) and Tg(M83$^{+/-}$:*Gfap*-luc$^{+/-}$) mice was determined by standard PCR by amplifying a 1 kb sequence within the *Gfap*-luc transgene. Primer sequences and cycling conditions used for PCR are listed in Table 2.1 and Table 2.2.

Table 2.1 PCR primers

Primer	Sequence 5` to 3`	Primer Type
Luc 1	TGG ATT CTA AAA CGG ATT ACC AGG G	forward
Luc 2	CCA AAA CAA CAA CGG CGG C	reverse

Table 2.2 PCR cycling conditions

	Step	Cycles	Temperature in °C	Time
Denaturation	1	1	97	5 min
Denaturation	2	35	94.5	40 s
Annealing	3		58	90 s
Extension	4		72	90 s
	5	1	72	10 min

The transgene encoding human α-synuclein with the familial A53T mutation was verified by real time PCR. Therefore, animal DNA was extracted from tail biopsies using the DNeasy Blood and Tissue Kit (Qiagen). Shortly, the tail tips were completely lysed in a Proteinase K containing buffer at 56 °C for 1 h and the insoluble components were separated by centrifugation for 2 min at 6000 x g. Lysates were loaded on silicia-membrane spin columns, purified by two washing steps and eluted in 40 µL distilled water. After the photometric quantification 90 ng of DNA was used for each real-time PCR reaction and samples were in triplicates. To follow the amplification reaction fluorescently labeled DNA oligonucleotides that bind downstream to one of the primers were used. In addition an internal positive control was carried along. Primers that were used for the amplification of the transgene, the internal positive control, and the 6-FAM -and Cyanine-5-labeled oligonucleotides are listed in Table 3. To normalize the fluorescent reporter signal a ROX reference dye (Thermo Fisher Scientific) was used. The fluorescence signal was measured in a 7900 HT Fast Real Time PCR system (Thermo Fisher Scientific) according to the cycling conditions listed in Table 2.4.

Table 2.3 Real-time PCR primers

Primer	Sequence 5` to 3`	Primer type
oIMR1544	CAC GTG GGC TCC AGC ATT	internal positive control (forward)
oIMR3580	TCA CCA GTC ATT TCT GCC TTT G	internal positive control (reverse)
oIMR1770	TGA CGG GTG TGA CAG CAG TAG	transgene
oIMR1771	CAG TGG CTG CTG CAA TG	transgene
TmoIMR0025	[6FAM] CCC TGC TCC CTC CAC TGT CTT CTG G [BHQ1]	transgene probe
TmoIMR0105	[Cyanine5] CCA ATG GTC GGG CAC TGC TCA A [BHQ3]	internal control probe

Table 2.4 Cycling conditions for the Real time PCR

	Step	Cycle	Temperature in °C	Time
Pre-denaturation	1	1	95	3 min
Denaturation	2	40	95	5 s
Extension	3		60	30 s

2.2 Inoculum preparation

2.2.1 Prion strains

The RML (Rocky Mountain Laboratory) prions were diluted from a 10 % stock concentration to a 0.2 % concentration in Ca^{2+}-and Mg^{2+}-free PBS with 5 % BSA (Thermo Fisher Scientific) under addition of 0.5 U/mL penicillin and 0.5 µg/mL streptomycin (Sigma).

2.2.2 Preparation of recombinant mouse α-synuclein fibrils

Recombinant mouse full-length wild-type α-synuclein (MyBioSource) in glycerol buffer (20mM Tris-HCl with pH 7.5, 10 % glycerol) was dialyzed against TBS aggregation buffer (20 mM Tris-HCl with pH 7.2, 150 mM NaCl with pH 7.2) through a semipermeable Slide-A-Lyzer dialysis cassette with a 3.5 kDa cut-off (Life Technology).

To reach a final concentration of 3 mg/mL the α-synuclein protein was concentrated in Amicon Ultra Tubes 3K (Millipore) by centrifugation. For fibril assembly 3 µg/µL protein was agitated together with one glass bead (VWR) in an orbital thermomixer (Eppendorf) at 800 rpm and 37 °C for a period of 5 days. Prior to injection, the harvested fibrils were diluted to 1 ug/uL in Ca^{2+} -and Mg^{2+}-free PBS and sonicated on ice for 1 min with a pulse of 1 s using a Sonoplus mini20 sonicator (Bandelin).

2.2.3 Preparation of recombinant human α-synuclein fibrils

The expression and purification of the recombinant human α-synuclein protein was conducted by Dr. Julius Tachu Babila at the German Center of Neurodegenerative Diseases, Bonn. Fibrils of the human wild-type α-synuclein were prepared as previously described in (Breid et al., 2016). Briefly, *E. coli* cells harboring the pET-3a expression plasmid (Novagen) for α-synuclein were grown at 37 °C in 1 L LB medium containing ampicillin, chloramphenicol, and 1 % glucose to an OD600 of 0.5. Protein expression was induced by 0.1 mM IPTG and the bacteria were grown for 5 h at 37 °C. Periplasmatic material was released into the buffer by an osmotic shock. Cells were pelleted by centrifugation at 6000 × g for 15 min, resuspended in a 35 % sucrose solution with 2 mM EDTA and 30 mM Tris-HCl (pH 7.2) and incubated for 15 min under shaking at RT. The cells were again harvested and resuspended in ice-cold water containing 5 mM $MgSO_4$. The periplasmatic material was boiled for 20 min and then centrifuged at 5000 × g for 30 min to subject the supernatant to fractional ammonium sulfate precipitation. Briefly, $(NH_4)_2SO_4$ crystals were added over 10 min to the supernatant to reach a 35 % saturation (19.4 g/ 100 mL) with gentle stirring on ice. Afterwards the centrifugation was repeated. Then 11.8 g/100 mL of $(NH_4)_2SO_4$ crystals were added over 10 min to take the concentration from 35 % to 55 % saturation with gentle stirring on ice. Finally the centrifugation was repeated. The pellet was re-suspended in 10 mL water and dialyzed three times for 3 h against 20 mM Tris-HCl (pH 8.0). α-Synuclein was purified from the supernatant by Resource Q anion exchange chromatography using 20 mM Tris-HCl (pH 8.0) as binding buffer and 500 mM NaCl in 10 mM Tris-HCl (pH 8.0) as elution buffer on an ÄKTA pure chromatography system (GE Healthcare). α-Synuclein was released from the column using a 30 mL linearly increasing gradient from the binding buffer towards the elution buffer and dialyzed against 150 mM NaCl in 20 mM Tris-HCl (pH 7.2). Fibril assembly for α-synuclein was performed in an orbital thermomixer

(Eppendorf) agitating 3 µg/µL protein at 800 rpm and 37 °C for 5 days. Prior to the injection, the fibrils were diluted in Ca^{2+}-and Mg^{2+}-free PBS to 1 µg/µL and sonicated for 1 min with a pulse of 1 s using a Sonoplus mini20 sonicator (Bandelin).

2.2.4 Preparation of MSA brain homogenate

Frozen brain tissue from the cortex of an MSA patient was homogenized in Ca^{2+}-and Mg^{2+}-free PBS (pH 7.4) by two 30 s cycles in a Precellys 24-Dual homogenizer (Peqlab) under addition of protease and phosphatase inhibitors (HALT Protease and Phosphatase Inhibitor Cocktail, Thermo Fisher Scientific). Initially a concentration of 50 % (w/v) homogenate was generated and further diluted into 20 %, 10 %, 5 % and 1 % (w/v) homogenates.

2.3 Transmission studies

2.3.1 Transmission by intracerebral injection

Mice were intracerebrally inoculated by a stereotactic surgery using a three-dimensional coordinate system (Kopf) to target the injection site. Animals were shortly anaesthetized in a gas anesthesia induction chamber using an isofluran/oxygen gas mixture at a flow rate of 3 L/min. After shaving the scull of the anesthetized mouse, the animal was placed in a head frame lying on a heated pad at 37°C. To fasten the position of the head the mouse was secured by two ear bars. Once the animal's head was in a defined position, the mouth was connected to the anesthesia tube with an isoflurane/oxygen flow rate of 2 L/min. To prevent dryness, the eyes were covered with Vaseline ointment (Molyduval). The scalp was opened by making a midline incision with an one-way scalpel (NeoLab). After cleaning the surgery area with Cutasept desinfection spray (Roth), a 27-gauge disposable hypodermic syringe (VWR) prepared with the inoculum was installed at the holding arm. The manipulator arm holding the syringe was moved along the three-dimensional coordinates to reach the striatum using the sutures and the bregma as anatomical landmarks (Fig. 2.2) (Cetin et al., 2006).

Injection coordinates for the striatum:

+ 0.2 mm in anterior-posterior direction relative to the bregma

+ 2.0 mm in medial-lateral direction relative to the sagittal suture

+ 2.6 mm in dorso-ventral direction through the cranium

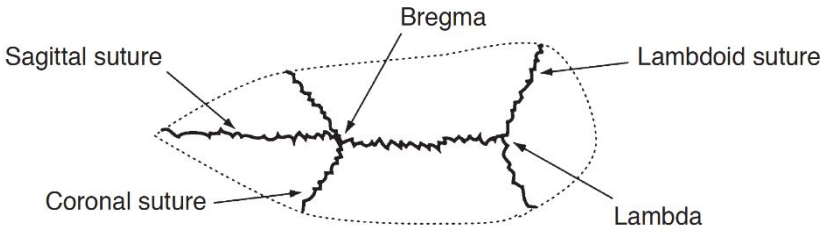

Fig. 2.2 Plan view to the cranium of a mouse. The anatomical point were the sagittal and the coronal sutures intersect each other is called the bregma and is localized in the rostral part of the cranium. The lambda is the anatomical point where the lambdoid suture crosses the sagittal suture in occipital orientation (Cetin et al., 2006).

First, the syringe was installed above the bregma and then moved to its appropriate position as indicated by the injection coordinates. To reach the + 2.6 mm dorso-ventral position, the needle was injected into the cranium. After a short adaption time of 1 min, the plunger of the syringe was shortly and gently pushed to carefully release the inoculum. For a better absorption and to avoid the loss of inoculum, an adaption pause of 3 min between every inoculum release was kept. After complete release of the inoculum, the syringe was left in place for another 15 min before it was removed and the scalp sutured with a veterinary tissue adhesive (3M Vetbond). To minimize local inflammation at the injection site, the animals received 15 µL antibiotics (Borgal solution 24%) into the scalp and the suture was treated with an antiseptic cream (Betaisodona). In addition, the mice received an intraperitoneal injection of 15 µL Carprofen as an analgesic (Rimadyl). Postoperative care also included injection of 300 µL 5% glucose solution (Braun) and 300 µL 0.9 % physiologic salt solution (Braun) into the peritoneum. Finally, the mice were constantly monitored, still lying on a heated pad, until they had completely recovered.

2.3.2 Transmission by intraglossal injection

Mice were anaesthetized by an intraperitoneal injection with ketamine and xylazine (100 mg/kg for ketamine 2 % and 10 mg/kg for xylazine 10 %, Ratiopharm) according to their body weight. The anesthesized animals were turned upside down and fixed on a heated pad using adhesive tape. To make the inner bottom side of the tongue accessible the mouth of the animal was opened with two forceps (FST) and by holding the tongue with another forceps the tongue was pulled forward. A 27-gauge disposable hypodermic syringe (VWR) was used to inject 5 µg of the recombinant mouse α-synuclein (1 µg/µL) or 10 µg of the recombinant human α-synuclein (2 µg/µL) and slowly injected into the right bottom side of the tongue in proximity to the right strand of the hypoglossal nerve. After a short adaption time of 5 s the needle was carefully retracted. Animals lying on a heated pad were constantly monitored until they had recovered completely.

2.3.3 Transmission by intraperitoneal injection

For injecting into the peritoneum the animals were shortly narcotized in an isoflurane/oxygen chamber at a flow rate of 2 L/min and injected with 50 µg of recombinant human α-synuclein using a 27-gauge disposable hypodermic syringe. The animals were monitored until they had completely recovered.

2.3.4 Inhalation

Mice were exposed to aerosols with pathological human α-synuclein derived from the brain of an MSA patient using a home-made inhalation chamber (Fig. 2.3). The exposure chamber was made of a plastic container with 7 holes with a diameter of 3 cm that were drilled into the sidewalls. Six 50 mL tubes (Nerbe plus) with space for six mice were inserted and sealed with a hot melt glue gun (Conrad). To allow nasal exposure of the animals the tube tips were cut off. The inhalation container was stabilized with additional tubes functioning as legs. The nebulizer device (Pari Boy SX, Pari) was connected to the 7th hole. Additionally, a filter unit (Sterivex, Millipore) was inserted into the container lid as an air vent trapping excessive aerosolized particles. To ensure its proper closure, clamps (Conrad) were clipped around the chamber. To prevent mice from changing their position within the tube, animals were fixated by addition of tissue paper before capping tubes. Animals were exposed to aerosols made from 1 mL PBS or MSA brain homogenate that was previously diluted to 20 %, 10 %, 5 %, 10 % or 1 % (w/v) in PBS. The nebulizer

device operates with a pressure of 1.6 bar and generates particles with a mass median diameter of 2.2 µm. During an exposure time of 10 min the animals inhaled aerosols by normal breathing trough the nasal tracts. After inhalation animals were carefully released from the tubes and returned to their cages.

Fig. 2.3 Inhalation chamber to expose mice to aerosols. The home-made inhalation chamber is connected to a nebulizer system (Pari Boy SX, Pari).

2.4 Bioluminescence imaging

For the non-invasive visualization of the bioluminescence signal from the brains of the Tg(*Gfap*-luc$^{+/-}$) and bigenic Tg(M83$^{+/-}$:*Gfap*-luc$^{+/-}$) mice. Animals were imaged once a week or every two weeks using an IVIS Lumina II imaging system (Caliper). Prior to imaging, the heads of mice were shaved and depilated with a special depilatory cream (Veet). To reduce an unspecific bioluminescence signal, the ears were colored in black using a non-irritating lab marker (Securline). Beforehand mice were shortly narcotized in an isoflurane/oxygene chamber with a flow rate of 2 L/min. The D-luciferin potassium salt (Acris) as substrate of the luciferase was dissolved in Ca^{2+}-and Mg^{2+}-free PBS to give a 30 mg/mL stock solution and intraperitoneally injected at 150 mg D-luciferin per kilogramm body weight. After 10 min incubation the animals were placed under continuous anesthesia into the imaging chamber. The emitted light was captured by a sensitive CCD camera for an exposure period of 60 s. BL emitted from the brain was quantified with Living Imaging 3.0 Software (Perkin Elmer).

2.5 Negative stain electron microscopy

The negative stain electron microscopy was conducted by Karen Tolksdorf at the department of neurology of the University of Bonn (Fig. 3.1A) and by Maria C.Garza and Dr. Holger Wille at the University of Alberta, in Edmonton, Alberta (Fig. 3.10A) (Breid et al., 2016). Transmission electron microscopy was performed with a Tecnai F20 TEM (FEI Company) operating at an acceleration voltage of 200 kV. Five µL sample were adsorbed for 30 s onto freshly glow discharged formvar/carbon coated 200 mesh copper grids. The grids were washed briefly with 0.1 M and 0.01 M ammonium acetate buffer (pH 7.4) and then stained with two 50 µL drops of freshly filtered 2% (w/v) uranyl acetate. The grids were allowed to dry overnight before viewing. The electron micrographs were recorded on an Eagle 4K CCD camera (FEI Company). Three different preparations of α-synuclein were characterized by thoroughly inspecting at least five different areas per grid.

2.6 Biochemical analysis

2.6.1 Purification of detergent-insoluble proteins

2.6.1.1 Extraction of sarcosyl-insoluble proteins

To collect brains, spinal cords, and tongues mice were shortly narcotized with isoflurane and killed by a spinal dislocation. Organs were dissected, snap-frozen on dry ice and stored at -80°C. For further processing, brain or spinal cord samples were homogenized and diluted (w/v) in Ca^{2+} -and Mg^{2+}-free PBS (pH 7.4) to a final concentration of 10% (w/v). Under addition of benzonase nuclease (Sigma) as well as protease and phosphatase inhibitors (HALT Protease and Phosphatase Inhibitor Cocktail, Thermo Fisher Scientific) the tissue was homogenized by two 30 s cycles with 6,000 rpm in a Precellys 24-Dual homogenizer (Peqlab). Tongues were also homogenized in PBS under addition of benzonase nuclease (Sigma) as well as protease and phosphatase inhibitors (HALT Protease and Phosphatase Inhibitor Cocktail, Thermo Fisher Scientific) to a final concentration of 10 % (w/v) by four 30 s cycles with 6,000 rpm in the Precellys 24-Dual homogenizer. To ensure that all cells were disrupted, all samples were sonicated twice for 10 s using a Sonoplus mini20 sonicator (Bandelin). After adjusting homogenates to 750 mM NaCl, they were centrifuged at 1,000 × g for 5 min at 4 °C to separate tissue debris. Protein concentration was determined by using the Pierce BCA Protein Assay (Thermo Fisher Scientific). One thousand µg of brain and tongue homogenates and

800 µg of the spinal cord homogenate were incubated on ice for 15 min with N-lauroylsarcosyl (Sigma) at a final concentration of 10 % (w/v). Homogenates were ultracentrifuged at 465,000 × g for 1 h at 4 °C over a 3 mL 10% (w/v) sucrose cushion in a TLA-110 rotor (Optima Max-XP, Beckman Coulter). The resulting pellets were resuspended in 45 µL of TD4215 denaturing buffer containing 4 % SDS, 2 % β-mercaptoethanol, 192 mM glycine, 25 mM Tris, and 5 % (w/v) sucrose. For heat denaturation samples were boiled at 100 °C for 5 min and loaded onto 4-12 % NuPage gels (Thermo Fisher Scientific) as previously described (Betemps et al., 2014). The further processing is described in 2.6.2.

2.6.1.2 Extraction of Triton X-100 and sarcosyl-insoluble proteins

To characterize the MSA brain homogenate that was used for inhalation experiments, the tissue was homogenized and diluted in Ca^{2+} -and Mg^{2+}-free PBS to reach a 50% (w/v) solution. After addition of benzonase nuclease (Sigma) as well as phosphatase and proteinase inhibitors (HALT Protease and Phosphatase Inhibitor Cocktail, Thermo Fisher Scientific), homogenates were sonicated twice for 10 s with a Sonoplus mini20 sonicator (Bandelin) and once for 10 min in a sonicator water bath (Bandelin). For buffer exchange, proteins were pelleted by ultracentrifugation at 100,000 x g for 30 min at 4°C and subsequently dissolved by vortexing in a Triton buffer containing 10 mM Tris-HCl (pH 7.4), 0.8M NaCl, 1 mM EGTA, 10 % sucrose and 1 % Triton X-100 (Sigma), sonicated for 10 min in a water bath and shaken in a thermocycler for 30 min at 37 °C at 800 rpm. Insoluble proteins were pelleted by ultracentrifugation at 100,000 x g for 30 min at 4 °C and again dissolved by vortexing in a sarcosyl buffer containing 10 mM Tris-HCl (pH 7.4), 0.8 M NaCl, 1 mM EGTA, 10 % sucrose and 1 % sarcosyl. Following another sonication step for 10 min in a water bath, proteins were shaken in a thermocycler for 30 min at 37 °C at 800 rpm. Finally samples were spun at 100,000 x g for 30 min and dissolved in Tris-HCl (pH 7.4) as previously described (Masuda-Suzukake et al., 2013).

2.6.2 Immunoblotting (SDS-PAGE)

For immunoblotting protein samples were resuspended in loading dye (New England BioLabs) and heat denatured at 100°C for 5 min. Denatured protein samples were loaded onto a NuPAGE 4-12 % Bis-Tris gel (Thermo Fisher Scientific) and further separated in a morpholineethanesulfonic acid (MES) buffer system (Thermo Fisher Scientific).

SeeBlue plus 2 pre-stained standard (Invitrogen) or Chameleon duo pre-stained protein standard (LI-COR Biosciences) were used as protein ladders. Proteins were separated by gel electrophoresis at 100 V and transferred onto PVDF membranes with a pore size of 0.45 µm (Millipore) by use of a semidry blotting system (Hoefer). After blotting for 1 h at 120 V, membranes were incubated in 0.4 % (v/v) formalin solution with Ca^{2+} -and Mg^{2+}-free PBS for 30 min on a rotor at RT to cross-link the proteins with the membrane. Membranes were blocked in a buffer containing TBS with 0.05 % (v/v) Tween 20 (MP Biomedicals) and 5 % (w/v) milk for 1 h under rotation at RT. Subsequently, the immunoblots were probed with a primary antibody diluted in blocking buffer overnight at 4 °C. For detection of the primary antibody a horseradish peroxidase-conjugated secondary antibody (Cayman) or an IRDye-conjugated antibody (LI-COR Biosciences) was incubated for 1 h at RT. The chemiluminescent reaction for the HRP antibodies was visualized with SuperSignal West Dura Extended Duration Substrate (Thermo Fisher Scientific) in a chemiluminescence reader (Stella, Raytek). To detect the fluorophore-conjugated secondary antibodies fluorescence was visualized with the Odyssey infrared imaging system (LI-COR Biosciences).

2.7 Immunohistochemistry

For immunohistochemical analysis mice were shortly anesthetized with isoflurane and transcardially perfused with 0.9 % NaCl solution followed by a 4 % paraformaldehyde buffer solution (Sigma) by using a perfusion pump (Ismatec). After removing the brain and the tongue, tissues were transferred into a 10 % PFA solution and incubated at 4°C overnight. For long-term storage all tissues were transferred into a 1 % PFA solution and kept at 4°C. To avoid over-fixation spinal cords were directly transferred into a 70 % EtOH bath and kept at 4 °C. For further processing, fixed mouse brains were sliced into four to five sections using an adult mouse brain matrix for coronal sectioning (WPI) (Fig. 2.4). In addition, mouse tongues were sliced into four coronal sections and spinal cords were separated in 6-8 short coronal parts. Tissue sections were dehydrated by a series of graded ethanol baths (70 %, 95 %, 100 %, 100 %, 100 %, 100 % EtOH), transferred into two xylol baths and finally infiltrated with paraffin waxes using a tissue processing station (Leica Biosystems). Tissue sections of brain, tongue, and spinal cord were embedded into tissue processing cassettes (Roth) under use of a paraffin station (Leica Biosystems). Embedded brains were cut into 8 µm and tongues cut into 5 µm coronal sections by using

a microtome (Leica) and mounted on adhesive Super Frost Plus glass slides (Schubert and Weiss).

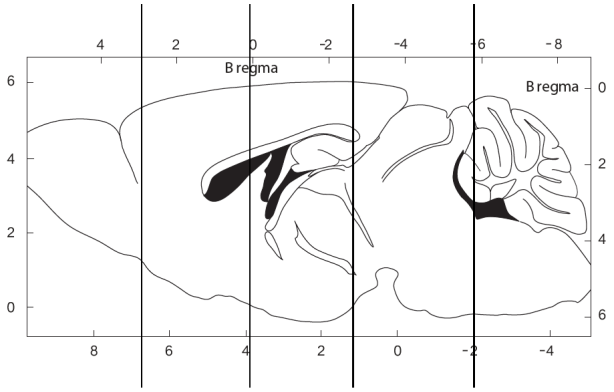

Fig. 2.4 Sectioning of the mouse brain. After fixation in paraformaldehyde brains were sliced into five parts to facilitate its infiltration with paraffin waxes. Embedded brain sections were further cut into 8 µm coronal sections (Franklin and Paxinos, 2008).

2.7.1 DAB staining

Brain sections were mounted on glass slides and incubated for 10 min at 60°C to melt the paraffin that surrounds the tissue. For deparaffinization the tissue was soaked in two xylol (Sigma) baths, transferred to an isopropanol/xylol bath for 5-10 min and rehydrated through a series of graded ethanol baths (100 %, 90 %, 70 %, 50 %, H_2O) with an incubation time of 5 min for each step. For antigen retrieval sections were incubated in citrate buffer for 10 min at RT and than cooked in a heated citrate buffer (pH 6.0) bath for 10 min in a microwave oven at 650 W. After cooling down, slides were transferred to a PBS bath for 10 min and further incubated with a 3 % hydrogen peroxide solution (Sigma) for 30 min to inhibit the endogenous peroxidases. After washing in PBS for 10 min and drawing a line around the tissue section with a hydrophobic barrier pen (Biozol Diagnostica), sections were blocked for 1 h at RT in blocking buffer containing 20 % (v/v) normal goat serum, 1 % (v/v) BSA (Thermo Fisher Scientific) and 0.5 % Triton X-100 (Sigma). The primary antibody diluted in 1 % (v/v) normal goat serum, 1 % (v/v) BSA, and 0.25 % Triton X-100 in PBS was incubated overnight at 4 °C. The antibodies used in this study with corresponding dilutions are listed in Table 2.5. To avoid drying of tissue sections the slides were stored in a wet chamber. After washing once with 0.25 % (v/v) Triton X-100 in PBS and twice with PBS sections were incubated with a secondary

peroxidase-conjugated antibody using the Vectastain ABC kit (Vector Laboratories) for rabbit antibodies and the MOM kit (Vector Laboratories) for mouse antibodies. For visualization sections were incubated in DAB (3-3'-diaminobenzidine, Biozol Diagnostica). Therefore the chemical was incubated for 30-60 s and reactions were inactivated in a 3 % hydrogen peroxide bath. After three washing steps for 10 min in distilled water acidic/negative charged structures like the DNA-containing nucleus were counterstained with Haematoxylin QS (Vector Laboratories) for 40 s. Slices were thoroughly washed in distilled water and bedewed with Vectamount mounting medium (Biozol) before they were covered with glass slides (Roth). After drying overnight at RT the slides were scanned on an Axio Scan.Z1 scanner (Carl Zeiss) and analyzed with the ZEN lite software (Carl Zeiss).

2.7.2 Fluorescence staining

Paraffin-embedded brain sections were incubated for 10 min at 60°C to melt the paraffin. Subsequently, sections were deparaffinized in two xylol and one isoprobanol/xylol bath for 5-10 min and finally hydrated through a series of graded ethanol baths (100 %, 90 %, 70 %, 50 %, H_2O). For antigen retrieval tissue sections were incubated for 5 min in citrate buffer and additionally boiled for 10 min at 650 W in a microwave oven. After the slides had cooled down for 20 min they were rinsed with PBS for 10 min. To minimize the antibody amount used, a hydrophobic barrier was drawn around the tissue sections (Biozol Diagnostica). Afterwards, sections were incubated for 1 h at RT in blocking buffer containing 20 % (v/v) normal goat serum, 1 % (v/v) BSA and 0.5 % Triton X-100. Sections were incubated with primary antibody diluted in 1 % (v/v) normal goat serum, 1 % (v/v) BSA, and 0.25 % Triton X-100 in PBS overnight at 4°C inside a wet chamber. The antibodies used in this study with corresponding dilutions are listed in Table 2.5. Slides were washed once with 0.25 % (v/v) Triton X-100 in PBS and twice with PBS for 20 min. Thus, tissue sections were stained with Alexa Fluor 488- or Alexa Fluor 594-conjugated (Thermo Fisher Scientific) anti-mouse or anti-rabbit secondary antibodies and the nuclear dye DAPI (4',6-diamidino-2-phenylindole, Thermo Fisher Scientific) diluted in 1 % (v/v) normal goat serum (Thermo Fisher Scientific) and 1 % (v/v) BSA in PBS for 1 h at RT. Secondary antibodies were used at a 1:1,000 working dilution and DAPI was diluted 1:50,000. After washing once with 0.25 % (v/v) Triton X-100 in PBS and twice with PBS for 10 min, slides were mounted with Fluoromount media (Omnilab) and

covered with glass slides (Roth). Finally, the slides were visualized with an LSM 700 confocal laser scanning microscope using the ZEN software (Carl Zeiss).

Table 2.5 Antibodies used for immunofluorescence (IF), immunohistochemistry (IHC) and western blotting (WB)

Antigen (antibody clone)	Source	Host	Immunogen	Dilution for IHC/IF	Antigen retrieval	Dilution for WB
Actin C4	Abcam	mouse	-	-	-	1:1000
p-α-Synuclein (phospho Ser 129) 81A	Covance	mouse	pSer129	1:200	citrate buffer	-
p-α-Synuclein (phospho Ser 129) pSyn #64	Wako	mouse	pSer129	1:1200	citrate buffer	-
p-α-Synuclein (phospho Ser 129) EP1536Y	Abcam	rabbit	pSer129	-	-	1:1000
human α-Synuclein Syn 211	Millipore	mouse	121-125	1:100	citrate buffer	1:2000
mouse α-Synuclein D37A6	Cell signaling	rabbit	103-110	1:100	citrate buffer	1:1000
Choline acetyltransferase (ChAT)	Millipore	rabbit	-	1:100	citrate buffer	-
Glial fibrillary acidic protein (GFAP)	Dako	rabbit	-	1:200	citrate buffer	-
Iba 1	Wako	rabbit	-	1:500	citrate buffer	-
Sequestosome 1 (p62)	Proteintech	rabbit	-	1:100	citrate buffer	-
Tyrosine hydroxylase	Abcam	rabbit	-	1:750	citrate buffer	-
Ubiquitin 1 Ubi-1	Millipore	mouse	-	1:500	citrate buffer	-

2.8 Behavioral analysis

To evaluate changes in the motor behavior, balance, coordination and grip strength of injected animals, their rotarod and wire-hang performance was tested after 30, 90, 180, 270, and 400 days post inoculation (dpi).

2.8.1 Rotarod test

A rotarod treadmill (Med associates) was used to assess motor learning, balance and coordination of the injected animals. Mice were tested four times per day on four consecutive days. Before each run the treadmill was cleaned with 70 % ethanol to minimize odor cues. Each mouse was placed on the horizontal rod, which accelerated speed from 4-400 rpm. The latency to fall was measured during a period of 5 min. Between each run the mice had 10 min time to recover. The first run on each day was considered a training session and not scored (Fig. 2.5). For the calculation of the running performance the training session at day one was considered as basal performance (= 100 % latency to fall) and the runs from the consecutive days were referred to them.

2.8.2 Wire-hang test

The neuromuscular strength of the injected animals and their balance were assessed by the wire-hang test. Previous to each testing the wire grids were disinfected with 70 % ethanol to minimize odor cues. Once the animal was placed on the wire grid the grid was slightly shaken to ensure that the animal gripped the wire. The time measurement started with the upside down turning of the wire grid. The latency to fall was measured with maximal 300 s as cut-off time. The mice were tested throughout one day with 5 hanging runs and with a regeneration time of 10 min between each trial. The first and second runs were considered as training sessions and the runs 3-5 were included to the calculation of the mean hanging performance (Fig. 2.5).

A) Rotarod performance-test protocol			
Training 1	Training 1	Training 1	Training 1
Training 2	Run 2	Run 2	Run 2
Training 3	Run 3	Run 3	Run 3
Training 4	Run 4	Run 4	Run 4

B) Wire hang test protocol
Training 1
Training 2
Run 1
Run 2
Run 3

Fig. 2.5 Overview about the testing protocols used for behavioral assays. A) The four-day protocol for the rotarod-performance test considered the entire first day and the first run of each consecutive day as training. To calculate the mean latency to fall, runs 2-4 on day two, three, and four were scored. B) For the wire-hang test animals were tested on a single day while the first two of five total sessions were considered as training. The mean of sessions 1-3 was calculated as the animals hanging performance for that day.

3 Results

3.1 Virulence of recombinant mouse α-synuclein fibrils injected into Tg(*Gfap*-luc$^{+/-}$) mice

3.1.1 Intracerebral injection with α-synuclein fibrils evoked mild neuropathology

To address whether intrastriatal injection of aggregated α-synuclein can induce widespread synucleinopathy in the brain, Tg(*Gfap*-luc$^{+/-}$) reporter mice were inoculated with recombinant mouse wild-type α-synuclein fibrils (Appendix Fig. 5.2 A). The visualization of the inoculum showed dot-like oligomeric and rod-shaped fibrillar forms of α-synuclein (Fig. 3.1 A). These fibrils were unilaterally injected into the striatum of the right brain hemisphere (Fig. 3.1 B).

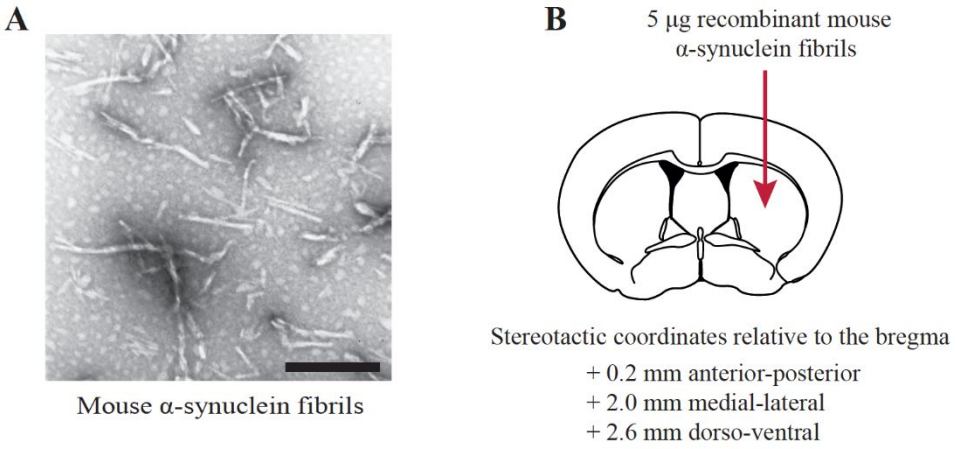

Fig. 3.1 Intrastriatal inoculation with α-synuclein fibrils. A) Negative stain electron microscopy image of aggregated mouse α-synuclein as oligomers and rod-shaped fibrils. Bar: 200 nm. B) Schematic view of the injection site. The striatum of the right brain hemisphere was targeted by the following stereotactic coordinates relative to the bregma: + 0.2 mm anterior-posterior, + 2.0 mm medial-lateral, + 2.6 mm dorso-ventral (Franklin and Paxinos, 2008).

During an observation time of 400 d, none of the inoculated animals showed any clinical symptoms of neurological disease. Histological analysis of the brains collected at 30, 90, 180 and 400 days post inoculation (dpi) revealed that mice injected with α-synuclein fibrils developed mild pathology showing inclusions of phosphorylated α-synuclein only at 400 dpi and not at earlier time points (Table 2.1).

Table 2.1 Overview about intracerebrally injected Tg(*Gfap*-luc$^{+/-}$) mice

Mouse line	Inoculum (amount)	Inoculation route	No. of mice with pathology/ no. of challenged mice	Survival time [dpi]
Tg(*Gfap*-luc$^{+/-}$)	mouse α-synuclein fibrils (5µg)	intracerebral	8/ 8 0/ 2 0/ 3 0/ 2	400 180 90 30
Tg(*Gfap*-luc$^{+/-}$)	PBS	intracerebral	0/ 9 0/ 3 0/ 3 0/ 2	400 180 90 30

For the immunohistochemical analysis, brain sections were stained with two different α-synuclein antibodies recognizing phosphorylation at serine 129. This phosphorylation site was previously described as the predominant post-translational modification of α-synuclein in human synucleinopathy lesions (Anderson et al., 2006; Fujiwara et al., 2002). Tissue sections probed with the 81A antibody indicated positive staining for phosphorylated and misfolded α-synuclein in cortical brain regions. Additional staining of tissue sections with the pSyn#64 antibody confirmed that α-synuclein pathology was restricted to the cortex (Fig. 3.2 A,B). The α-synuclein pathology was found throughout the entire cortex rostral and caudal from the injection site in both hemispheres, but not inside the striatum. The α-synuclein deposits showed a specific filamentous structure as characterized in humans as LNs and were distributed in the following interconnected regions: a) somatosensory cortex, b) insular cortices including the granular, dysgranular and agranular cortex and c) more caudal regions, including the ectorhinal, perirhinal and entorhinal cortices (Fig. 3.2 C). Surprisingly, and in contrast to brain sections from animals analyzed at 400 dpi, deposits of phosphorylated α-synuclein were not detectable at 30, 90 or 180 dpi (data not shown).

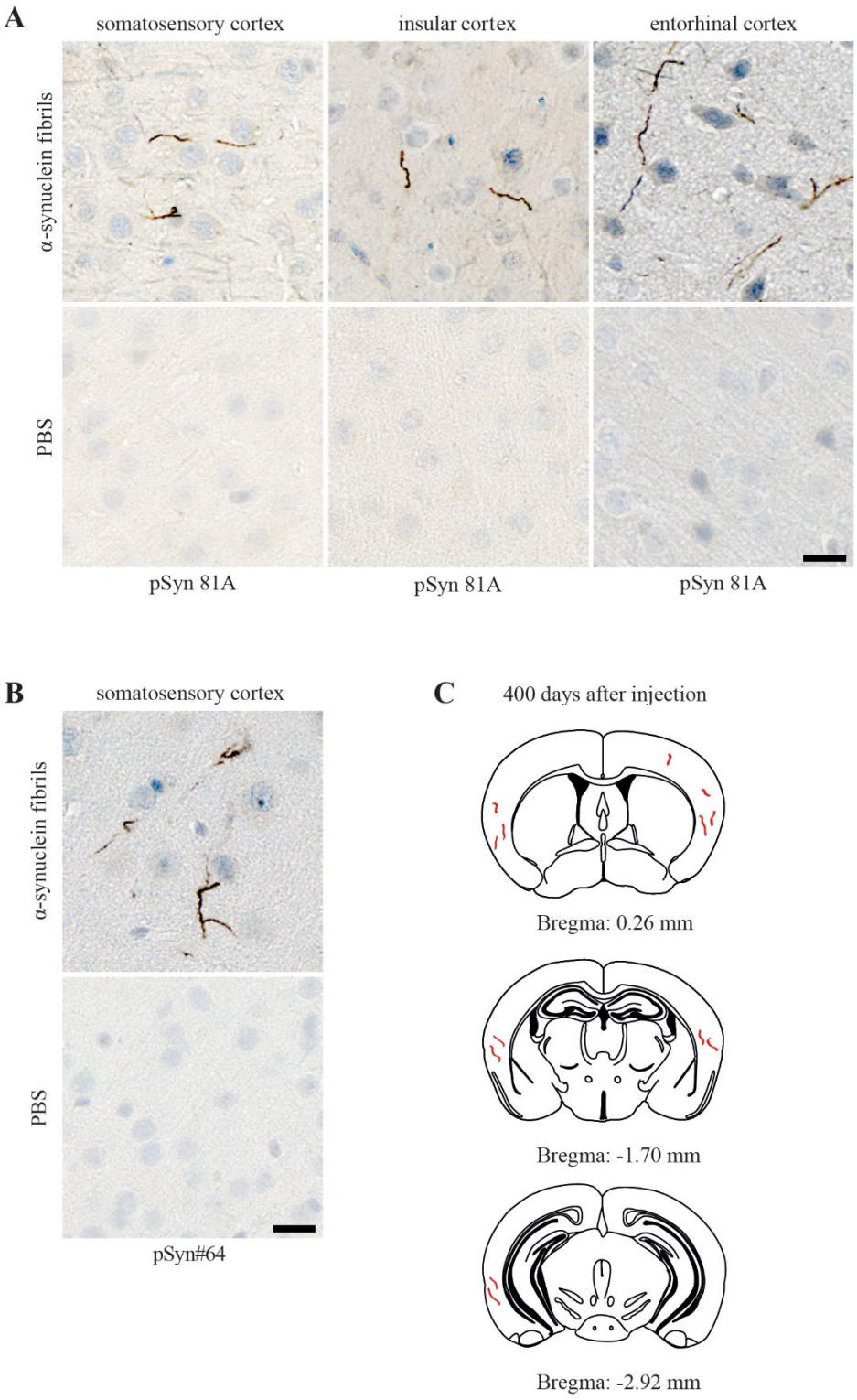

Fig. 3.2 Intrastriatal injection of recombinant mouse α-synuclein fibrils into Tg(*Gfap*-luc$^{+/-}$) mice induced mild α-synuclein pathology in their brains. Immunohistochemical staining with A) the pSyn#64 antibody or B) the 81A antibody detected filamentous aggregates of phosphorylated α-synuclein at 400 dpi. The pathology was restricted to the somatosensory cortex, insular cortices, and rhinal cortices as schematically shown in C) LNs are depicted by the red symbols. The distribution of pathology as detected with both antibodies was similar. The location of each coronal region is defined by its relative position to the bregma (Franklin and Paxinos, 2008). Bar = 20 µm.

Despite the presence of phosphorylated α-synuclein aggregates in the cortex at 400 dpi as detected by immunohistochemistry, high-molecular-weight species composed of sarcosyl-insoluble and phosphorylated α-synuclein extracted from whole brain homogenates could not be visualized by biochemical techniques (Fig. 3.3). The absence of insoluble α-synuclein oligomers was also evident at the earlier time points.

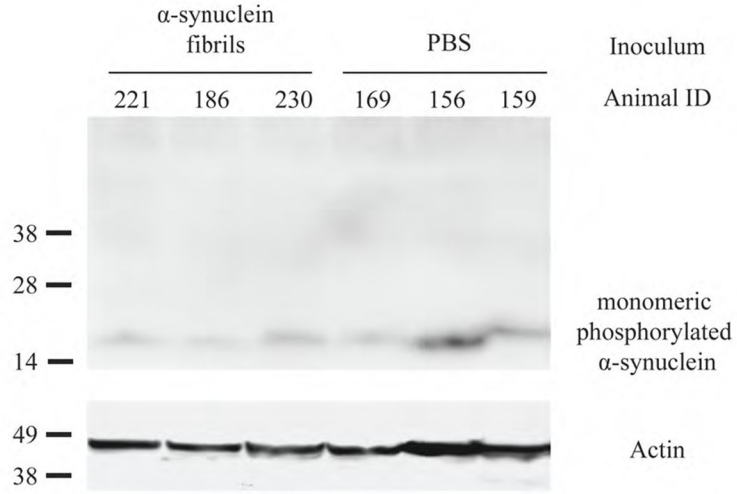

Fig. 3.3 Detergent-insoluble species of phosphorylated α-synuclein were not detectable in the brains of Tg(*Gfap*-luc$^{+/-}$) mice. Brain homogenates of mice intracerebrally injected with PBS or α-synuclein fibrils were analyzed at 400 dpi by immunoblotting. Probing with the EP1536Y antibody did not reveal the presence of oligomeric forms of phosphorylated α-synuclein. Equal sample loading was confirmed with an antibody against actin. Three animals were exemplary depicted for each treatment group.

3.1.2 α-Synuclein fibrils intraglossally injected did not neuroinvade the brain

To elucidate if α-synuclein fibrils injected into the tongue muscle show a similar propensity to seed pathology and neuroinvade the brain, Tg(*Gfap*-luc$^{+/-}$) mice were intraglossally injected with recombinant α-synuclein fibrils or PBS into the lower bulk of the tongue muscle (Appendix Fig. 5.2 B). During the observation period of 400 d none of the animals showed obvious behavioral changes or signs of neurological disease (Table 2.2).

Table 2.2 Overview about intraglossally injected Tg(*Gfap*-luc$^{+/-}$) mice

Mouse line	Inoculum (amount)	Inoculation route	No. of mice with α-synuclein pathology/ no. of challenged mice	Survival time [dpi]
Tg(*Gfap*-luc$^{+/-}$)	mouse α-synuclein fibrils (5µg)	intraglossal	0/ 8 0/ 4 0/ 2 0/ 4	400 180 90 30
Tg(*Gfap*-luc$^{+/-}$)	PBS	intraglossal	0/ 9 0/ 2 0/ 3 0/ 5	400 180 90 30

In addition, immunohistochemical analyses were performed in various brain areas that are interconnected to the cranial nerves to innervate the tongue. The stainings did not reveal deposits of phosphorylated α-synuclein when using both phosphorylation-specific antibodies pSyn#64 or 81A. The tongue is prevalently innervated by the bilaterally proceeding hypoglossal nerve originating at the hypoglossal nucleus. After none of the examined incubation periods, 30, 90, 180 or 400 dpi, misfolded and phosphorylated α-synuclein was detectable in the hypoglossal nucleus. Exemplary, the hypoglossal nuclei at 30 and 400 dpi were depicted to demonstrate the lack of pathology in animals injected with α-synuclein fibrils or PBS (Fig. 3.4).

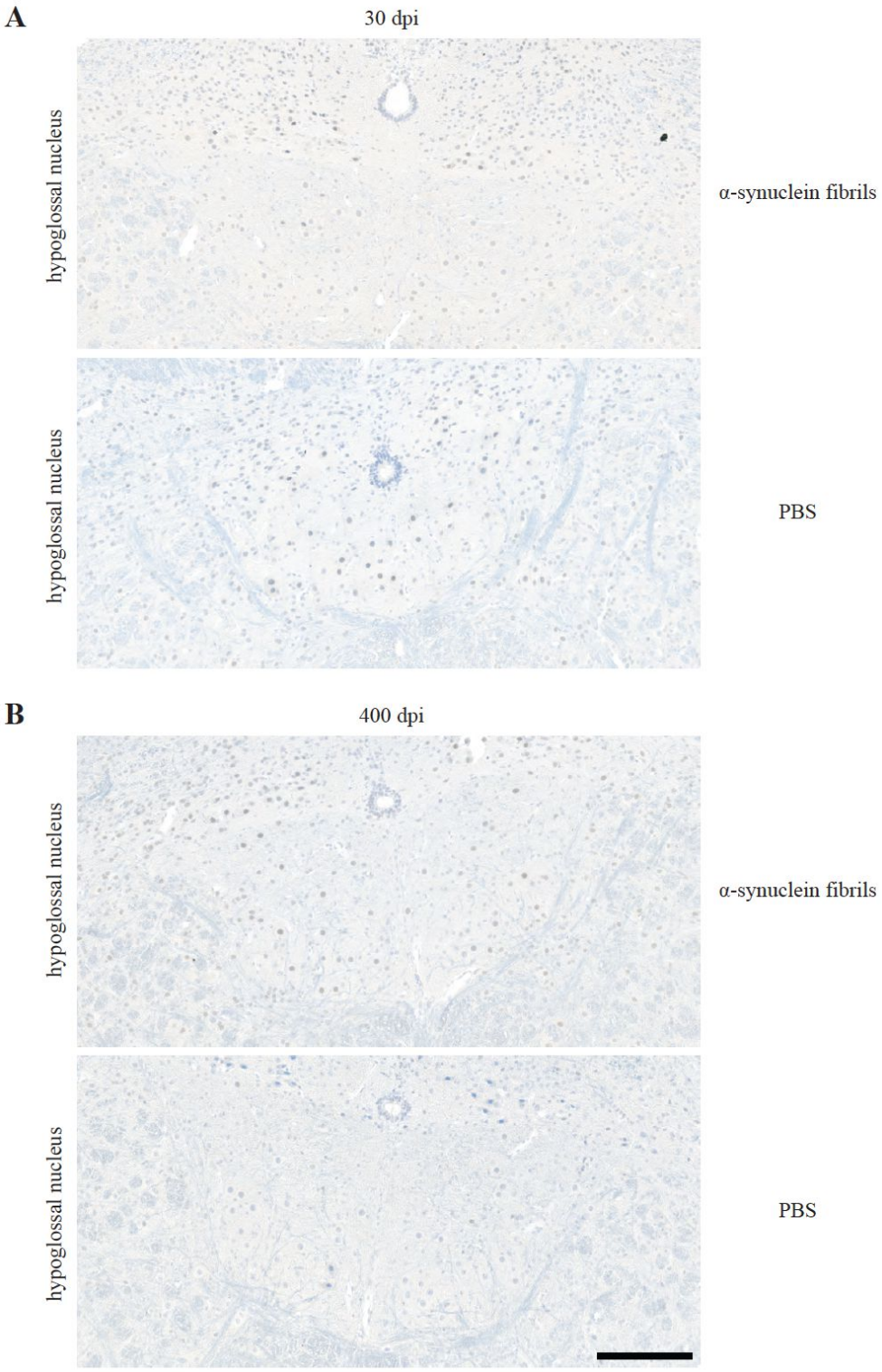

Fig. 3.4 Tg(*Gfap*-luc$^{+/-}$) mice intraglossally injected with α-synuclein fibrils did not reveal any α-synuclein pathology in their hypoglossal nuclei. For the immunohistochemical analysis brain sections were stained with the pSyn#64 antibody that recognizes phosphorylated α-synuclein. None of the fibril- or PBS-injected animals showed deposits of phosphorylated α-synuclein in their hypoglossal nuclei. Shown here are only results for brains collected at 30 (A) and 400 dpi (B). Bar = 200 µm.

Moreover, biochemical analysis by immunoblotting revealed that the sarcosyl-insoluble fractions of the animal brains intraglossally injected with α-synuclein seeds or PBS did not contain any high-molecular weight species of phosphorylated α-synuclein. The lack of phosphorylated aggregates was obvious at all examined time points as exemplary shown at 30 dpi (Fig. 3.5).

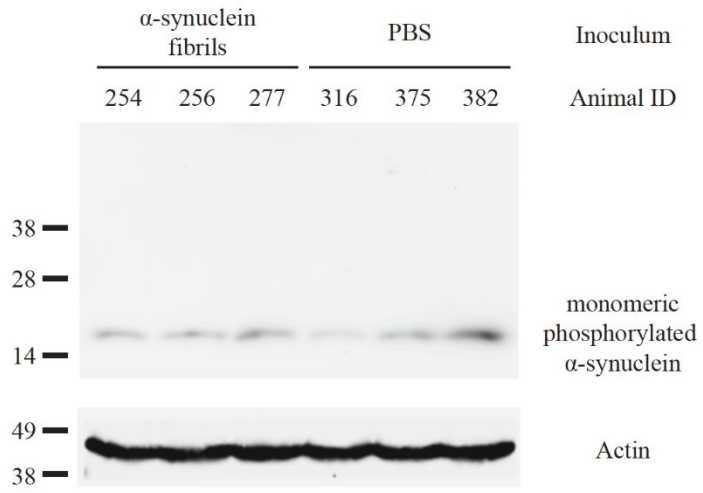

Fig. 3.5 Intraglossally injected Tg(*Gfap*-luc$^{+/-}$) mice did not show any insoluble and phosphorylated α-synuclein aggregates in their brains. For biochemical analysis sarcosyl-insoluble fractions were extracted at 30 dpi from the brains of mice intraglossally injected with α-synuclein fibrils or PBS. Detection with the EP1536Y antibody revealed only a weak signal for the monomeric form of phosphorylated α-synuclein with approximately 14 kDa. Equal protein loading was confirmed with an antibody against actin. Samples from three different animals are shown for each treatment group.

To investigate whether the injected fibrils may have seeded disease-associated deposits around the injection site, the tongues of the injected mice were immunohistochemically analyzed with the pSyn#64 antibody. The analysis did not reveal the presence of phosphorylated α-synuclein in any of the analyzed tongues, including those collected at 30 dpi (Fig. 3.6). In particular, the epithelial layers, the skeletal muscles, the surrounding epithelium of blood vessels, and the nerve bundles remained free of misfolded α-synuclein. Equally, biochemical analysis by immunoblotting with the EP1536Y antibody did not detect sarcosyl-insoluble phosphorylated α-synuclein extracted from whole tongue homogenates at all examined time points.

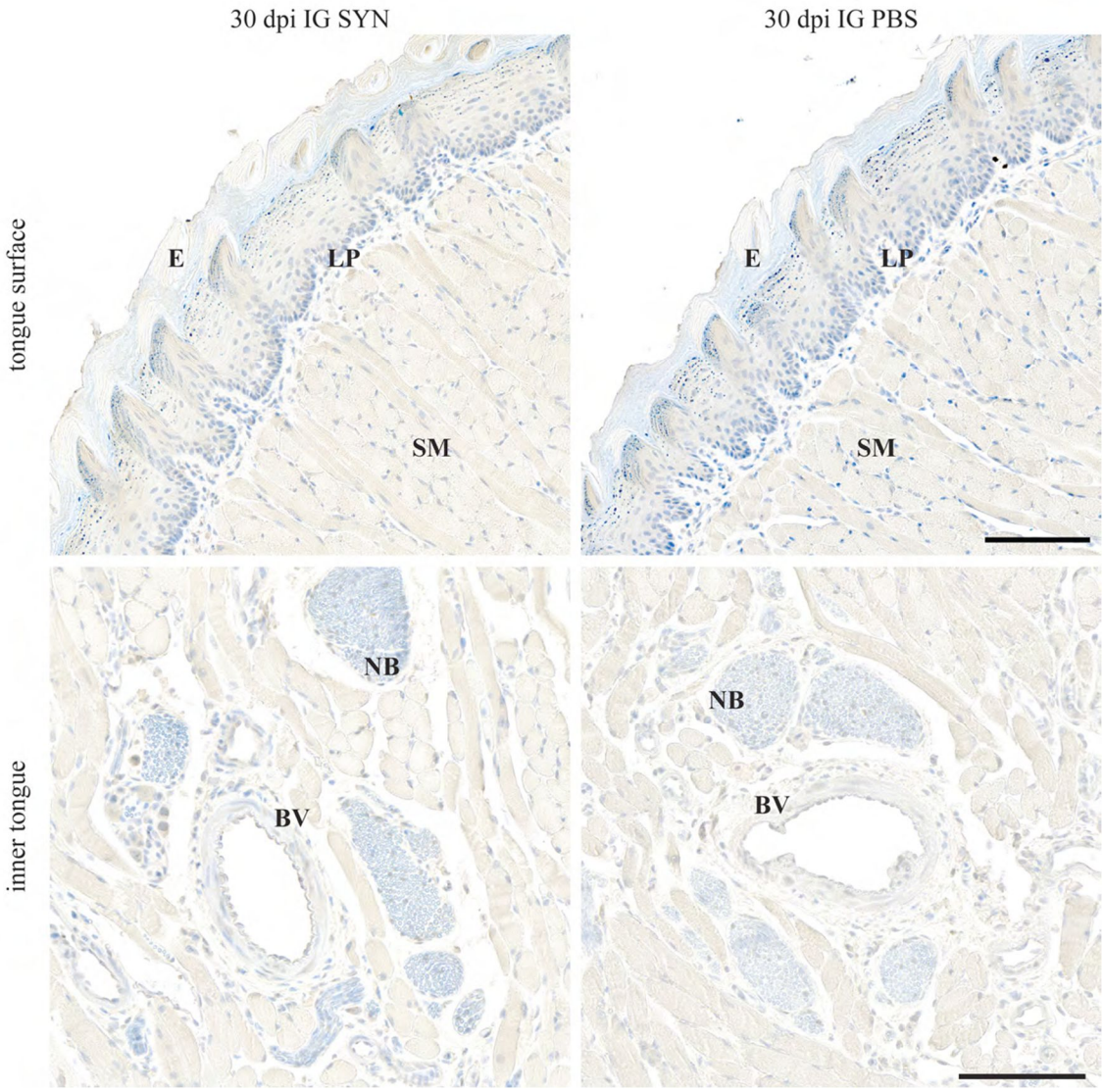

Fig. 3.6 Tg(*Gfap*-luc$^{+/-}$) mice intraglossally injected with α-synuclein fibrils did not accumulate phosphorylated α-synuclein in their tongues. Tongues of mice intraglossally injected were immunohistochemically analyzed at 30 dpi with the phosphorylation specific pSyn#64 antibody. None of the α-synuclein- (SYN) or PBS-injected animals showed deposits of phosphorylated α-synuclein in their tongues as illustrated for the epithelium (E), the lamina propria (LP), the skeletal muscles (SM), the fibers of nerve bundles (NB) and the surrounding tissue of blood vessels (BV). Bar = 100 µm.

3.1.3 Inoculated mice did not display motor deficits

To uncover abnormalities in motor behavior and performance caused by neuronal failure, the behavior of intracerebrally (Fig. 3.7 A,B) or intraglossally (Fig. 3.7 C,D) injected Tg(*Gfap*-luc$^{+/-}$) mice was analyzed. Therefore, animals were tested in the rotarod-performance (Fig. 3.7 A,C) and the wire-hang test (Fig. 3.7 B,D). The rotarod-performance test provides information regarding an animal's ability to maintain balance

and coordination. The wire-hang assay measures an animal's grip strength. Both tests demonstrated that fibril-injected animals did not diminish performance when compared to PBS-injected control mice. However, an age-dependent reduction in performance became apparent at least at 360 dpi in both assays independent of the inoculum or the injection route (Fig. 3.7).

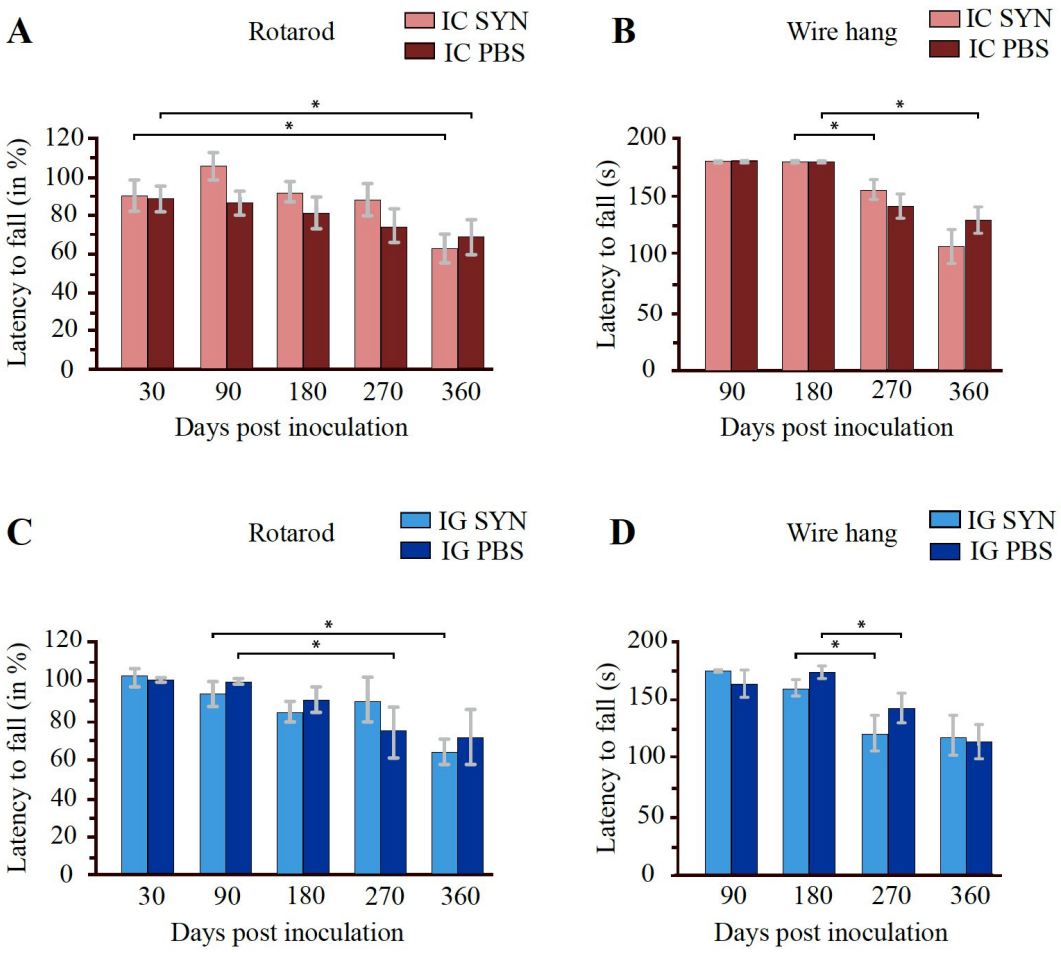

Fig. 3.7 Intracerebrally and intraglossally inoculated Tg(*Gfap*-luc$^{+/-}$) mice did not show behavioral deficits. Neither the rotarod-performance test (A and C) nor the wire-hang test (B and D) revealed any significant differences between animals injected intracerebrally (A and B) with α-synuclein fibrils (light red) or PBS (dark red). Similarly, animals intraglossally injected (C and D) with α-synuclein fibrils (light blue) or PBS (dark blue) did not show any behavioral deficits for both tests. At least eight animals were tested for each treatment group in the rotarod-performance test at 30, 90, 180, 270, and 360 dpi. In the wire-hang-test at least five animals were tested at 90, 180, 270, and 360 dpi. Error bars indicate SEM. * $P < 0.05$ (paired t-test).

3.1.4 Injected mice did not develop persistent CNS inflammation

Since Tg(*Gfap*-luc$^{+/-}$) mice express luciferase from the GFAP (Glial fibrillary acidic protein) promoter the activity of astrocytes can be easily monitored by bioluminescence imaging (BLI) as previously shown in these mice after infection with prions (Tamgüney et al., 2009a). To assess whether injection of α-synuclein fibrils or PBS in Tg(*Gfap*-luc$^{+/-}$) reporter mice causes sustained neuroinflammation, the activity of astrocytes was monitored by BLI throughout the entire experimental time course. Tg(*Gfap*-luc$^{+/-}$) mice were intracerebrally injected with RML prions as a positive or with PBS as a negative control. Prion-infected animals began to show an increased radiance ~10 weeks before they finally developed neurological signs of prion disease and had to be sacrified (Fig. 3.8A). Approximately eight weeks after prion injection, animals emitted from their brains bioluminescence (BL) levels above a threshold of 1.5 million photons/s/cm^2/sr. In this setting, this value was indicative for astrocytic activation. In contrast, PBS-injected negative control animals did not show an increase in BL throughout the entire 19 weeks of the experiment. An initial increase exceeding 1.5 million photons/s/cm^2/sr in prion- and PBS-injected mice at 2 weeks post inoculation was caused by the inoculation-induced trauma resulting in transient astrogliosis. For Tg(*Gfap*-luc$^{+/-}$) mice that were either intracerebrally or intraglossally injected with α-synuclein fibrils or PBS, BLI did not reveal an increase in BL throughout the observation course of 54 weeks (Fig. 3.8 B,C). In comparison to the intraglossal injections, injections into the cerebrum, transiently led to elevated BL as a result of surgery-induced inflammation.

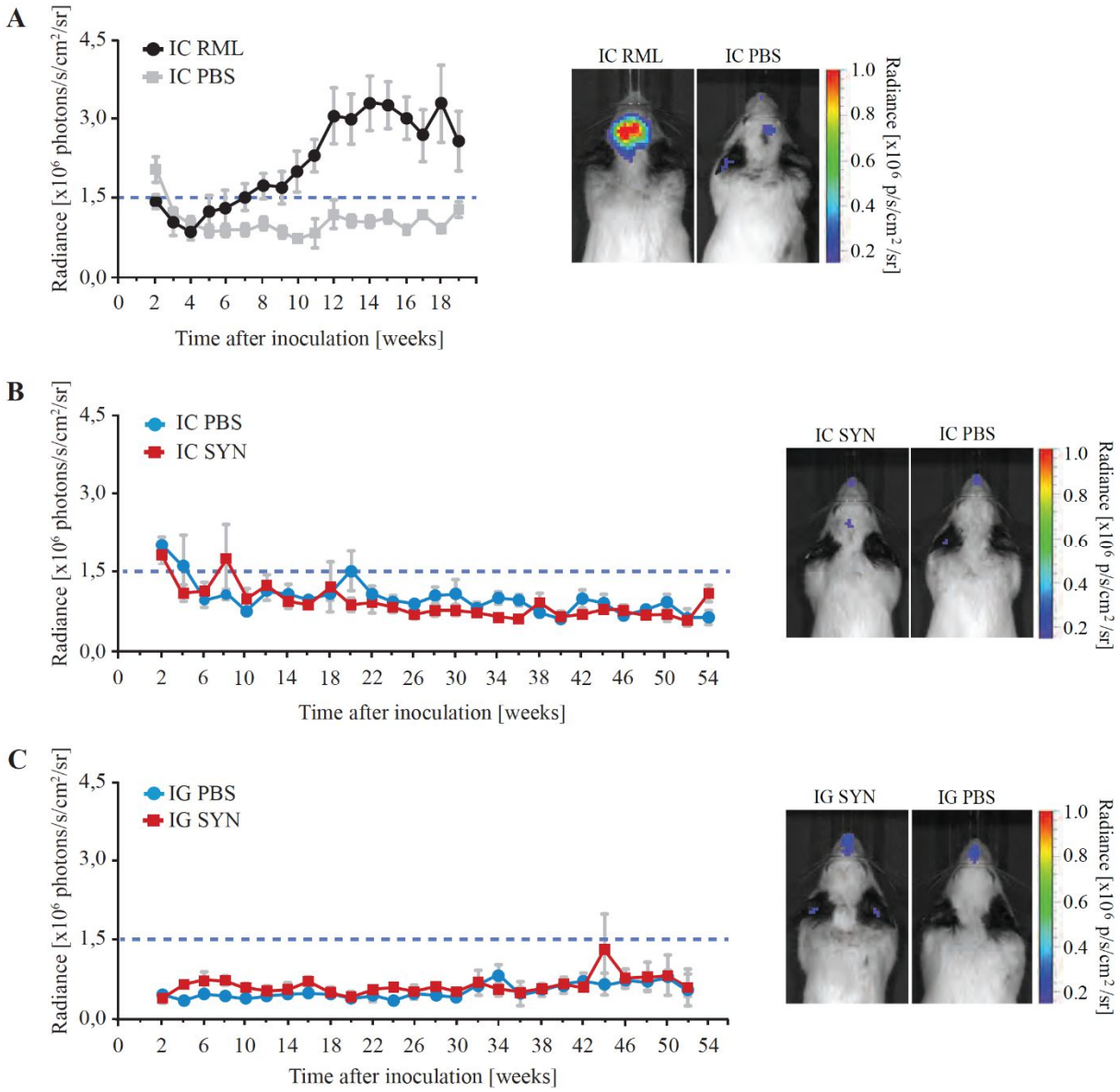

Fig. 3.8 Intracerebral and intraglossal challenge with α-synuclein prionoids did not cause astrocytic gliosis in Tg(*Gfap*-luc$^{+/-}$) mice. The activation of astrocytes in the brains of intracerebrally or intraglossally injected Tg(*Gfap*-luc$^{+/-}$) mice was measured by BLI every first to second week. A) Mice intracerebrally injected with RML prions displayed elevated BL signals exceeding a threshold of 1.5x10^6 photons/s/cm^2/sr (indicated as blue-dotted line) at 8 weeks post inoculation (black circles). Intracerebral injection with PBS did not induce astrocytic activation (grey squares). B) BL measured from the brains of animals intracerebrally injected with α-synuclein fibrils (red squares) or PBS (blue circles) remained predominantly under the threshold of 1.5 x10^6 photons/s/cm^2/sr. C) BL did not significantly increase when animals were intraglossally injected with α-synuclein fibrils (red squares) or PBS (blue circles). Images are representative of animals that were quantified for BLI at the latest time point. At least 13 animals were used for BLI at each time point for all conditions. Error bars indicate SEM.

Since the cortex of intracerebrally injected animals exclusively accumulated phosphorylated α-synuclein, it might be the most probable brain region, beside the injection site, to develop signs of neuroinflammation. Immunohistochemical staining with an antibody against GFAP did not show any signs of astrocytic gliosis in the striatum and cortical regions of Tg(*Gfap*-luc$^{+/-}$) mice injected with α-synuclein fibrils or PBS (Fig. 3.9 A). The injection did not lead astrocytes to change their morphology or to proliferate. Furthermore, to analyze whether these animals had reactive microgliosis, brain sections were additionally stained with an antibody to ionized calcium-binding adapter molecule 1 (IBA-1). IBA-1 is a marker for activated microglia that is also known as AIF-1 (allograft inflammatory factor 1). Animals sacrified at 400 dpi did not reveal signs for reactive microgliosis showing comparable number of cells with unchanged morphology between all treatment groups (Fig. 3.9 B).

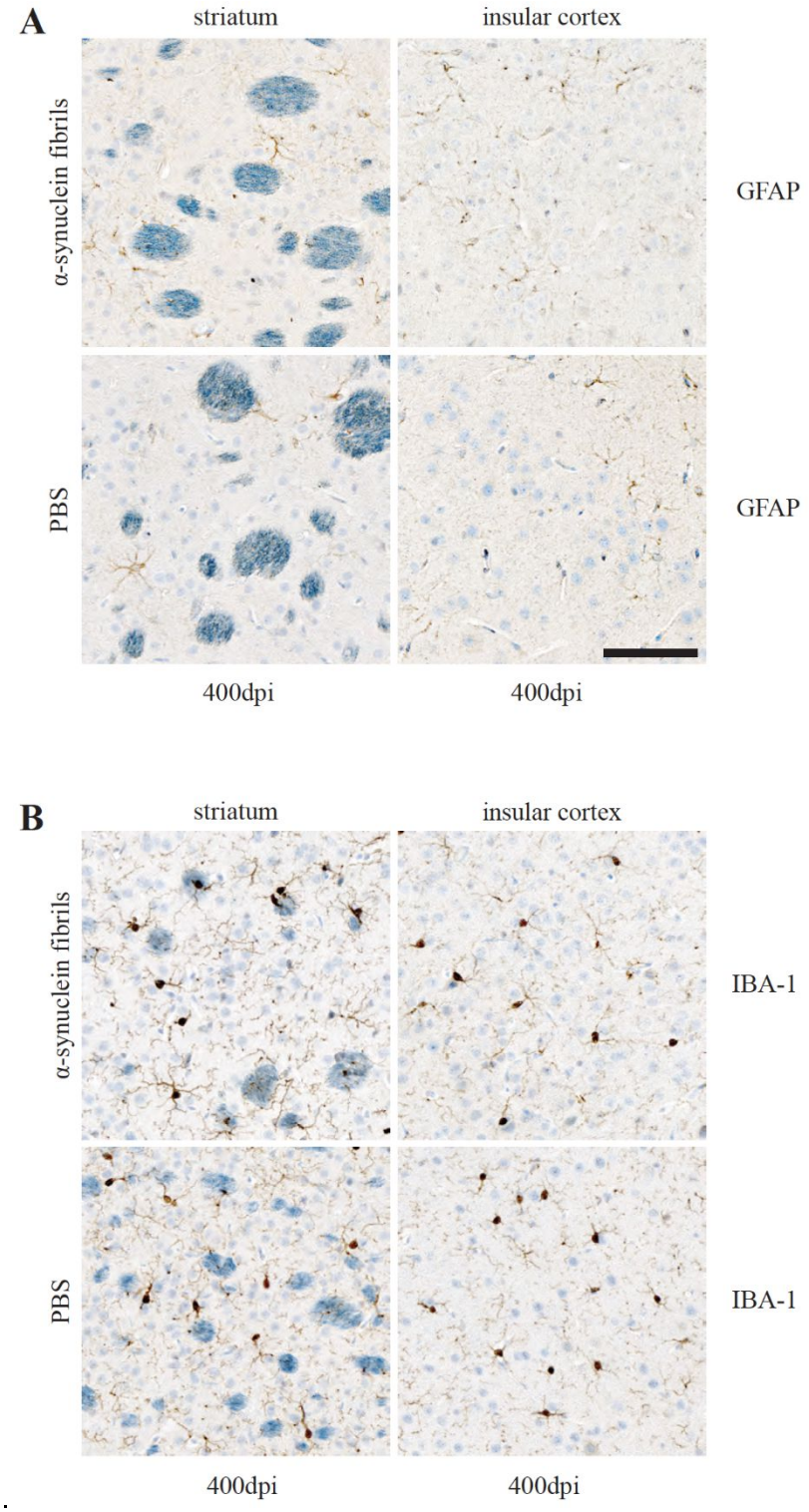

Fig. 3.9 Intracerebral injections of α-synuclein fibrils in Tg(*Gfap*-luc$^{+/-}$) mice did not cause neuroinflammation. A) Immunohistochemical analysis did not reveal differences between PBS- and α-synuclein injected animals after staining brain sections of animals sacrified at 400 dpi with an antibody to GFAP. Animals in both treatment groups did not display any signs for astrocytic gliosis. B) Staining with an IBA-1 antibody equally confirmed the absence of microgliosis in both treatment groups at 400 dpi. Representatively, stained sections of the striatum and the insular cortex are shown. Bar = 100 µm.

3.2 Susceptibility of Tg(M83$^{+/-}$:Gfap-luc$^{+/-}$) mice to peripherally injected α-synuclein fibrils

3.2.1 Injection of α-synuclein fibrils induced neuropathology and neurologic disease

To investigate whether animals overexpressing the A53T mutant of human α-synuclein would develop α-synuclein pathology after peripheral challenge, bigenic, hemizygous Tg(M83$^{+/-}$:*Gfap*-luc$^{+/-}$) reporter mice were peripherally injected with misfolded α-synuclein. As also previously reported, the Tg(M83$^{+/-}$:*Gfap*-luc$^{+/-}$) mice did not develop any spontaneous neurological disease or neuropathology for at least 22 months of age (Watts et al., 2013). For the peripheral challenge, Tg(M83$^{+/-}$:*Gfap*-luc$^{+/-}$) mice were injected with human α-synuclein fibrils into the tongue or peritoneal cavity (Appendix 5.2 C). The inoculum contained clusters of rod-shaped fibrils of different length (Fig. 3.10 A).

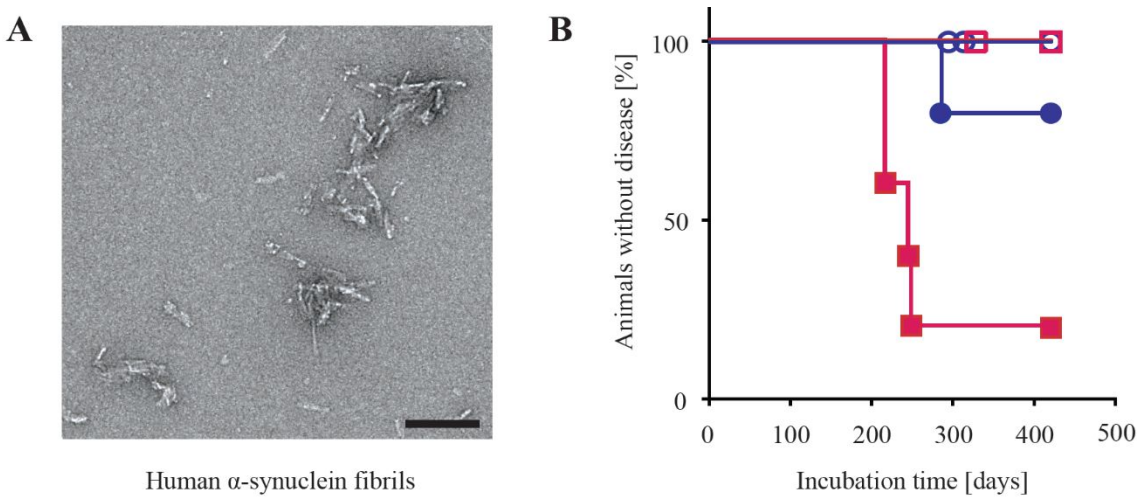

Fig. 3.10 Intraperitoneal or intraglossal challenge with α-synuclein fibrils caused disease in Tg(M83$^{+/-}$:*Gfap*-luc$^{+/-}$) mice. A) The electron microscopy image shows recombinant wild-type human α-synuclein as clusters of rod-shaped aggregates of different length. Bar = 100 nm. B) The Kaplan-Meier survival curves indicate that 4 mice of 5 intraperitoneally injected with α-synuclein fibrils developed neurological dysfunction and disease in 229 ± 17 days (mean ± SD; red filled squares), whereas none of the PBS-injected control mice (n = 5) developed signs of neurological illness within 420 dpi (red framed squares). Among the intraglossally injected animals only one of five died after 285 dpi (blue filled circles), whereas the residual four animals as well as the PBS-injected mice (n = 5) (blue framed circles) did not show any signs of disease.

Intraglossal injection of Tg(M83$^{+/-}$:*Gfap*-luc$^{+/-}$) mice with recombinant human α-synuclein fibrils caused neurologic disease in only one mouse of five, which died after 285 d as presented in the Kaplan-Meyer survival curve (Fig. 3.10 B, Table 2.3). All other mice, including those intraglossally injected with PBS did not develop neurologic disease during 420 d of observation. The intraperitoneal challenge of Tg(M83$^{+/-}$:*Gfap*-luc$^{+/-}$) mice with recombinant human α-synuclein fibrils induced clinical symptoms of neurologic disease in four of five animals with marked signs of paralysis of the hindlimb muscles, kyphosis, tail rigidity, and reduced activity within 229 ± 17 d (mean ± SD) (Fig. 3.11). Whereas Tg(M83$^{+/-}$:*Gfap*-luc$^{+/-}$) mice injected with PBS remained healthy throughout the observation period of 420 days (Fig. 3.10 B, Table 2.3) (Breid et al., 2016).

Table 2.3 Overview about peripherally injected Tg(M83$^{+/-}$:*Gfap*-luc$^{+/-}$) mice

Mouse line	**Inoculum (amount)**	**Inoculation route**	**No. of sick mice/ no. of challenged mice**	**Mean survival time ± SD [dpi]/ harvesting**
Tg(M83$^{+/-}$:*Gfap*-luc$^{+/-}$)	human α-synuclein fibrils (50µg)	intraperitoneal	4/ 5	229 ± 17
Tg(M83$^{+/-}$:*Gfap*-luc$^{+/-}$)	PBS	intraperitoneal	0/ 5	420
Tg(M83$^{+/-}$:*Gfap*-luc$^{+/-}$)	human α-synuclein fibrils (10µg)	intraglossal	1/ 4	285/ 420
Tg(M83$^{+/-}$:*Gfap*-luc$^{+/-}$)	PBS	intraglossal	0/ 5	420

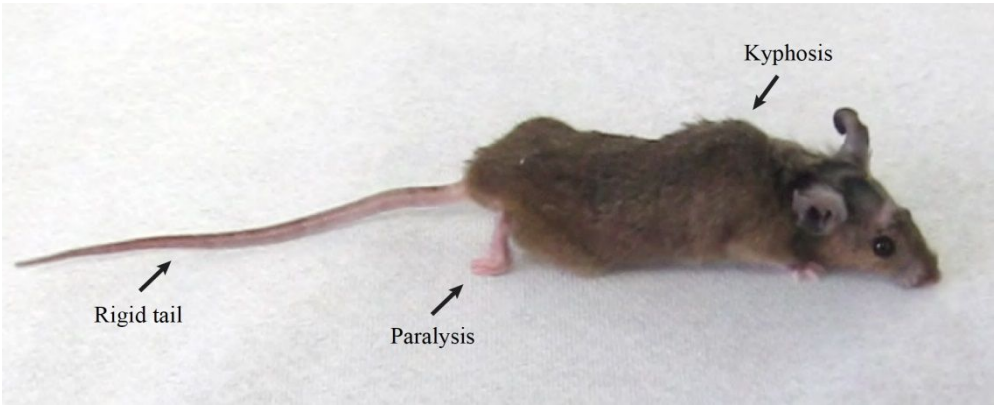

Fig. 3.11 Diseased Tg(M83$^{+/-}$:*Gfap*-luc$^{+/-}$) mouse after intraperitoneal injection with α-synuclein fibrils. The mouse intraperitoneally inoculated with α-synuclein fibrils developed severe neurological symptoms with paralysis of the hindlimbs, kyphosis, tail rigidity, and reduced activity at 215 dpi.

3.2.2 Intraglossally injected mice developed neurologic disease

Intraglossally injected Tg(M83$^{+/-}$:*Gfap*-luc$^{+/-}$) mice were weighed weekly and continued to gain weight, except for animal 121 that had been injected with fibrils and started to lose weight eight weeks before it became terminally sick and died (Fig. 3.12 A,B). Biochemical analysis revealed that the diseased animal had accumulated aggregated species of phosphorylated α-synuclein in its CNS; in both the brain and spinal cord sarcosyl-insoluble fractions of oligomeric α-synuclein species were detectable by the phosphorylation specific antibody EP1536Y (Fig. 3.12 C). A pronounced signal was achieved for an oligomeric form below 38 kDa. The equal protein loading was shown by probing the immunoblot with an actin antibody. The non-diseased, healthy animals did not accumulate aggregated and phosphorylated α-synuclein species in their brains or spinal cords, equally to the PBS-inoculated controls. The endogenous monomeric α-synuclein in the brain samples was detectable to a similar extend in the healthy and diseased animals. In contrast, the endogenous, monomeric and phosphorylated α-synuclein in the spinal cord samples was less abundant in the non-diseased animals than in the affected mouse 121 (Fig. 3.12 C) (Breid et al., 2016).

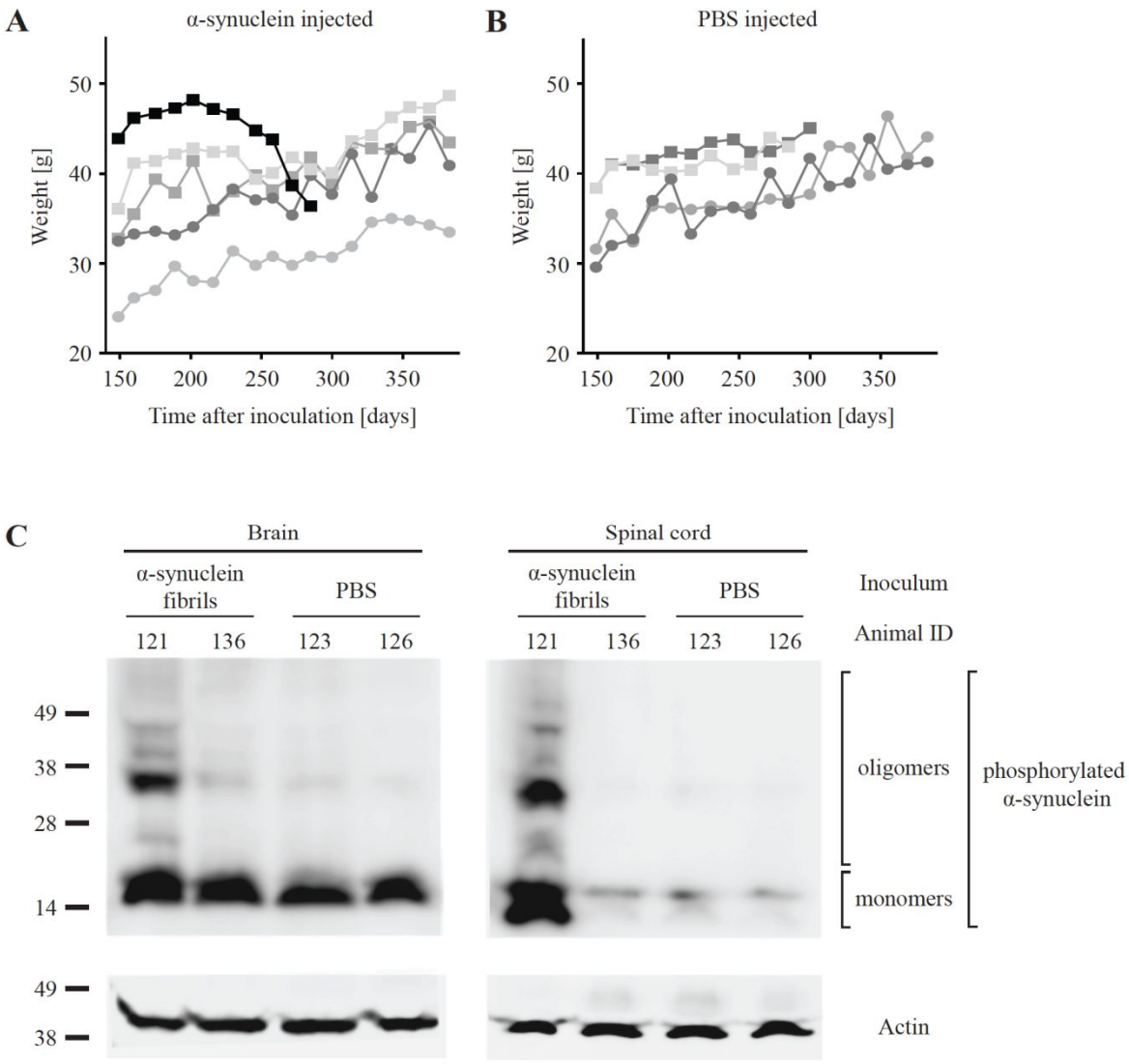

Fig. 3.12 The intraglossally injected and diseased Tg(M83$^{+/-}$:*Gfap*-luc$^{+/-}$) animal lost its bodyweight and accumulated phosphorylated α-synuclein in its CNS. A) Animal 121 began to lose weight at least 8 weeks before it died after intraglossal injection of α-synuclein fibrils (black squares). In contrast, the other animals intraglossally injected with α-synuclein fibrils remained healthy throughout the 420 d period of the experiment and continuously gained weight (grey shaded symbols), B) as did all PBS-injected animals. In panels A) and B) female mice are respresented by circles and male mice by squares. C) For biochemical analysis the brain and spinal cord tissues were harvested once animals showed clinical symptoms or finally at 420 dpi. The diseased animal 121 had accumulated sarcosyl-insoluble aggregates of phosphorylated α-synuclein in its brain and spinal cord, which were detected with the EP1536Y antibody recognizing phosphorylated α-synuclein. In contrast, mice that did not develop disease after intraglossal injection showed only the monomeric form of phosphorylated α-synuclein in their brain and spinal cord extracts. The molecular weight is shown in kilodalton. Equal sample loading in each lane was confirmed by detection of actin.

Surprisingly, none of the animals intraglossally injected with α-synuclein fibrils revealed any accumulations of phosphorylated α-synuclein in their brains or spinal cords, when they were analyzed by immunohistochemistry. Brains and spinal cords were collected at 420 dpi and the tissue sections were probed with an antibody detecting phosphorylation at serine 129 of α-synuclein (pSyn#64). Analysis was performed for the entire brain and spinal cord including the cortex, striatum, hippocampus, amygdala and hypoglossal nucleus as well as cervical, thoracic and lumbar parts of the spinal cord (data not shown). Even the hypoglossal nucleus in the brainstem that is directly connected to the tongue by the bilateral hypoglossal nerve did not display any aggregates of phosphorylated α-synuclein, which is a likely route for neuroinvasion as it has been shown for prions after intraglossal inoculation (Bartz et al., 2003) (Fig. 3.13).

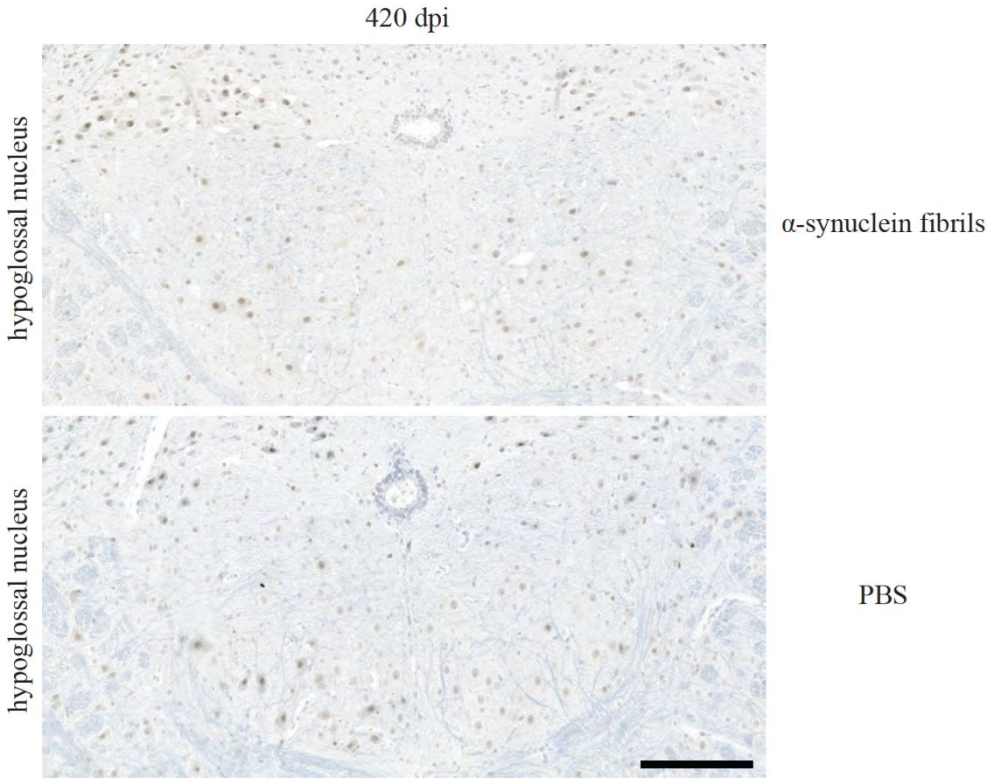

Fig. 3.13 The hypoglossal nuclei of Tg(M83$^{+/-}$:*Gfap*-luc$^{+/-}$) mice injected with α-synuclein fibrils did not contain detectable deposits of disease-associated α-synuclein. For immunohistochemical analysis the brains of intraglossally injected animals at 420 dpi were stained with the phosphorylation-specific pSyn#64 antibody. None of the animals injected with α-synuclein fibrils (n=5) or PBS (n=5) displayed deposits of phosphorylated α-synuclein. Bar = 400 µm.

To analyze whether α-synuclein prionoids injected into the tongue muscle seeded aggregation of phosphorylated α-synuclein out of the injection site, tongues were dissected at 420 dpi and stained with the phosphorylation specific antibody pSyn#64. Animals injected with α-synuclein fibrils or PBS did not accumulate any deposits of phosphorylated α-synuclein throughout the entire tongue muscle. All types of tissues including the epithelial layers, the skeletal muscles, the surrounding epithelium of blood vessels, and the nerve bundles were free of pathology (Fig. 3.14).

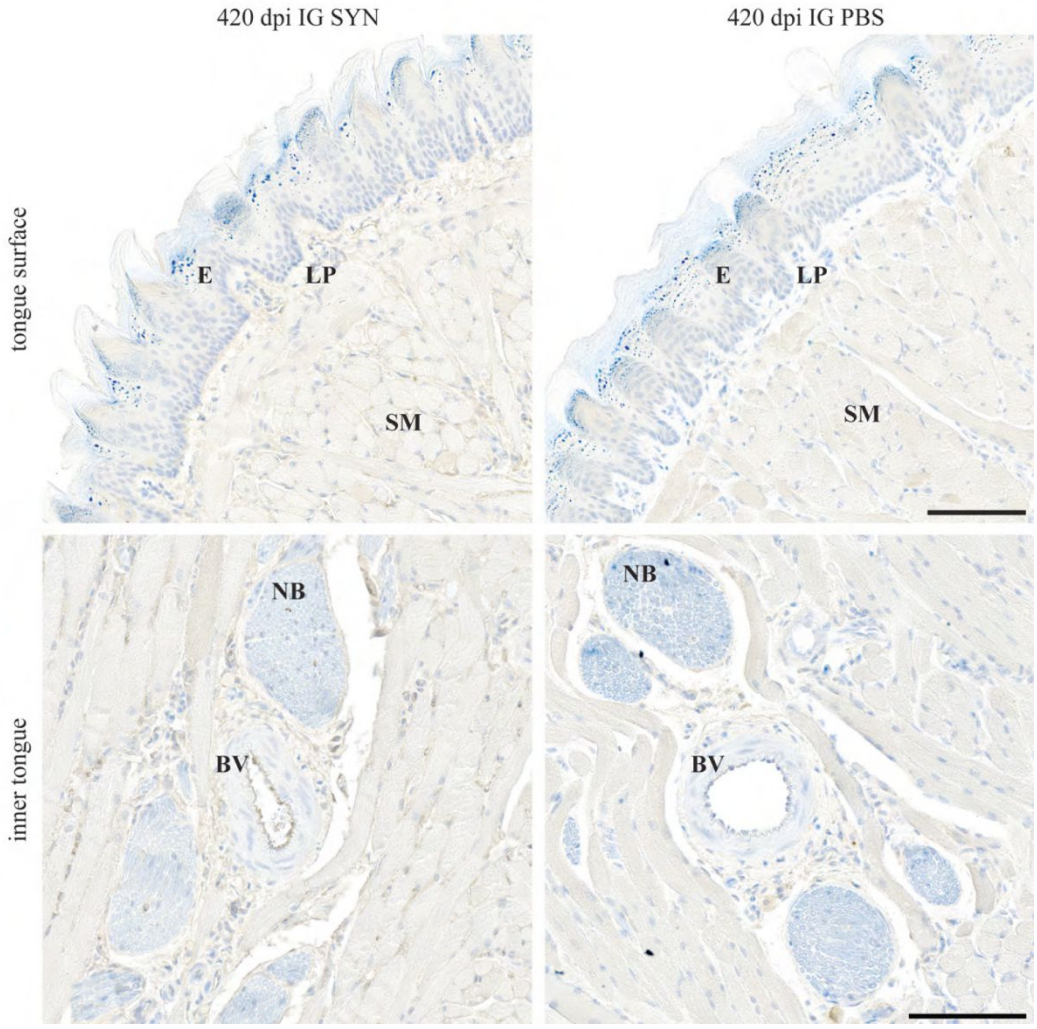

Fig. 3.14 Tg(M83$^{+/-}$:*Gfap*-luc$^{+/-}$) mice intraglossally injected with α-synuclein fibrils did not show any signs of α-synuclein pathology in their tongues. For the immunohistochemical analysis the tongues of mice intraglossally injected with α-synuclein fibrils or PBS were collected at 420 dpi and stained with the phosphorylation-specific pSyn#64 antibody. None of the injected animals had accumulated any phosphorylated deposits of α-synuclein in the tongue as illustrated for the epithelium (E), lamina propria (LP), skeletal muscles (SM), fibers of nerve bundles (NB) or surrounding tissue of blood vessels (BV). Bar = 100 µm

3.2.3 Severe neurologic illness in intraperitoneally injected mice

Further characterization of the intraperitoneally injected Tg(M83$^{+/-}$:*Gfap*-luc$^{+/-}$) mice revealed that in comparison to PBS-injected healthy controls, fibril-injected animals strikingly lost bodyweight beginning six-to-eight weeks before they developed signs of neurologic disease (Fig. 3.15 A,B). In contrast, animals that did not develop disease, continuously gained weight over the entire 420 d observation period. To detect disease-associated α-synuclein species, sarcosyl-insoluble protein fractions from brains and spinal cords of all mice were biochemically analyzed. Similar to the animal (mouse 121) diseased after intraglossal injection, the intraperitoneally injected and diseased mice also accumulated sarcosyl-insoluble aggregates of phosphorylated α-synuclein in their brains and spinal cords (Fig. 3.15 C).. By probing the immunoblots with the phosphorylation specific antibody EP1536Y, aggregated and phosphorylated species of α-synuclein were detected as additional bands above the molecular weight of monomeric α-synuclein with 14 kDa.

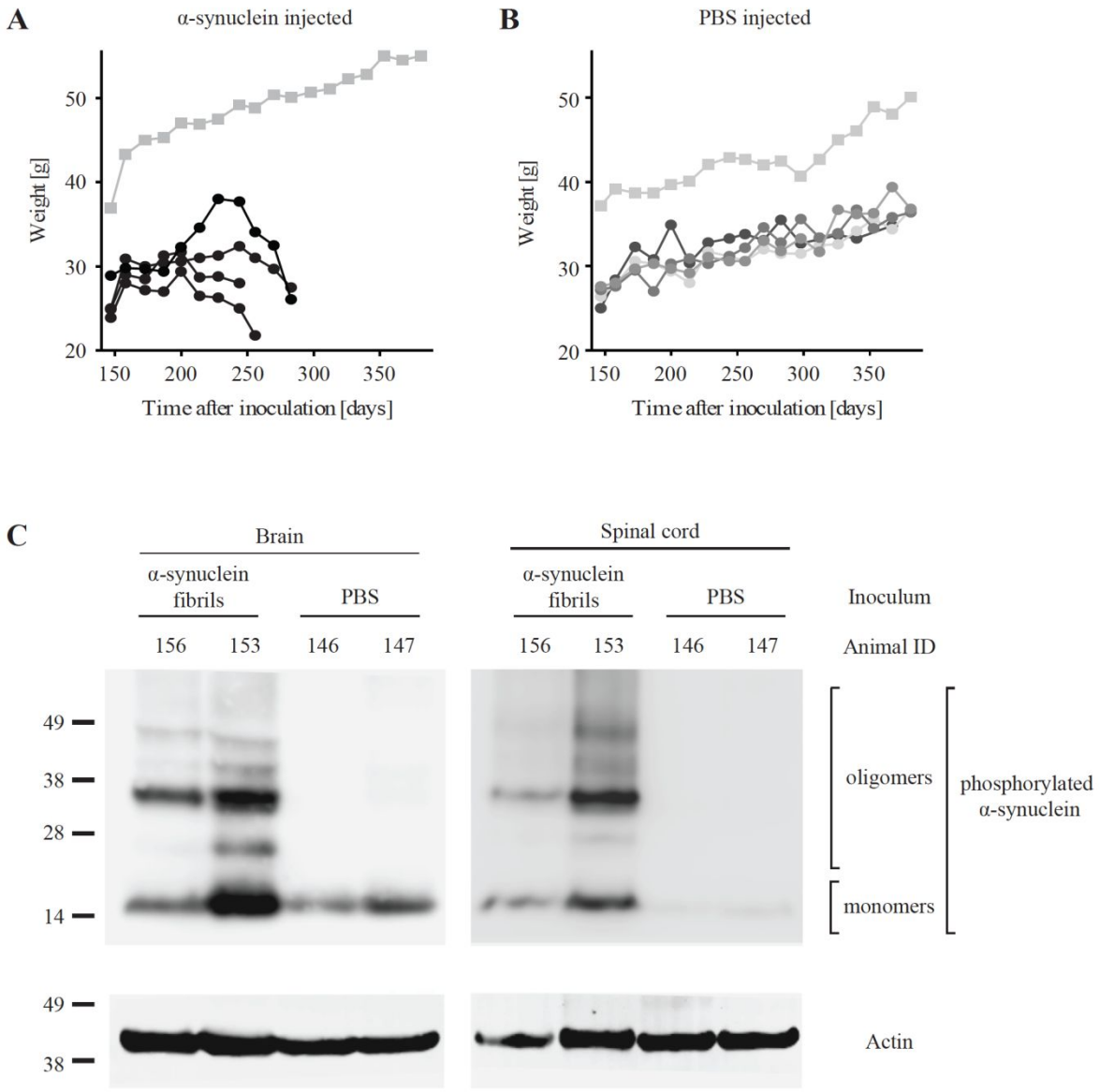

Fig. 3.15 Intraperitoneally with α-synuclein fibrils injected and diseased Tg(M83$^{+/-}$:*Gfap*-luc$^{+/-}$) mice showed a severe loss of weight and accumulated phosphorylated α-synuclein in their CNS. A) Animals that received an intraperitoneal injection of α-synuclein fibrils and developed neurological illness first began to lose weight 6-8 weeks before they developed signs of neurologic disease (black circles). The one animal that did not get sick gained weight throughout the entire observation period as also shown for B) PBS-injected animals (grey shaded symbols). Circles represent female mice and squares represent male mice. C) Sick fibril-injected mice had accumulated high-molecular weight species of sarcosyl-insoluble phosphorylated α-synuclein in their brains and spinal cords when probed with the EP1536Y antibody. PBS injected control animals exhibited monomeric α-synuclein only in extracts from their brains, but not spinal cord. Molecular weight is shown in kilodalton. Equal sample loading in each lane was verified by detection of actin.

3.2.3.1 Distribution of neuropathology in the brains and spinal cords of diseased mice

To define the neuroanatomical distribution of neuropathological lesions in brains and spinal cords of diseased Tg(M83$^{+/-}$:*Gfap*-luc$^{+/-}$) mice, immunohistochemical staining with two different antibodies against phosphorylated α-synuclein, pSyn#64 and pSyn81A were performed. In the brains of the diseased animals abundant deposits of phosphorylated α-synuclein were found in neuronal cell bodies or their processes, whereas the brains of PBS-injected control mice were free of pathology (Fig. 3.16). Both the antibodies marking phosphorylated α-synuclein revealed a similar distribution pattern of pathology. In diseased animals deposits of phosphorylated α-synuclein were widespread throughout the cerebrum but absent in the cerebellum and the rostral lying areas of the olfactory bulb. The highest abundance of neuronal inclusions was detected in the hypothalamus, amygdala and brainstem as summarized in the pathology distribution map (Fig. 3.17). Equally, the fibril-injected animal, that did not develop neurologic disease until 420 dpi, was free of pathological deposits in its brain (data not shown).

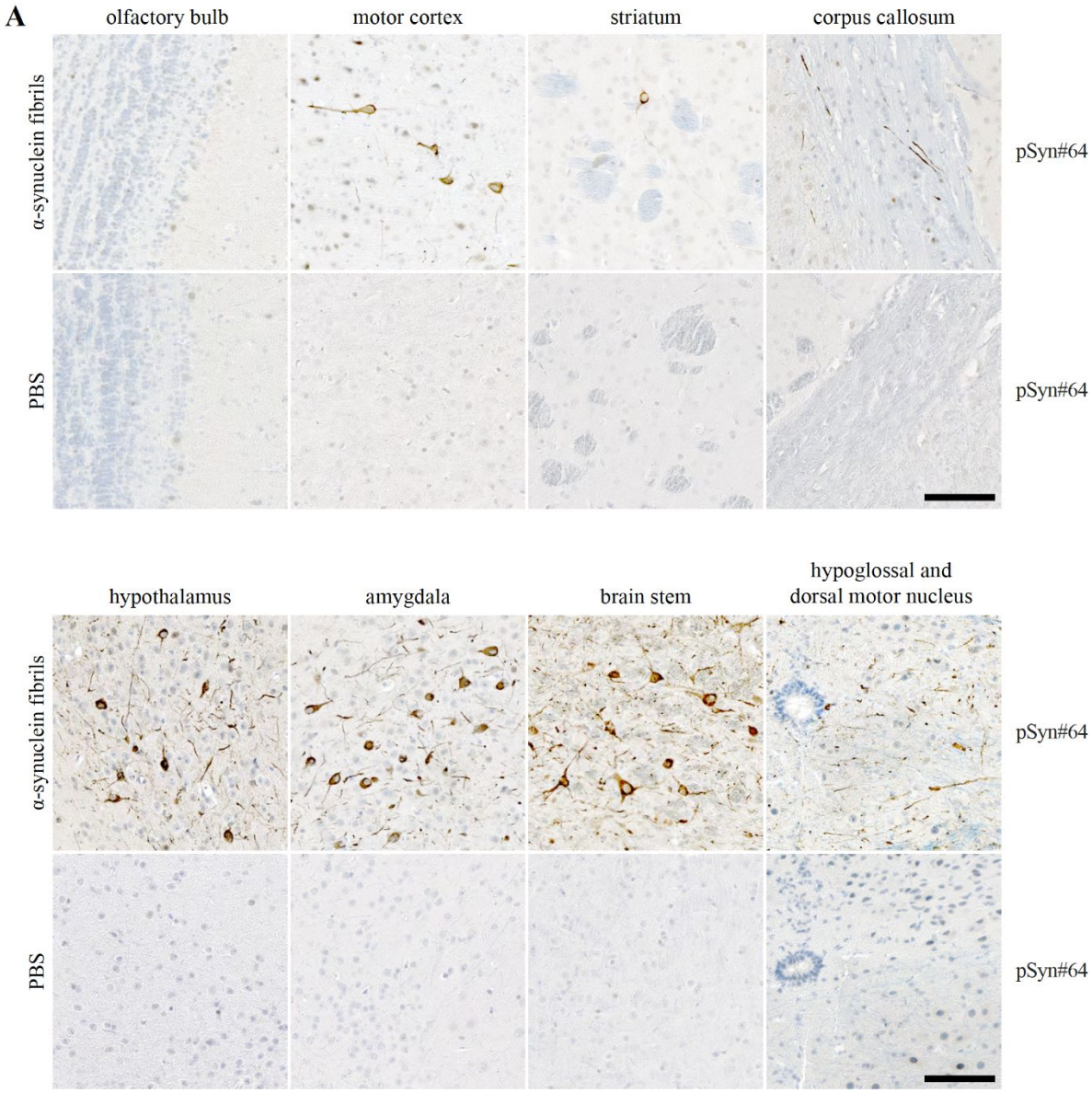
A
olfactory bulb
motor cortex
striatum
corpus callosum
α-synuclein fibrils
PBS
pSyn#64
pSyn#64
hypothalamus
amygdala
brain stem
hypoglossal and
dorsal motor nucleus
α-synuclein fibrils
PBS
pSyn#64
pSyn#64

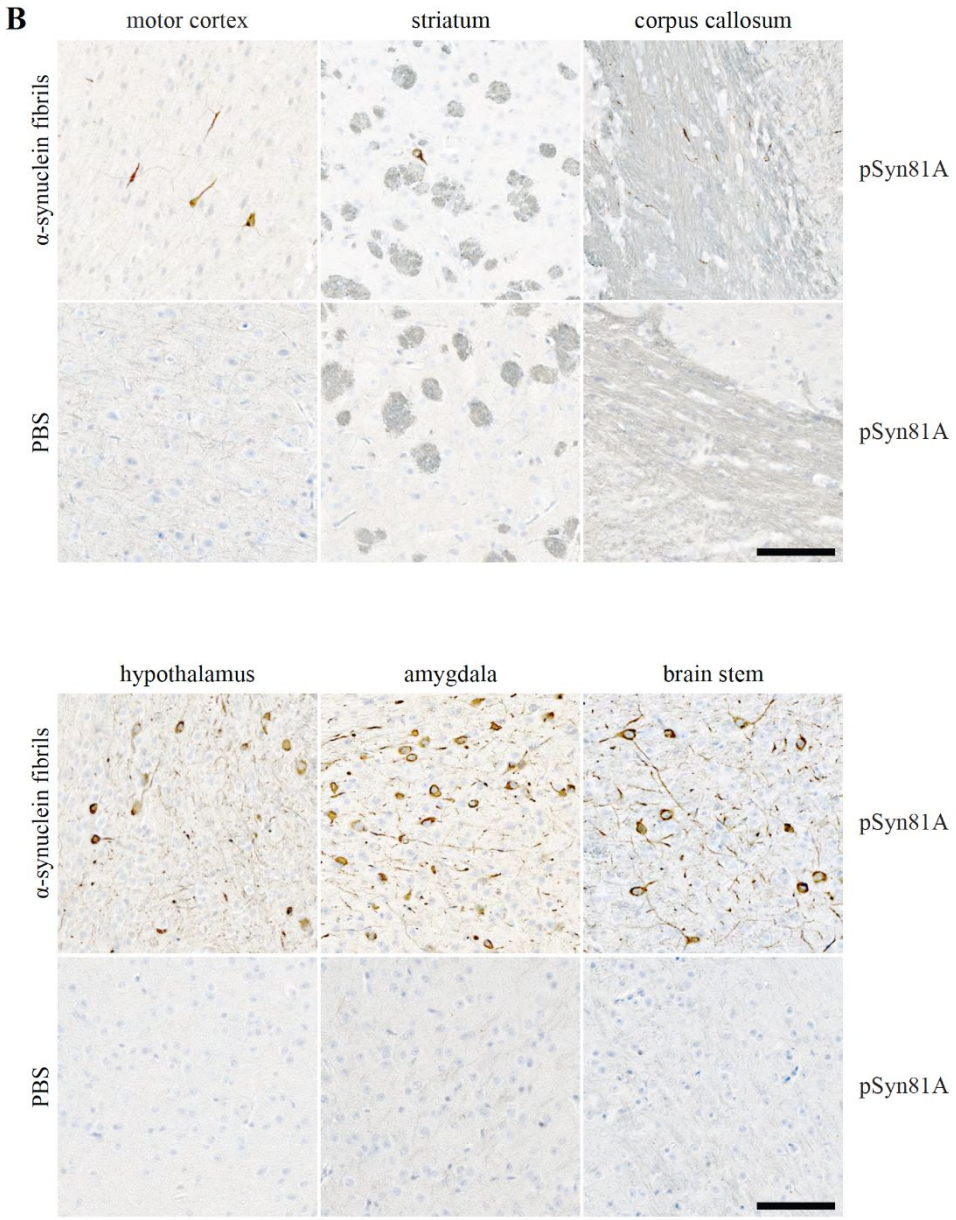

Fig. 3.16 Tg(M83$^{+/-}$:*Gfap*-luc$^{+/-}$) mice developed severe neuropathology in their brains after intraperitoneal injection with α-synuclein prionoids. A) Once the animals developed clinical signs of disease or at 420 dpi their brains were analyzed immunohistochemically. Brain sections were immunostained with the (A) pSyn#64 and (B) 81A antibody recognizing phosphorylation at serine 129 of α-synuclein. Diseased animals accumulated abundant deposits of phosphorylated α-synuclein throughout their brains including the motor cortex, striatum, corpus callosum, hypothalamus, amygdala, and brain stem with the hypoglossal and dorsal motor nuclei. The olfactory bulb was free of α-synuclein pathology. Deposits of phosphorylated α-synuclein were abundant in neuronal cell bodies and their neurites. The PBS-injected mice did not display any CNS pathology. Bar = 50 µm.

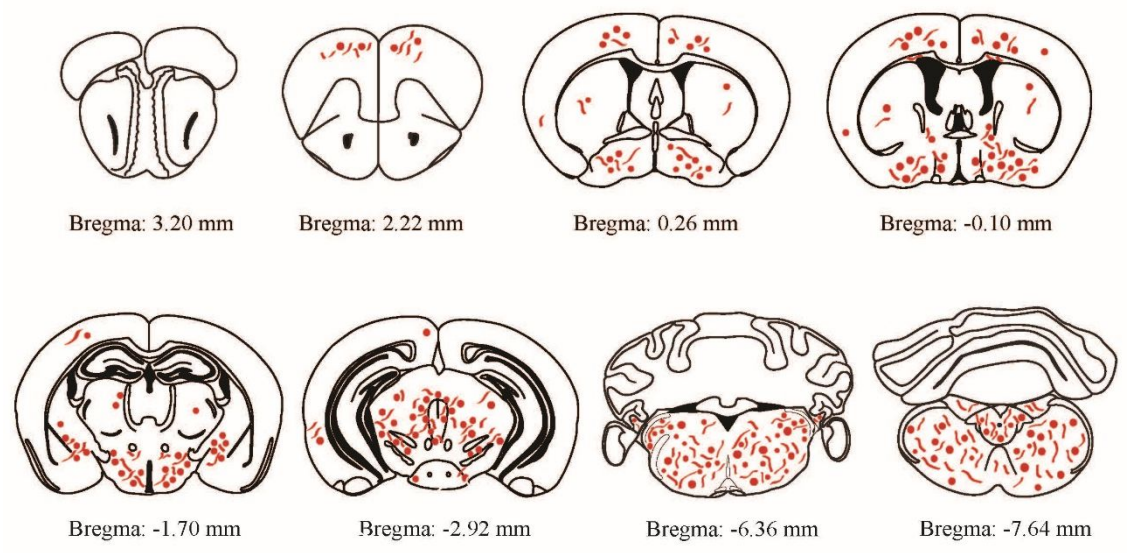

Fig. 3.17 Distribution of misfolded and phosphorylated α-synuclein in the brains of diseased Tg(M83$^{+/-}$:*Gfap*-luc$^{+/-}$) mice. The schematic view depicts the distribution of α-synuclein deposits as detected by two antibodies, pSyn#64 and pSyn81A. Abundant deposits of phosphorylated α-synuclein were found throughout the cerebrum except the olfactory bulb and the cerebellum that remained free of pathology. Deposits of phosphorylated α-synuclein were present within neuronal cell bodies (red circles) and neurites (red rods). The position of each coronal brain section is stated relative to the bregma (Franklin and Paxinos, 2008).

Immunostaining of spinal cord sections revealed that neuronal deposits of phosphorylated α-synuclein were widely and consistently distributed in the gray matter of its cervical, thoracic and lumbar segments (Fig. 3.18 A,B). The use of antibodies that are specific for mouse or human α-synuclein (Appendix 5.1) showed that deposits of aggregated α-synuclein in the CNS of diseased animals did not only consist of transgenically expressed mutant human α-synuclein as detected with the Syn 211 antibody, but also of endogenously expressed mouse α-synuclein as detected with the D37A6 antibody. In contrast, α-synuclein deposits were not found in the spinal cord of PBS-injected control mice (Fig. 3.18 A).

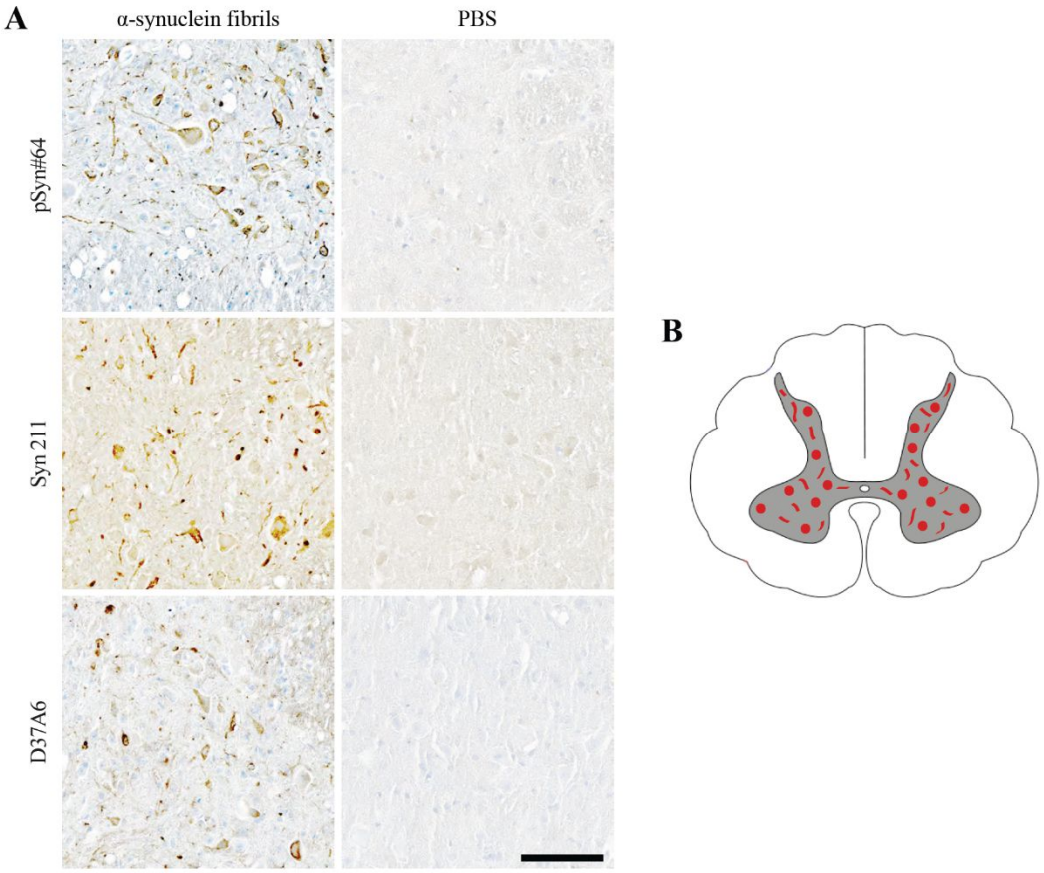

Fig. 3.18 The Tg(M83$^{+/-}$:*Gfap*-luc$^{+/-}$) mice developed neurophathology in their spinal cords after intraperitoneal injection with α-synuclein fibrils. A) Immunohistochemical staining of spinal cord sections with the pSyn64# antibody displayed abundance of phosphorylated α-synuclein within the gray matter. The antibodies Syn211 and D37A6 specifically recognize human or mouse α-synuclein and revealed that both proteins were abundant in deposits within the gray matter. Bar = 50 µm. B) The schematic coronal view through the spinal cord depicts that α-synuclein deposits were restricted to the gray matter. Phosphorylated α-synuclein deposits were located in cell bodies (red circle) and within neurites (red rods). A similar pathology distribution was observed throughout the entire spinal cord including cervical, thoracic and lumbar segments.

To specify which type of neuron in the spinal cord was affected by deposition of α-synuclein, additional immunofluorescence analyses for cholinergic motor neurons that innervate extrafusal muscle fibers, and phosphorylated α-synuclein were performed. Co-staining with antibodies to phosphorylated α-synuclein and cholinergic acetyltransferase (ChAT) revealed that deposits of misfolded α-synuclein clearly localized to cholinergic motor neurons in the ventral horn of diseased animals. Whereas, α-synuclein pathology was not detectable in PBS-injected control mice (Fig. 3.19).

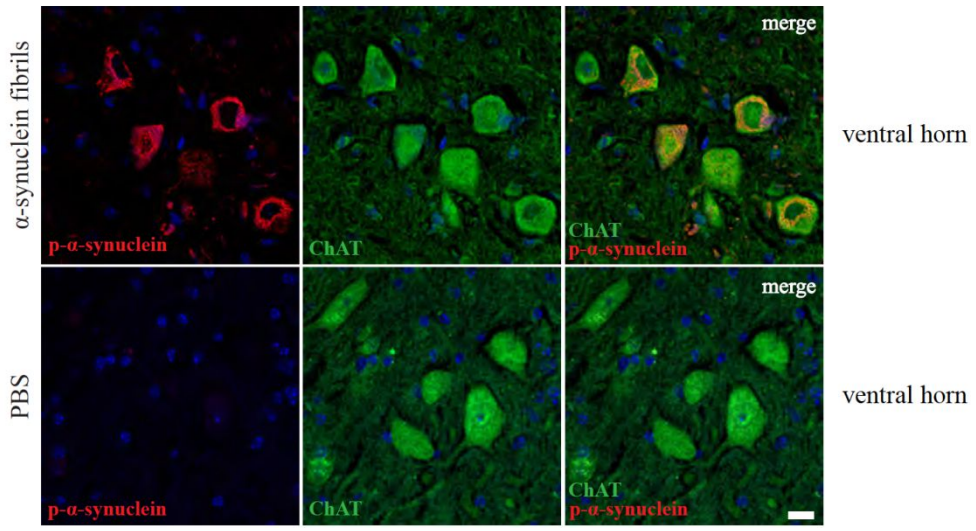

Fig. 3.19 Deposits of phosphorylated α-synuclein were present in motorneurons of diseased Tg(M83$^{+/-}$:*Gfap*-luc$^{+/-}$) mice. Immunofluorescence analysis with the pSyn64# antibody against phosphorylated α-synuclein and an antibody against choline acetyltransferase (ChAT) revealed deposits of phosphorylated α-synuclein within cholinergic neurons in the spinal cord of diseased animals. Healthy control animals were free of pathology. Nuclear staining with DAPI is shown in blue. Bar = 20 µm.

3.2.3.2 Deposits of phosphorylated α-synuclein colocalized with ubiquitin and p62

For further characterization of α-synuclein positive deposits in the CNS of diseased mice, brain and spinal cord sections were immunofluorescently labeled with antibodies against phosphorylated α-synuclein and ubiquitin. Phosphorylated α-synuclein was found to colocalize with ubiquitin in the brains and spinal cords of diseased animals indicating a dysregulated protein degradation and homeostasis (Fig. 3.20 A,B). Similarly, phosphorylated α-synuclein also colocalized with the ubiquitin-binding protein p62 (sequestosme-1) in brain and spinal cord sections of diseased animals (Fig. 3.20 C,D). In contrast, stained brain and spinal cord sections of PBS-injected healthy control mice did not reveal aggregates or colocalization for any of these proteins (Fig. 3.20 A-D).

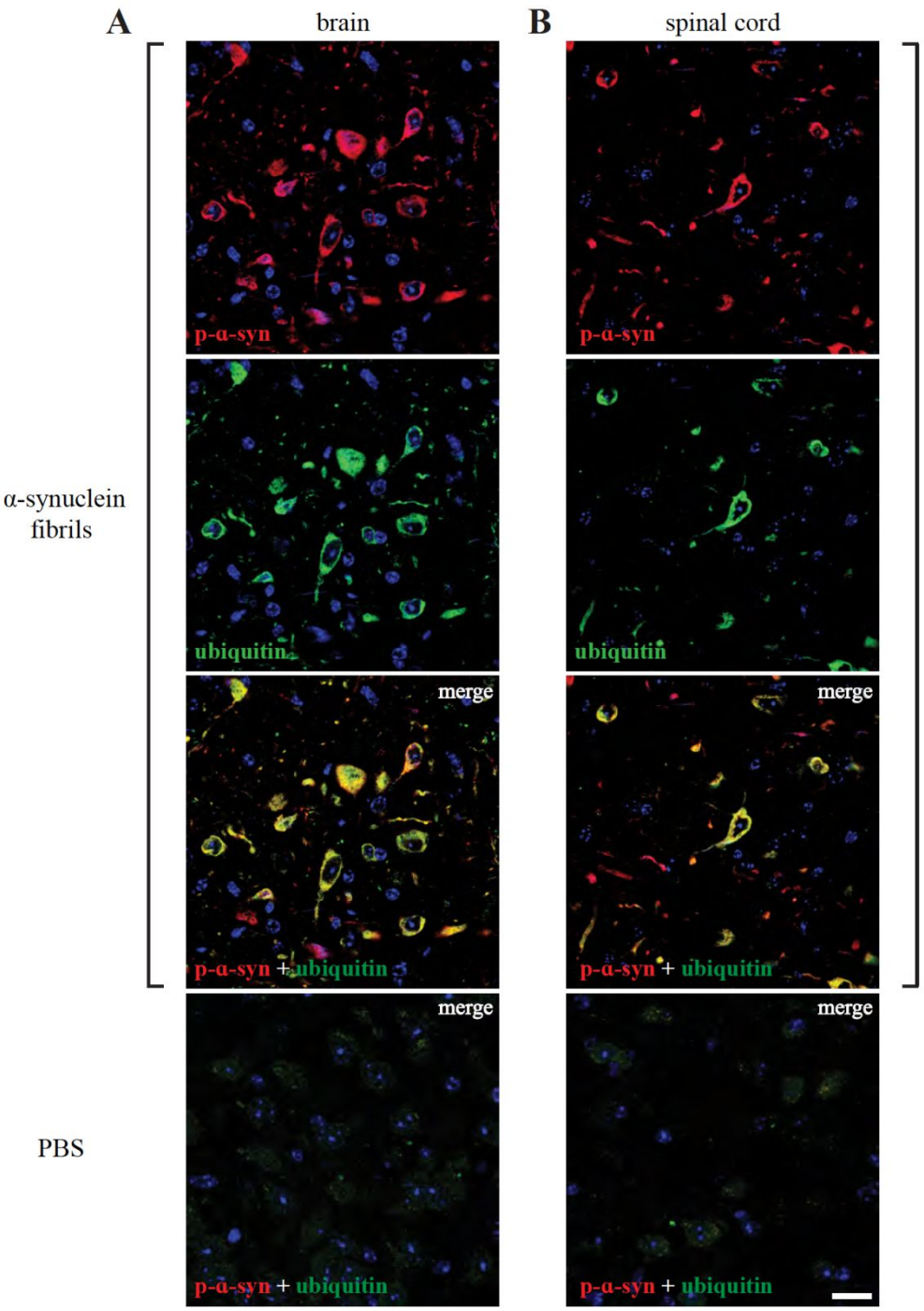
A
brain
B
spinal cord
α-synuclein fibrils
PBS
p-α-syn
ubiquitin
merge
p-α-syn + ubiquitin

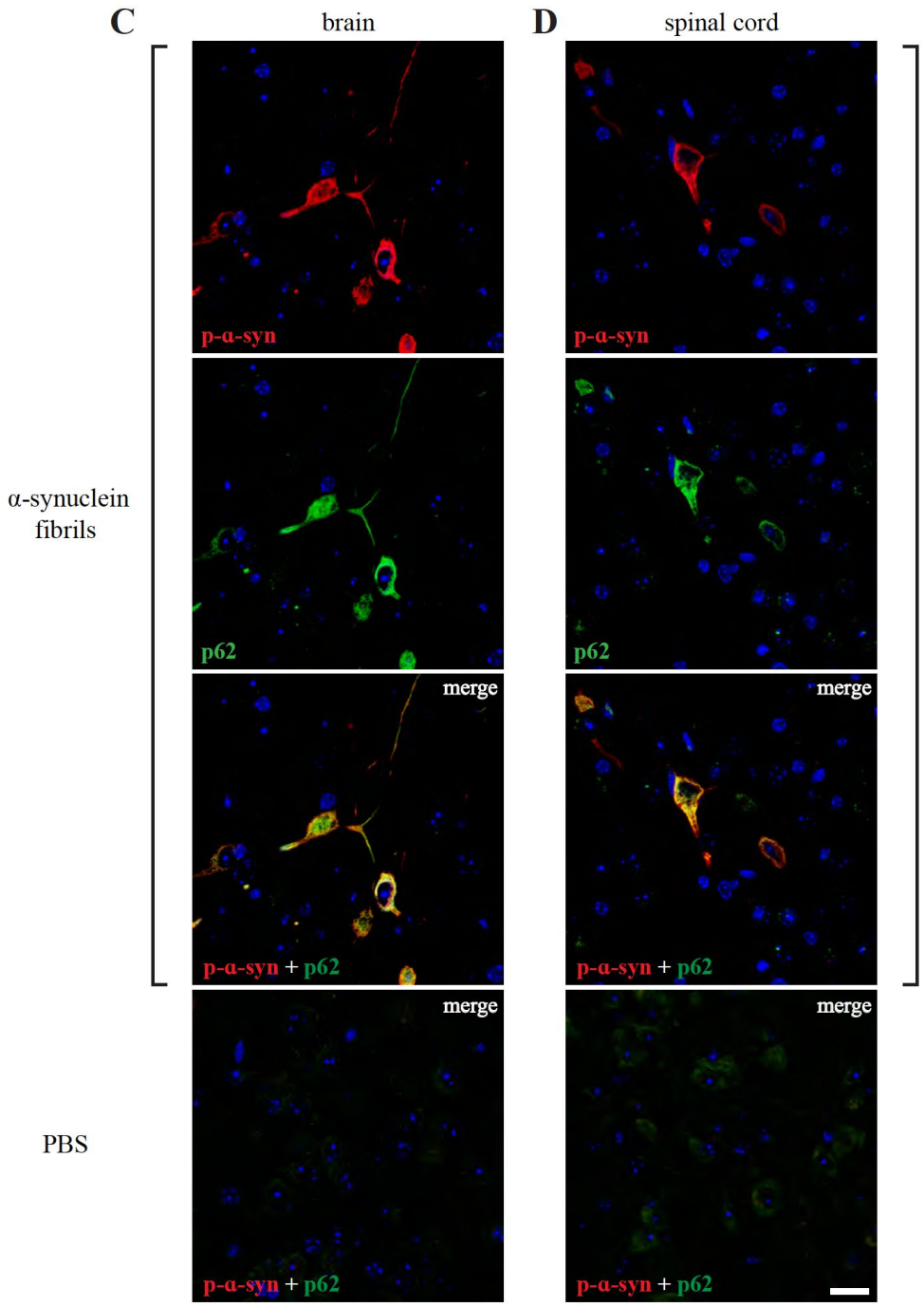

Fig. 3.20 Colocalization of misfolded and phosphorylated α-synuclein with ubiquitin and p62 in diseased Tg(M83$^{+/-}$:*Gfap*-luc$^{+/-}$) mice. Immunofluorescence staining for phosphorylated α-synuclein with the EP1536Y antibody and an antibody against ubiquitin revealed colocalization of both proteins in deposits in the (A) brain and (B) spinal cord of diseased mice. In contrast, the brain and spinal cord of PBS-injected animals did not display any deposits or colocalization of these proteins as shown in a merged view. In addition, when (C) brain and (D) spinal cord sections were stained for phosphorylated α-synuclein with the pSyn64# antibody and an antibody against p62 (sequestosme-1) an unambiguous colocalization was detectable. PBS-injected control animals did not show aggregation or colocalization for any of these proteins in brain or spinal cord, as indicated in the merged image. Nuclear staining with DAPI is shown in blue. Bar = 20 µm.

3.2.3.3 Phosphorylated α-synuclein colocalized with dopaminergic neurons in the substantia nigra

Since loss or dysfunction of dopaminergic neurons may be causative for an impaired locomotor activity (Masliah et al., 2000), it was examined whether deposits of phosphorylated α-synuclein are formed in dopaminergic neurons within the substantia nigra of diseased mice. Therefore, co-immunofluorescence stainings with antibodies detecting tyrosine hydroxylase (TH) that is expressed in dopaminergic neurons and phosphorylated α-synuclein were perfomed. The deposits of phosphorylated α-synuclein clearly colocalized with TH-positive neurons of the substantia nigra (Fig. 3.21).

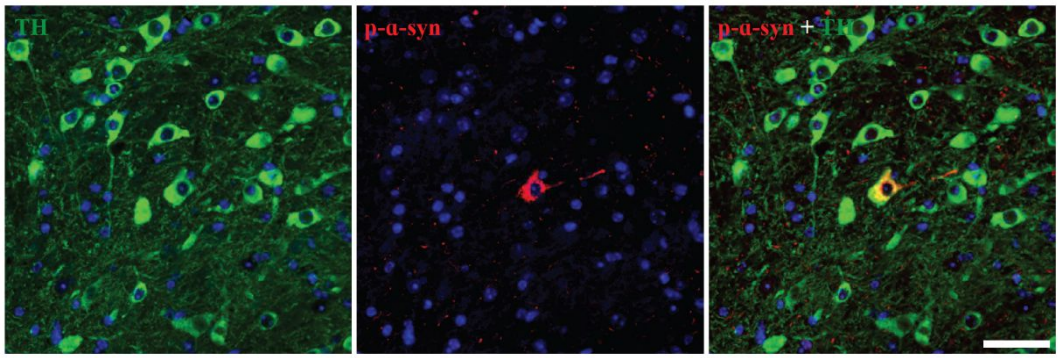

Fig. 3.21 Diseased Tg(M83$^{+/-}$:*Gfap*-luc$^{+/-}$) mice accumulated α-synuclein deposits in their substantia nigra. Immunofluorescence staining with the pSyn#64 antibody against phosphorylated α-synuclein and an antibody against tyrosine hydroxylase (TH) showed clear localization of phosphorylated α-synuclein deposits in dopaminergic neurons. Nuclear staining with DAPI is shown in blue. Bar = 50 µm.

3.2.4 Reactive astrogliosis and microgliosis in diseased animals

Because neurodegenerative diseases are often associated with neuroinflammation characterized by activated microglia and astrocytes, the brains of intraperitoneally and intraglossally injected Tg(M83$^{+/-}$:*Gfap*-luc$^{+/-}$) mice were monitored for these neuroinflammatory markers. Immunofluorescence staining with an antibody to GFAP visualizes astrocytes and an antibody to phosphorylated α-synuclein revealed reactive astrocytic gliosis in regions with phosphorylated α-synuclein deposits (Fig. 3.22 A). Abundance of activated astrocytes was found in the brainstem as shown here for the gigantocellular reticular nucleus. In contrast, stained tissue sections of healthy PBS-injected control mice did not present any α-synuclein deposits or activated astrocytes. Furthermore, to determine if microglia are also activated, the brain sections were stained for IBA-1. The sections derived from the brainstem of diseased Tg(M83$^{+/-}$:*Gfap*-luc$^{+/-}$)

mice showed abundant activated microglia in the presence of deposits of phosphorylated α-synuclein. Whereas in the brains of PBS-injected control mice, IBA-1 positive cells were less abundant and still showed a more ramified morphology indicative of an absence of microgliosis (Fig. 3.22 A).

As a second non-invasive measure to monitor astrocytic gliosis, BL emitted from the brains of injected Tg(M83$^{+/-}$:*Gfap*-luc$^{+/-}$) reporter mice was regularly measured throughout the course of the experiment. The intraperitoneally with α-synuclein fibrils injected and diseased mice displayed increased radiance (>2 x 10^6 photons/s/cm^2/sr) emitted from their brains shortly before they developed signs of neurologic disease with a mean incubation time of 229 ± 17 days (Fig. 3.22 B). As shown in the left photograph, intraperitoneal injection with α-synuclein fibrils not only induced an increase in BL in the brain but also in the spinal cord of diseased animals (Fig. 3.22 C, left image). Animals that did not develop disease did not show BL above the threshold of 2 x 10^6 photons/s/cm^2/sr. Elevated BL indicative for reactive astrogliosis was also measured for animal 121 two weeks before it died at 285 dpi after intraglossal injection with α-synuclein prionoids (Fig. 3.22 B,C, center image). Thus, aggregation of phosphorylated α-synuclein in diseased Tg(M83$^{+/-}$:*Gfap*-luc$^{+/-}$) mice was accompanied by neuroinflammation consisting of reactive gliosis and microgliosis.

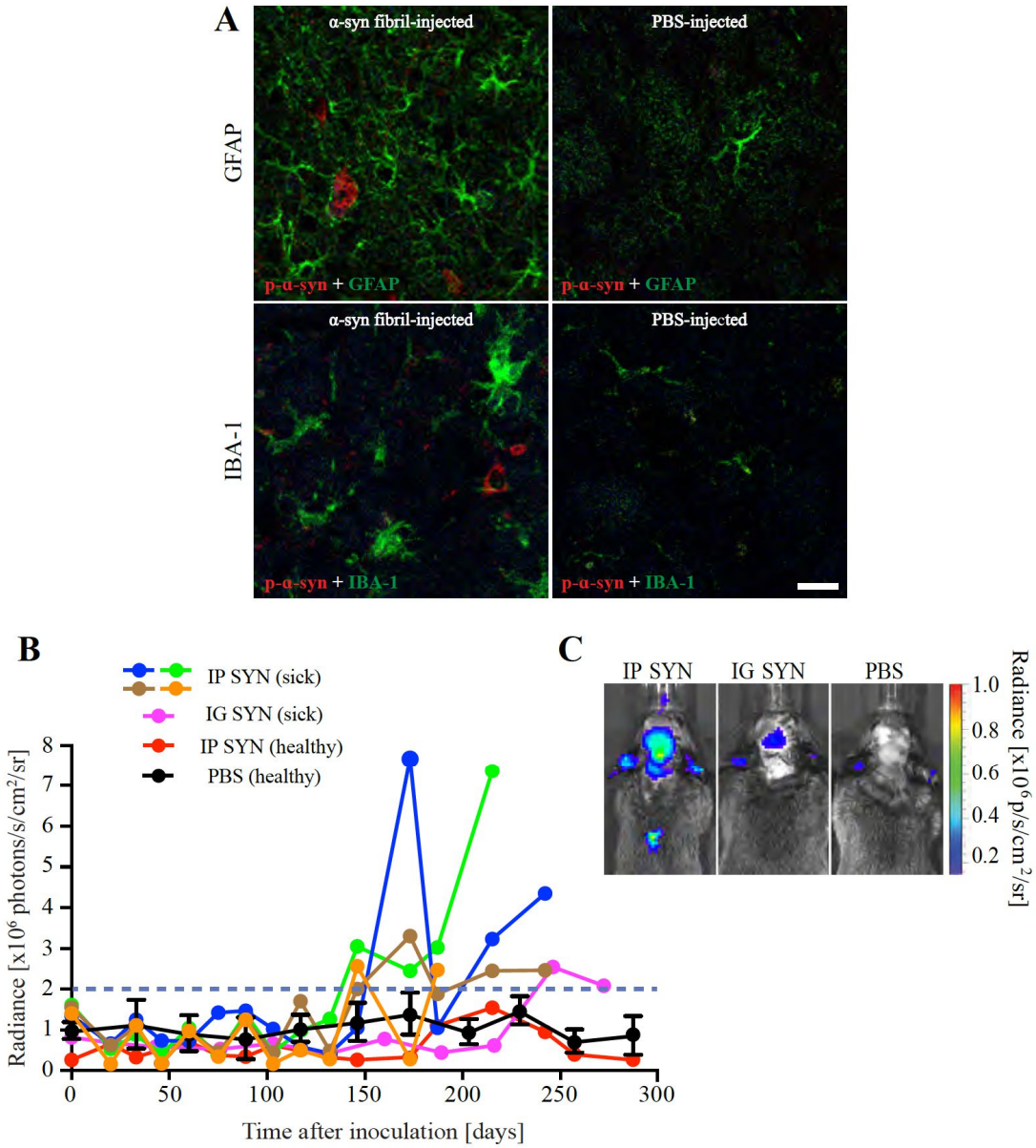

Fig. 3.22 Fibril-injected Tg(M83$^{+/-}$:*Gfap*-luc$^{+/-}$) mice developed neuroinflammation shortly before signs of neurologic illness appeared. A) Immunofluorescence staining with an antibody against GFAP and an antibody to phosphorylated α-synuclein revealed that diseased mice had accumulated reactive astrocytes in regions with deposits of α-synuclein. Healthy animals did not show signs of astrogliosis. Staining with an antibody to the microglial marker IBA-1 and an antibody for phosphorylated α-synuclein displayed microgliosis near deposits of phosphorylated α-synuclein. In healthy animals deposits of α-synuclein and IBA-1 positive cells were less abundant. Bar = 20 µm. B) After intraperitoneal challenge of Tg(M83$^{+/-}$:*Gfap*-luc$^{+/-}$) mice with α-synuclein fibrils, elevated levels of BL with >2 x 10^6 photons/s/cm^2/sr were measured from the brains of four mice (blue, green, brown, and orange circles) a few weeks before they developed neurologic symptoms. One animal never showed elevated BL and did not develop disease (red circles). One of five mice intraglossally injected with α-synuclein fibrils showed increased BL levels shortly before it died (magenta circles). PBS-injected control animals never exhibited elevated BL that exceed the threshold of 2 x 10^6 photons/s/cm^2/sr (black circles). Error bars show SD (n=4). C) Intraperitoneally fibril-injected Tg(M83$^{+/-}$:*Gfap*-luc$^{+/-}$) mice emitted elevated BL from their brains and spinal cords. After intraglossal injection with α-synuclein fibrils, only animal 121 developed signs of reactive gliosis. Control animals injected with PBS did not emit elevated BL from their brains.

3.3 Aerosols made of MSA brain homogenate did not induce neuropathology

To elucidate whether disease-associated species of α-synuclein have the propensity to pass the olfactory epithelium and to induce neurodegeneration similar to prions, Tg(M83$^{+/-}$:*Gfap*-luc$^{+/-}$) reporter mice were nasally exposed to aerosolized α-synuclein particles originating from MSA brain homogenate (Appendix Fig. 5.1 D). Biochemical analysis of the MSA brain homogenate revealed that it contained detergent-insoluble, phosphorylated α-synuclein species of high-molecular weight exceeding that of monomeric α-synuclein (Fig. 3.23).

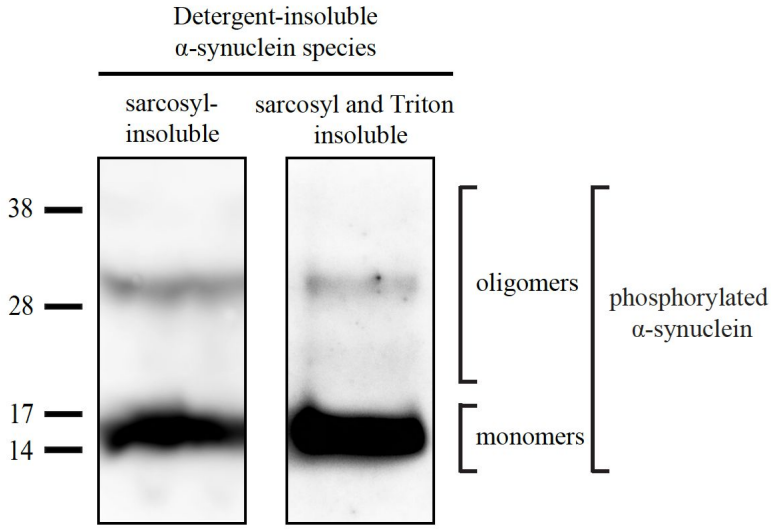

Fig. 3.23 MSA brain homogenate with detergent-insoluble α-synuclein species. Sarcosyl or Triton X-100 insoluble protein fractions were extracted from the MSA brain homogenate and analyzed by probing the immunoblot with the EP1536Y antibody. Both extraction protocols revealed the presence of monomeric and oligomeric species of phosphorylated α-synuclein in the MSA brain homogenate. Molecular weight is shown in kilodalton.

The infection dynamics of Tg(M83$^{+/-}$:*Gfap*-luc$^{+/-}$) mice nasally exposed to aerosols made from 1 %, 5 %, 10 %, 20 % (w/v) MSA brain homogenate in PBS and the control group are shown in Table 2.4.

Table 2.4 Aerosol transmission experiments in Tg(M83$^{+/-}$:*Gfap*-luc$^{+/-}$) mice

Mouse line	Inoculum (amount)	Inoculation route	No. of sick mice/ no. of challenged mice	Survival time [dpi]
Tg(M83$^{+/-}$:*Gfap*-luc$^{+/-}$)	PBS	inhalation	0/ 5	600
Tg(M83$^{+/-}$:*Gfap*-luc$^{+/-}$)	1 % MSA brain homogenate	inhalation	0/ 5	600
Tg(M83$^{+/-}$:*Gfap*-luc$^{+/-}$)	5 % MSA brain homogenate	inhalation	0/ 5	600
Tg(M83$^{+/-}$:*Gfap*-luc$^{+/-}$)	10 % MSA brain homogenate	inhalation	0/ 10	600
Tg(M83$^{+/-}$:*Gfap*-luc$^{+/-}$)	20 % MSA brain homogenate	inhalation	0/ 5	600

Animals were monitored for up to 600 dpi without developing any signs of neurologic illness. Throughout the entire experimental course all animals were also assessed for neuroinflammatory changes by measuring the BL emitted from their brains. Neither animals exposed to MSA nor to PBS showed notable changes in BL during the observation course of 600 d. Thus, indicating that these animals did not develop any signs of astrocytic gliosis following exposure to aerosols (Fig. 3.24).

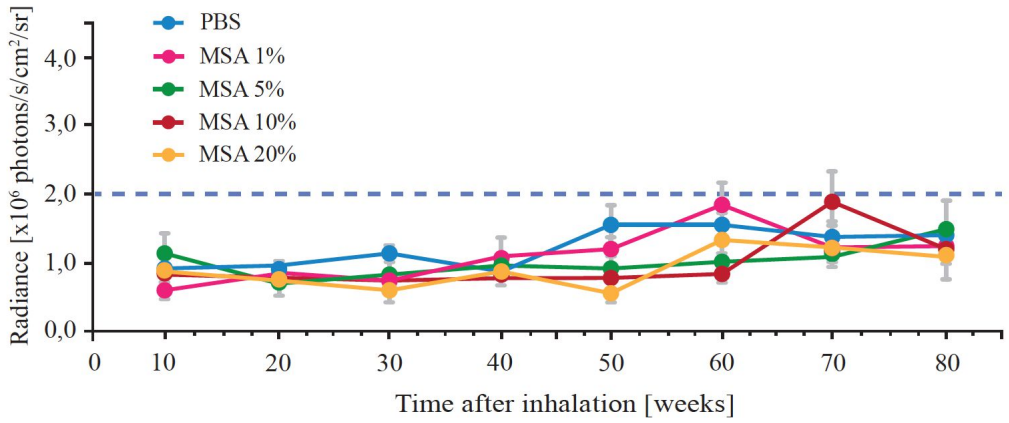

Fig. 3.24 Tg(M83$^{+/-}$:*Gfap*-luc$^{+/-}$) challenged with aerosols of MSA brain homogenate did not show signs of astrocytic glisis. BL measured from the brains of Tg(M83$^{+/-}$:*Gfap*-luc$^{+/-}$) reporter animals exposed to aerosolized brain homogenates of 20 % (yellow circles), 10 % (red circles), 5 % (green circles), and 1 % (pink circles) was not elevated when compared to control animals (PBS, blue circles). The radiance was measured in photons/s/cm^2/sr. Error bars show SEM [20 % MSA: n=5; 10 % MSA: n=10; 5 % MSA: n=5; 1 % MSA: n=5; PBS: n=5].

Immunohistochemical analysis of brains and spinal cords of all treatment groups (PBS, 1 % MSA, 5 % MSA, 10 % MSA, and 20 % MSA) harvested at 600 dpi did not reveal accumulation of disease-associated α-synuclein species. Staining for phosphorylated α-synuclein with the pSyn#64 antibody was negative throughout the entire cerebrum, including the striatum, amygdala, hippocampus, and brain stem. In particular, the olfactory bulb, which is directly connected to the olfactory epithelium, was free of pathology (Fig. 3.25).

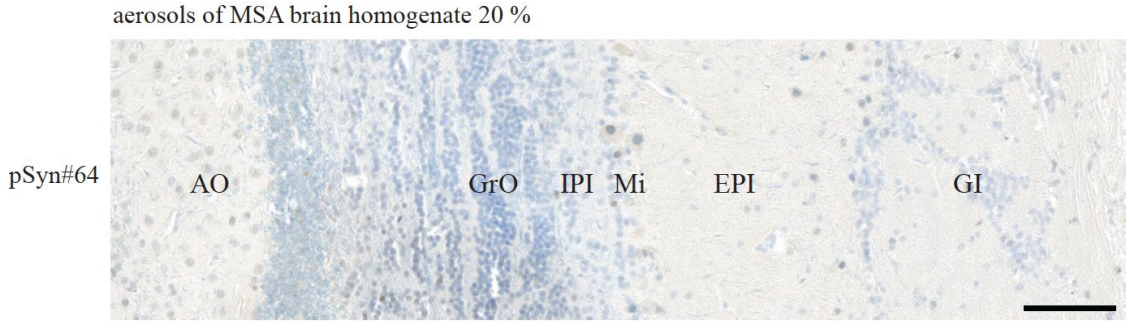

Fig. 3.25 Exposure of Tg(M83$^{+/-}$:*Gfap*-luc$^{+/-}$) mice to aerosols containing pathological α-synuclein did not induce neuropathology in the olfactory bulb. Immunohistochemical analysis with the pSyn64# antibody of brains of animals exposed with 20 % MSA brain homogenate did not show any deposition of phosphorylated α-synuclein at 600 dpi. AO: anterior olfactory area, GrO: granule cell layer, IPI: internal plexifrom layer, Mi: mitral cell layer, EPI: external plexiform layer. Bar = 100 µm.

4 Discussion

4.1 Virulence of α-synuclein prionoids inoculated into Tg(*Gfap*-luc$^{+/-}$) mice

4.1.1 Intracerebral injection of α-synuclein prionoids induced mild α-synuclein pathology

It has been previously shown that an intracerebral injection either with recombinant α-synuclein or patient derived pathogenic α-synuclein species causes prion-like spreading and formation of α-synuclein deposits in the CNS of wild-type mice (Luk et al., 2012a; Masuda-Suzukake et al., 2013; Recasens et al., 2014; Sacino et al., 2013a). Luk et al. (2012a) observed phosphorylated α-synuclein in inclusions to a high extend already at 30 dpi. They reported a time-dependent spreading of α-synuclein inclusions from the striatum to more distal interconnected brain regions such as the amygdala and the olfactory bulb in both hemispheres. In this work intrastriatal injection of mouse α-synuclein fibrils only caused a mild neuropathology in the cortex of Tg(*Gfap*-luc$^{+/-}$) mice after a long incubation time of 400 d (3.1.1). Injection of α-synuclein fibrils into the striatum did not result in deposition of phosphorylated α-synuclein around the injection site at none of the examined time points for up to 400 d. Opposite to previous findings (Luk et al., 2012a) and probably due to the mild α-synuclein pathology, the animals inoculated in this study did not display any behavioral deficits in the wire hang or rotarod-performance test. Thus, their motor neurons innervating skeletal muscles remained unaffected.

Considering that the genetic background of Tg(*Gfap*-luc$^{+/-}$) mice is essentially wild-type as far as α-synuclein is concerned, these mice are comparable to the non-transgenic animals used in previous studies. However, the degree of neuropathology and its spatio-temporal spreading greatly differs between individual studies (Masuda-Suzukake et al., 2013; Sacino et al., 2013b; Sacino et al., 2014b). Different experimental outcomes in different studies may be explained by differing experimental conditions affecting the infectivity of α-synuclein fibrils, and important factors include: a) inoculum preparation, b) amount of inoculum, and c) injection site (Uchihara and Giasson, 2016). Some practical aspects of the mentioned factors are discussed in the following paragraphs.

a) Inoculum preparation: Buffer composition, shaking and sonication settings might affect the assembly of monomeric α-synuclein into fibrils (see 2.2.2 and 2.2.3). The conditions for fibril assembly often differ between studies (Luk et al., 2012a; Masuda-Suzukake et al., 2013; Sacino et al., 2014b). In comparison to the protocol of Masuda-Suzukake et al. (2013), the buffer used in the present study contained additional NaCl that could have resulted in the formation of fibrils with different properties. A buffer composition with reduced salt concentrations has been shown to cause different structural α-synuclein conformations, e.g. so-called ribbons, which show different seeding and propagation properties (Bousset et al., 2013). It has also to be considered that the assembly solution does not contain only fibrils but also oligomeric and prefibrillar α-synuclein intermediates. These intermediates might be toxic and could also affect seeding properties (Karpinar et al., 2009; Winner et al., 2011). In contrast to one other protocol (Masuda-Suzukake et al., 2013), in the present study fibrils were not separated by centrifugation. Since different aggregation states can be distinguished in part by molecular weight, a separation of fibrils and intermediates by sedimentation velocity could improve characterization of aggregated α-synuclein species (Mok and Howlett, 2006). Further influencing factors might be the duration of fibril assembly as well the sonication protocol that could generate divers α-synuclein species with different seeding efficiencies. For instance Masuda-Suzukake et al. (2013) only centrifuged and did not sonicate their fibrils during the entire assembly protocol. Whereas in the protocol of Luk et al. (2012) and the protocol used in the present study fibrils were only sonicated and not centrifuged after assembly.

b) Amount of inoculum: The amount of α-synuclein seeds injected into mice might also influence their ability to form α-synuclein deposits and to cause neurodegeneration. In the present study 5 µg of α-synuclein fibrils were used for intracerebral injections. This amount has been reported to be sufficient to induce widespread α-synuclein pathology (Luk et al., 2012a). Masuda-Suzukake and colleagues injected 10 µg of fibrils, twice the amount that was injected by Luk et al. or in this study, which induced widespread α-synuclein pathology but only after long incubation times (Masuda-Suzukake et al., 2013). Dose-dependency has been shown in a report by Sacino et al. (2013b) injecting 2 µg vs. 25 µg into neonatal mice. In contrast to the low concentration that was not able to induce any signs of pathology, rare inclusions were found after injecting 25 µg of fibrils. Similarly, a dose-dependent induction of pathology has been reported in mice that received injections with viral vectors overexpressing α-synuclein (Oliveras-Salva et al.,

2013; Sacino et al., 2013a). A correlation between the amount of α-synuclein inoculated and its pathogenicity has also been confirmed in primary neurons where the extent of induced pathology depends on the amount of α-synuclein inoculated (Volpicelli-Daley et al., 2014).

c) Injection site: α-synuclein seeds injected into different brain regions might result in a different distribution and severity of α-synuclein pathology. The injection of α-synuclein fibrils e.g into the substantia nigra has been shown to be less virulent than the injection into the striatum (Luk et al., 2012a; Masuda-Suzukake et al., 2013).

All the above-mentioned factors might synergistically influence each other and a detailed analysis is necessary to better understand how pathogenicity and disease progression is influenced.

In general, the immunohistochemical or biochemical techniques utilized to assess α-synuclein pathology could also affect the outcome of the results. In the present study, phosphorylated α-synuclein may have been detectable only at 400 dpi and not earlier by immunohistochemical techniques due to its low abundance. The detection of phosphorylated α-synuclein might be optimized by the pretreatment of tissue sections with formic acid or proteinase K to enhance the signal for α-synuclein deposits and reduce the signal for endogenous non-aggregated α-synuclein (Beach et al., 2008). Pathology restricted to the cortex might explain why phosphorylated α-synuclein was not detected after immunoblotting of sarcosyl-insoluble fractions extracted from whole-brain homogenate. Due to a higher protein concentration extracted from the entire tissue, immunoblotting is generally considered as a more sensitive method than immunohistochemistry. In this respect, extracting from specifically dissected anatomical regions, such as the cortex, might enable detection of phosphorylated α-synuclein oligomers by immunoblotting.

Since brain surgery is always accompanied by local inflammation, resulting changes in brain homeostasis might as well influence prion-like propagation efficiency. It has been clearly shown that persistent neuroinflammation caused by LPS promotes the development of neuropathology and neurodegeneration in a mouse model overexpressing α-synuclein (Gao et al., 2011). However, according to the present data, the short, local inflammation caused by surgery is not accompanied by obvious long-term effects that possibly change disease progression (3.1.4). Despite the local inflammatory response,

induction of persistent neuroinflammation was not detectable as also observed in another study addressing the intracerebral injection of α-synuclein fibrils (Masuda-Suzukake et al., 2013). It is likely that the low abundance of α-synuclein inclusions restricted to the cortex was insufficient to activate astrocytes or microglia. Nevertheless, previous *in vitro* experiments have shown that misfolded α-synuclein activates microglia and can be directly transferred from primary neurons to astrocytes inducing an inflammatory response (Lee et al., 2010; Zhang et al., 2005). The induction of an inflammatory response might not only result from the accumulation of misfolded α-synuclein itself. It has been discussed that other circumstances like neuronal death and release of aggregated protein into the extracellular space might promote neuroinflammation (Glass et al., 2010). Moreover, α-synuclein aggregates that are posttranslationally modified by nitration have been shown to efficiently activate microglia and induce a neurotoxic response (Reynolds et al., 2008). In this respect, posttranslational modification like nitration might influence the capability of aggregated α-synuclein to activate immune cells.

4.1.2 Intraglossal injection of α-synuclein prionoids did not induce neuropathology

In contrast to prions that propagate within only two weeks from the tongue to the hypoglossal nucleus in the brainstem (Bartz et al., 2003), in the present work, injection of human α-synuclein fibrils into the tongue of Tg(*Gfap*-luc$^{+/-}$) mice did not induce any neuropathology. Even within the tongue muscle, α-synuclein fibrils did not cause any protein deposition for up to 400 dpi (3.1.2). It may be supposed that prion-like propagation of pathogenic α-synuclein depends on the conversion of endogenous α-synuclein. The assumption that the endogenous protein concentration is relevant for aggregate formation and seeding is supported by experiments in primary neurons. Exogenous addition of α-synuclein fibrils to primary neurons lead to an enhanced formation of aggregates when the concentration of endogenous α-synuclein was increased as in mature neurons (Volpicelli-Daley et al., 2011). The availability of neurons in the tongue muscle is limited to a few cranial nerves and therefore, it is likely, that the muscular tissue of the tongue might not express enough native α-synuclein to support its efficient conversion.

4.2 Mice overexpressing human α-synuclein are susceptible to peripherally injected α-synuclein fibrils

4.2.1 Intraglossal injection of α-synuclein prionoids induced α-synuclein pathology

The present work shows that in comparison to the Tg(*Gfap*-luc$^{+/-}$) mice, bigenic Tg(M83$^{+/-}$:*Gfap*-luc$^{+/-}$) mice overexpressing the A53T mutant of the human α-synuclein were more susceptible to exogenous challenge with α-synuclein fibrils via the tongue. It has been previously reported that homozygous Tg(M83$^{+/+}$) mice develop a lethal movement disorder caused by widespread CNS accumulation of pathological α-synuclein (Giasson et al., 2002). For the present study, only heterozygous Tg(M83$^{+/-}$) mice were used. These mice did not spontaneously accumulate pathogenic α-synuclein and remained free of neurologic disease for over 21 months as also reported by others (Watts et al., 2013). However, the heterozygous overexpression of human α-synuclein was sufficient to induce distinct neuropathology in the CNS of one of five animals intraglossally injected with α-synuclein prionoids at 285 dpi (3.2.1 and 3.2.2). These results differ from a previous study, which reports no neuroinvasion in bigenic Tg(M83$^{+/-}$:*Gfap*-luc$^{+/-}$) mice injected intraglossally with 5 µL of 1 % MSA brain homogenate and sacrificed at 220 dpi (Prusiner et al., 2015).

The intraglossal injection experiments into monogenic Tg(*Gfap*-luc$^{+/-}$) and bigenic Tg(M83$^{+/-}$:*Gfap*-luc$^{+/-}$) mice cannot be directly compared. Tg(M83$^{+/-}$:*Gfap*-luc$^{+/-}$) mice were injected with 10 µg of α-synuclein fibrils, whereas Tg(*Gfap*-luc$^{+/-}$) animals were injected with only 5 µg. For prions it has been shown that prion infectivity increases proportional to the concentration of prions intracerebrally inoculated (Tamgüney et al., 2009a). As already discussed in 4.1.1 dose-dependency has also been shown to be relevant for injections with α-synuclein. Therefore, it might be interesting to verify if more inoculum may induce neuropathology in Tg(*Gfap*-luc$^{+/-}$) mice or even increase the number of diseased Tg(M83$^{+/-}$:*Gfap*-luc$^{+/-}$) mice. Another explanation for the limited rate and severity of neuroinvasion after fibril challenge into the tongue muscle is that injections were not directly targeted to the bilateral hypoglossal nerve (cranial nerve XII). All intrinsic and extrinsic muscles of the tongue are innervated by the hypoglossal nerve, which originates from the hypoglossal nucleus (nucleus XII) in the brainstem (McClung and Goldberg, 2000). This nerve is the prevalent but not the only conduit innervating the tongue. Other cranial nerves such as the glossopharyngeal nerve also innervate the tongue

and might act as additional routes for α-synuclein seeds to neuroinvade the CNS. The hypoglossal nerve of LBD patients has been reported not to accumulate phosphorylated α-synuclein although other cranial nerves like the oculomotor, trigeminal, and the glossopharyngeal-vagus nerves, together with their roots display obvious α-synuclein pathology (Nakamura et al., 2016). Deposition of phosphorylated α-synuclein in both the brain and the spinal cord after intraglossal challenge supports the hypothesis of an initial retrograde axonal transport to the brainstem and from there to the spinal cord. Consequently, the findings of the present work, reaffirm that the intraglossal route is not only a pathway for *bona fide* prions (Bartz et al., 2003) but also for α-synuclein prionoids to neuroinvade the CNS. Although neuroinvasion of α-synuclein prionoids via the tongue is inefficient and takes seven weeks longer than that of prions, these findings indicate that α-synuclein prionoids have characteristics that are very similar to prions.

4.2.2 Intraperitoneally injected α-synuclein fibrils induced severe neuropathology and neurologic illness

The present work is the first to show that human α-synuclein prionoids can neuroinvade the CNS and induce neurologic disease in Tg(M83$^{+/-}$:*Gfap*-luc$^{+/-}$) mice after a single intraperitoneal injection with α-synuclein fibrils (3.2.1 and 3.2.3). Neuroinvasive properties were primarily described for *bona fide* prions (Kimberlin and Walker, 1986) and also found for β-amyloid and the tau protein (Clavaguera et al., 2014; Eisele et al., 2010). Similar to our findings, a prion-like behavior was evident when brain extracts containing misfolded β-amyloid were injected into the peritoneum of APP23 mice. These animals, which express the human β-amyloid precursor protein with the Swedish mutation, developed β-amyloidosis in their brains after injection (Eisele et al., 2010). Similarly, intraperitoneal injection of brain stem extracts containing pathogenic tau aggregates into animals expressing the P301S mutant of tau, induces pathology in their brains (Clavaguera et al., 2014). Comparing the transmission routes and incubation times of α-synuclein prionoids to neuroinvade the CNS of Tg(M83$^{+/-}$:*Gfap*-luc$^{+/-}$) mice indicates that the efficiency to induce neuropathology along the intraperitoneal route is similar to the direct intracerebral route. Intraperitoneal injection causes disease only two weeks later (229 dpi) than after intracerebral injection with brain homogenate from diseased Tg(M83$^{+/+}$) mice (216 dpi) (Watts et al., 2013). Unexpectedly, injection of human α-synuclein prionoids into the hindlimb muscles, the gastronemicus or the biceps

femoris, was reported to induce a much faster disease onset with obvious motor symptoms already at 129 dpi (Sacino et al., 2014a).

There is evidence that the level of endogenous substrate protein expression is generally relevant for the seeded conversion of α-synuclein into its pathogenic form that is associated with disease as discussed in 4.1.2. In the Tg(APP23) mouse model for Alzheimer's disease, which was intraperitoneally injected with β-amyloid, the level of cerebral β-amyloidosis was clearly dependent on the amount of endogenous amyloid precursor protein (APP) expressed (Eisele et al., 2014). For α-synuclein it is not yet clear, if overexpression of endogenous α-synuclein is a prerequisite to induce disease after intraperitoneal injection with α-synuclein fibrils. The results presented in 3.1.1 are in line with previous studies and show that endogenous overexpression is not a precondition for α-synuclein prionoids to cause CNS disease via the intracerebral route. Because intracerebrally injected α-synuclein fibrils are able to induce neuropathology in mice that are wild-type for α-synuclein (Luk et al., 2012a; Masuda-Suzukake et al., 2013; Sacino et al., 2013b). Only additional experiments in WT mice will help to clarify whether overexpression of α-synuclein is necessary for peripheral infection or not. Moreover, seeding efficiency might not only be determined by the level of endogenous protein expressed but also by molecular compatibility, which is often determined by sequence homology between native, endogenous α-synuclein and its fibrillary seed (Luk et al., 2016). It has been shown in mice, that mouse α-synuclein fibrils show a higher propensity to seed aggregation than human α-synuclein fibrils. Substitution of a single amino acid in the mouse sequence was sufficient to alter its propensity to fibrillize *in vitro* and to seed misfolding of endogenous α-synuclein after injection into mice (Luk et al., 2016). As presented in 3.2.3.1 the aggregates found in the spinal cord of diseased animals were composed of endogenous mouse α-synuclein as well as transgenically expressed human α-synuclein. This clearly indicates that although the inoculated seed was human origin, both native mouse and transgenically expressed human α-synuclein are involved in the pathological process accelerating and amplifying the disease progression.

The underlying mechanisms of how α-synuclein prionoids enter the CNS after intraperitoneal injection have not been thoroughly investigated yet. For prions it has been discussed that neuroinvasion might be possible by a) retrograde spreading of infectivity along peripheral nerves, or b) the hematogenous route (Siso et al., 2010).

Retrograde axonal transportation via peripheral nerves as a probable route for neuroinvasion of α-synuclein was confirmed by several inoculation studies. α-synuclein prionoids injected into the gastrocnemicus- or biceps femoris muscle of the hindlimb have shown to induce α-synuclein pathology in the CNS of Tg(M83$^{+/-}$) or Tg(M83$^{+/+}$) mice (Sacino et al., 2014a). The dissection of the sciatic nerve lead to a delayed or diminished induction of neuropathology indicating that the sciatic nerve is a probable route for neuroinvasion. However, since the induction of disease could not be completely abolished by nerve dissection, α-synuclein prionoids might also use additional routes, e.g. other peripheral nerves to enter the CNS. It has also been reported that human PD brain lysate or recombinant α-synuclein fibrils injected into the intestinal wall of rats were retrogradely transmitted via the vagus nerve to the brain stem causing neuropathology (Holmqvist et al., 2014). A similar long-distance propagation, was described after injection of human α-synuclein expressed from adeno-associated viruses into the vagus nerve in the rat neck (Ulusoy et al., 2013). The assumption that neuronal circuits are the prevalent transmission routes for disease-associated α-synuclein to neuroinvade the CNS was suggested after histopathological studies in patients with Lewy body disorders. The histological data revealed that α-synuclein pathology is not only restricted to the central or peripheral nervous system but also found in its innervated tissues and organs (Beach et al., 2010). The tissues along the digestive system, from the submandibular gland to the rectum, have been observed to be the most affected tissues and probably play an important role for the long-distance transmission of proteinaceous agents (Beach et al., 2010; Cersosimo and Benarroch, 2012; Hilton et al., 2014).

The finding that red blood cells bear high concentrations of α-synuclein strengthens the possibility that blood could act as a reservoir for the replication, seeding, and dissemination of α-synuclein prionoids in the body (Barbour et al., 2008). Studies in rats have also suggested that misfolded α-synuclein species can cross the blood-brain barrier (BBB) after intravenous injection (Peelaerts et al., 2015). The induction of neuroinflammation as response to LPS has been shown to increase the permeability of the BBB (Banks and Erickson, 2010). Notably, in contrast to wild-type mice, Tg(SNCA$^{-/-}$) mice that are deficient for α-synuclein did not change their BBB permeability (Jangula and Murphy, 2013). These findings indicate that the presence of native α-synuclein is sufficient to enhance the permeability of the BBB and consequently to make the brain accessible for pathogens. For prions it has been reported that they can replicate outside of nervous tissue in follicular dendritic cells and secondary lymphoid tissues (Bruce et al.,

2001; McCulloch et al., 2011). Whether α-synuclein prionoids can replicate in non-nervous tissue and organs like such as the lymphatic system has not been investigated yet. Transmission of synucleinopathies by blood transfusion or organ transplantation has not been reported. In this respect it has to be considered that incubation times for the iatrogenic transmission of synucleinopathies are not known and could span several decades as has been observed for human prion diseases like kuru, which can take up to 60 years (Collinge et al., 2006). Beside the iatrogenic transmission of prion diseases there is evidence that also amyloid-β associated with Alzheimer's disease may have been transmitted via treatment with contaminated growth hormone or by dural grafting (Frontzek et al., 2016; Jaunmuktane et al., 2015a; Rudge et al., 2015).

The results presented in 3.2.3.1 show that despite the wide distribution of α-synuclein pathology in the brains of Tg(M83$^{+/-}$:*Gfap*-luc$^{+/-}$) mice intraperitoneally injected with α-synuclein fibrils certain anatomical regions were devoid of neuropathology. Detailed analysis of the brains revealed that neurons of the olfactory bulb, hippocampus, and cerebellum, including Purkinje and granule cells did not show any signs of α-synuclein deposition. Similar findings regarding this lack of pathology in these brain regions have been previously described but cannot be fully attributed to the prion promoter, which controls α-synuclein expression in M83 mice (Giasson et al., 2002). Indeed, the prion promoter is well known to drive expression in the hippocampus and Purkinje cells of the cerebellum (Tremblay et al., 2007). Since the complete lack of pathology is restricted to anatomical regions that contain granule cell populations (Franklin and Paxinos, 2008) it may be assumed that these neurons in the white matter do not support replication of misfolded α-synuclein. Also, in the spinal cord of diseased animals, α-synuclein pathology was restricted to the grey matter and not found within the white matter (3.2.3.1). These observations support the idea that long unmyelinated axons, as they are abundantly found in the grey matter, are more accessible and vulnerable than neurons surrounded by myelin sheets (Braak and Del Tredici, 2004). In particular, the cholinergic neurons of the ventral horn and the dopaminergic neurons of the substantia nigra accumulated deposits of misfolded α-synuclein (3.2.3.1 and 3.2.3.3). Both cell types are involved in controlling locomotor activity and their impairment possibly caused motor dysfunction in these mice.

Moreover, the present results show that mice intraperitoneally injected with α-synuclein fibrils develop beside α-synuclein pathology, neuroinflammation in form of microgliosis

and reactive astrogliosis. Reactive astrocytes were detectable by BLI a few weeks before animals became terminally sick, similar to findings previously reported after intracerebral injection of MSA brain homogenate into Tg(M83$^{+/-}$:*Gfap*-luc$^{+/-}$) mice (Watts et al., 2013). The variability in BL intensities detected over time might be caused by dynamic regulation of GFAP expression, which is regulated by various signaling molecules (Sofroniew, 2009). Such mediator molecules are released by several cell types including microglia, oligodendrocytes, or leukocytes and gradually trigger the activity state of astrocytes. A rapid GFAP upregulation might also be explained by ependymal stem cells that are prompt to migrate to the CNS lesion and differentiate into astrocytes to stem the acute injury (Johansson et al., 1999). Despite such variability in measuring astrocytic gliosis, BLI can be used as surrogate marker to detect neuronal lesions some weeks before motor symptoms appear.

4.3 Aerosols of pathogenic α-synuclein did not transmit disease

In PD, neurons of the olfactory bulb or the enteric nervous system have been described as initiation points from where the disease progression could start (Braak et al., 2003a; Braak et al., 2004). The data presented in 3.3.1 show that aerosols made from MSA brain homogenate did not enter the olfactory epithelium and did not induce neuropathology or disease within 600 d in Tg(M83$^{+/-}$:*Gfap*-luc$^{+/-}$) mice. Similarly, direct instillation of recombinant α-synuclein fibrils or brain extracts containing pathogenic α-synuclein species from a LBD patient did not induce neuropathology in WT mice in 640 days when treated with weekly doses over one month (Masuda-Suzukake et al., 2013). In contrast, other agents like lipopolysaccharides LPS or MPTP (see intoxication mouse models 1.5.1) have been shown to easily enter the brain by passing the nasal mucosa and induce PD-like pathology when directly instilled into the nostrils of rodents (He et al., 2013; Rojo et al., 2006). In addition, the nasal route via the olfactory epithelium was described as a very efficient route through which aerosolized CWD prions could enter the brain and induce disease in Tg(cerPrP) mice that express cervid PrP^{C} (Denkers et al., 2010). Interestingly, aerosol mediated prion transmission has been shown to be more efficient than the direct instillation of infectious material into the nose. With regard to the present study, it cannot be completely excluded that pathogenic α-synuclein entered the olfactory epithelium, but remained under the threshold for immunohistochemical detection. Therefore it is recommendable to analyze whether the brain homogenates of mice exposed to aerosols might possibly seed aggregation *in vitro* and *in vivo*. In particular,

passage of the potentially pathogenic brain homogenates into mice would finally answer the question whether α-synuclein aerosols are able to mediate disease.

However, one crucial factor that may influence particle absorption by the nasal mucosa is the size of the aerosolized particles. Since the nebulizer used for the present work (2.3.4) produced particles with a median diameter of 2.2 µm, it can be assumed that impaction is the major mechanism for their deposition in the nasal tracts (Vidgren and Kublik, 1998). For rodents it has been shown that aluminosilicate particles with a diameter larger than 3 µm are preferentially deposited in the nasal-pharyngeal region. For a particle size smaller than 3 µm, the deposition in the lung and bronchial airways increases (Raabe et al., 1988). This might explain why a supposedly sufficient amount of pathogenic α-synuclein to induce pathology may not have entered the nasal tracts and its epithelium. Beside the particle size, the short exposure time might also play a role in limiting the uptake of α-synuclein aerosols via receptor nerve endings. Therefore the influence of aerosol particle size and exposure times on the uptake of the pathogenic α-synuclein via receptor nerve endings needs to be further investigated. In this respect, it should be considered that particles that enter the nasal tracts may also be transported by swallowed saliva to the gastrointestinal tract. According to the "dual hit hypothesis" this pathway is another potential route for α-synuclein to neuroinvade the CNS (Hawkes et al., 2007, 2009).

4.4 Conclusions

The findings described here clearly show that similar to prions α-synuclein prionoids cause CNS neuropathology and disease after direct injection into the CNS and by neuroinvasion via several peripheral routes after peripheral injection.

The findings in wild-type mice and mice overexpressing α-synuclein clearly show a direct correlation between the severity of α-synuclein pathology and the resulting disease phenotype. Intracerebral challenge of α-synuclein wild-type mice could recapitulate mild neuropathology as similarly observed in sporadic PD but not pathophysiological features like behavioral deficits and neuroinflammation. Induction of neuropathology via the intraglossal route in mice overexpressing α-synuclein shows that following oral ingestion pathogenic α-synuclein could be transmitted to the CNS via the cranial nerves. In particular, this pathway may have relevance when a superficial wound in the tongue facilitates the uptake of pathogenic α-synuclein or the entrance for other toxic agents. Moreover, the presented data provide the first evidence that the peritoneum is a potential entry site for α-synuclein prionoids to neuroinvade the CNS and cause neuropathology. Intraperitoneal injection of α-synuclein fibrils into mice overexpressing human α-synuclein resembles important characteristics of human synucleinopathies recapitulating a distinct correlation between pathological, inflammatory, and physical hallmarks. In this respect, BLI is a suitable indicator for neuroinflammation preceding the appearance of motor symptoms. Moreover, intraperitoneal injection presents a suitable model to study peripheral routes through which α-synuclein possibly enters the CNS. The peritoneum and in particular the gastrointestinal system is of great interest since the progression of PD may start here. Although pathogenic α-synuclein aerosols did not pass the olfactory epithelium of mice and induce neuropathology, it remains recommendable to study this route more extensively since the olfactory cells are among the first cell populations affected in PD. In this respect, also the role of environmental factors like air pollution and pesticides entering the nose during daily life, should be included in further research. Despite many parallels with prions, it has to be further elucidated whether α-synuclein prionoids can overcome species barriers and are transmissible between organisms to induce disease.

5 Appendix

5.5 Alignment of the amino acid sequences of mouse and human α-synuclein

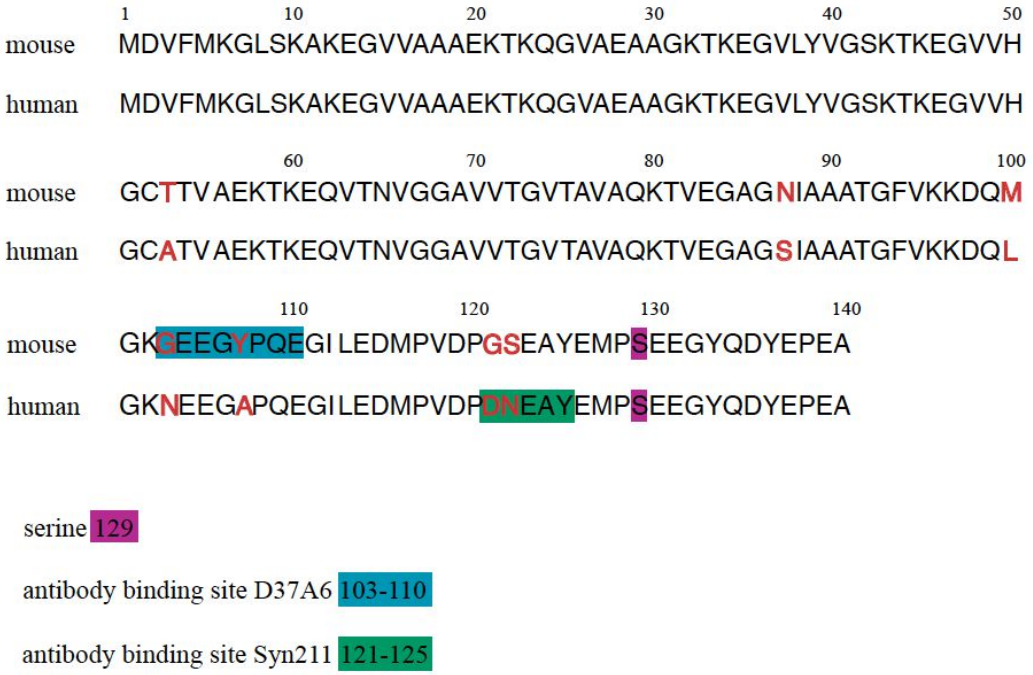

Fig. 5.1 Amino acid sequence of mouse and human α-synuclein. Both sequences differ in seven amino acids (red). The prevalent phosphorylation site of α-synuclein is at serine 129 (purple). Binding sites of the specific mouse and human antibodies are indicated: antibody D37A6, mouse specific (blue) and antibody Syn211, human specific (green).

5.6 Experimental overview

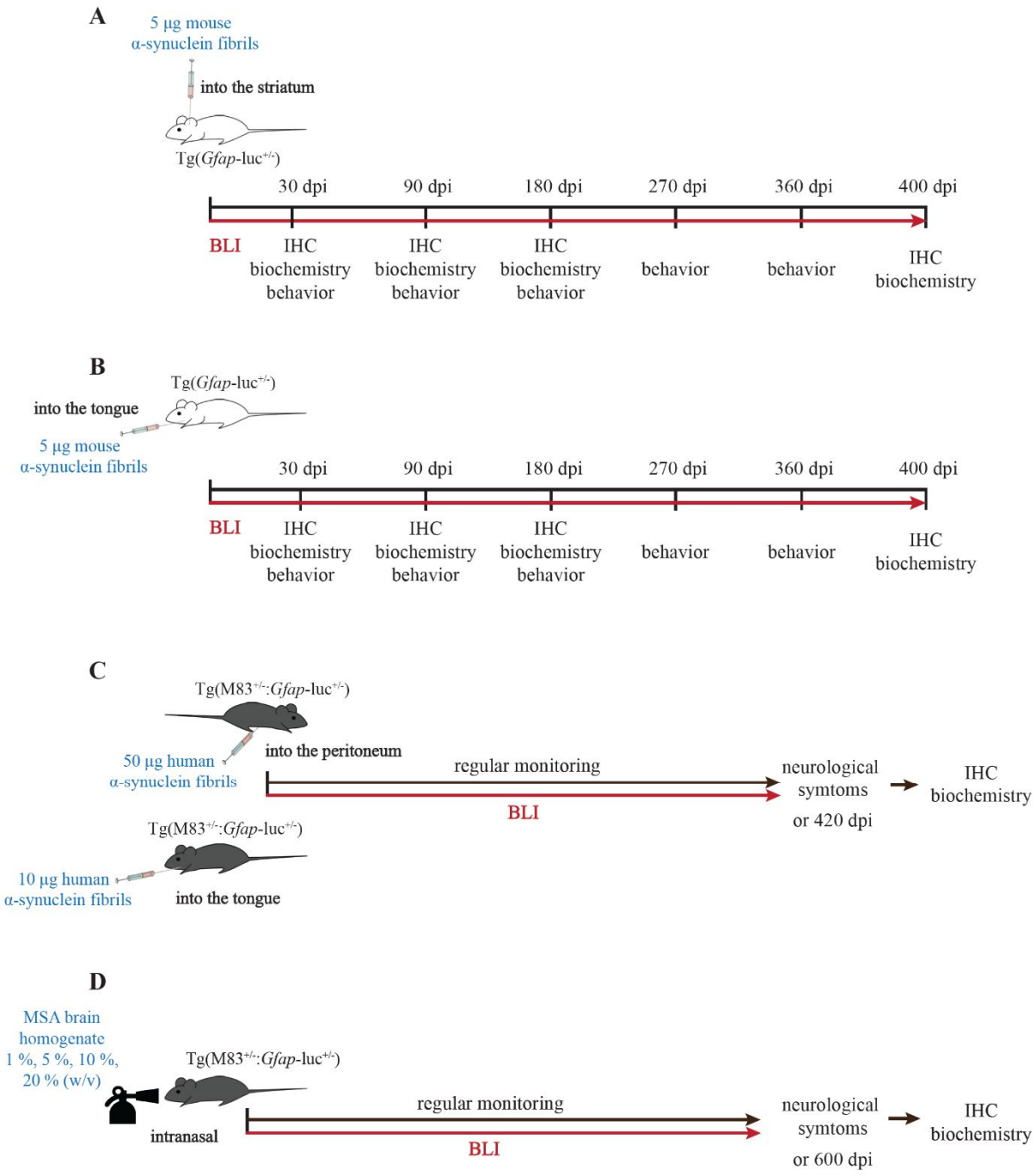

6 Abbreviations

AD	Alzheimer`s disease
AIF 1	allograft inflammatory factor 1
ALP	autophagy-lysosomal pathway
APP	amyloid precursor protein
BBB	blood-brain barrier
BL	bioluminescence
BLI	bioluminescence imaging
bp	base pair
BSE	bovine spongiform encephalopathy
ChAT	cholinergic acetyltransferase
CJD	Creutzfeldt-Jakob disease
CNS	central nervous system
$CuSO_4$	copper sulfate
CWD	chronic wasting disease
DA	dopamine
DAB	3-3'-diaminobenzidine
DNA	deoxyribonucleic acid
d	day
dpi	days post inoculation
E. coli	Escherichia coli
EDTA	ethylenediaminetetraacetic acid
EGTA	ethylene glycol-bis (β-aminoethyl ether)-N,N,N',N'-tetraacetic acid
EtOH	ethanol
GCI	glial cytoplasmic inclusions
GFAP	glial fibrillary acidic protein
HCL	hydrochloric acid
Hbb	human β-globin intron 2
HPLC	high performance liquid chromatography
HRP	horseradish peroxidase
ic/ IC	intracerebral
ID	identification number
IF	immunofluorescence

ig /IG	intraglossal
IHC	immunohistochemistry
IL-1β	interleukin 1β
IL-6	interleukin 6
ip /IP	intraperitoneal
IPTG	isopropyl β-D-1-thiogalactopyranoside
kDa	kilodalton
LB	Lewy body
LB	lysogeny broth
LBD	Lewy body dementia
LBVAD	Lewy body variant of Alzheimer`s disease
LN	Lewy neurite
LPS	lipopolysaccharide
Luc2	luciferase gene 2
kb	kilobase
rpm	rotation per minute
MAPT	microtubule associated protein tau
$MgSO_4$	magnesium sulfate
MSA	multiple system atrophy
MPP^+	1-methyl-4-phenyl-pyridium
MPTP	1-methyl-4-phenyl-1,2,3,6-tetrahydropyridine
NaCl	sodium chloride
$(NH_4)_2SO_4$	ammonium sulfate
No./ no.	number
nTg	non transgenic
OD	optical density
TBS	Tris-buffered saline
TH	tyrosine hydroxylase
p	phospho
PCR	polymerase chain reaction
PBS	phosphate-buffered saline
PD	Parkinson`s disease
PDGF β	platelet-derived growth factor-β
PFA	paraformaldehyde

PFF	preformed fibrils
PolyQ	polyglutamine
PrP	prion protein
PVDF	polyvinylidene difluoride
RML	RML (Rocky mountain laboratory) prion
ROI	region of interest
RT	room temperature
SD	standard deviation
Ser129	serine 129
SEM	standard error of the mean
SNc	substantia nigra pars compacta
Snca	gene encoding mouse α-synuclein
SOD1	superoxide dismutase 1
SYN	α-synuclein
TEM	transmission electron microscopy
TH	tyrosine hydroxylase
TME	transmissible mink encephalopathy
TNF-α	tumor necrosis factor α
UPS	ubiquitin-proteasomal system
vCJD	variant Creutzfeldt-Jakob disease
w/v	weight per volume
WB	western blot
6-OHDA	6-hydroxdopamine

7 Contributions

Expression and purification of recombinant human α-synuclein protein was performed by Dr. Julius Tachu Babila at the German Center of Neurodegenerative Diseases, Bonn. The mouse α-synuclein fibrils in Fig. 3.1 were analyzed by electron microscopy by Karen Tolksdorf at the Department of Neurology of the University of Bonn. The human α-synuclein fibrils in Fig. 3.9 were analyzed by electron microscopy by Dr. Maria C. Garza and Dr. Holger Wille at the University of Alberta in Edmonton, Alberta.

8 Bibliography

Abeliovich, A., Schmitz, Y., Farinas, I., Choi-Lundberg, D., Ho, W.H., Castillo, P.E., Shinsky, N., Verdugo, J.M., Armanini, M., Ryan, A., *et al.* (2000). Mice lacking α-synuclein display functional deficits in the nigrostriatal dopamine system. Neuron *25*, 239-252.

Aguzzi, A. (2009). Cell biology: Beyond the prion principle. Nature *459*, 924-925.

Aguzzi, A., and Lakkaraju, A.K. (2016). Cell Biology of Prions and Prionoids: A Status Report. Trends Cell Biol *26*, 40-51.

Aguzzi, A., and Rajendran, L. (2009). The transcellular spread of cytosolic amyloids, prions, and prionoids. Neuron *64*, 783-790.

Ahmed, I., Liang, Y., Schools, S., Dawson, V.L., Dawson, T.M., and Savitt, J.M. (2012). Development and characterization of a new Parkinson's disease model resulting from impaired autophagy. J Neurosci *32*, 16503-16509.

Allen, N.J., and Barres, B.A. (2009). Neuroscience: Glia - more than just brain glue. Nature *457*, 675-677.

Amor, S., Peferoen, L.A., Vogel, D.Y., Breur, M., van der Valk, P., Baker, D., and van Noort, J.M. (2014). Inflammation in neurodegenerative diseases--an update. Immunology *142*, 151-166.

Anderson, J.P., Walker, D.E., Goldstein, J.M., de Laat, R., Banducci, K., Caccavello, R.J., Barbour, R., Huang, J., Kling, K., Lee, M., *et al.* (2006). Phosphorylation of S-129 is the dominant pathological modification of α-synuclein in familial and sporadic Lewy body disease. J Biol Chem *281*, 29739-29752.

Banks, W.A., and Erickson, M.A. (2010). The blood-brain barrier and immune function and dysfunction. Neurobiol Dis *37*, 26-32.

Barbour, R., Kling, K., Anderson, J.P., Banducci, K., Cole, T., Diep, L., Fox, M., Goldstein, J.M., Soriano, F., Seubert, P., *et al.* (2008). Red blood cells are the major source of α-synuclein in blood. Neurodegener Dis *5*, 55-59.

Bartels, T., Choi, J.G., and Selkoe, D.J. (2011). α-Synuclein occurs physiologically as a helically folded tetramer that resists aggregation. Nature *477*, 107-110.

Bartz, J.C., Kincaid, A.E., and Bessen, R.A. (2002). Retrograde transport of transmissible mink encephalopathy within descending motor tracts. J Virol *76*, 5759-5768.

Bartz, J.C., Kincaid, A.E., and Bessen, R.A. (2003). Rapid prion neuroinvasion following tongue infection. J Virol *77*, 583-591.

Beach, T.G., Adler, C.H., Sue, L.I., Vedders, L., Lue, L., White Iii, C.L., Akiyama, H., Caviness, J.N., Shill, H.A., Sabbagh, M.N., *et al.* (2010). Multi-organ distribution of phosphorylated α-synuclein histopathology in subjects with Lewy body disorders. Acta Neuropathol *119*, 689-702.

Beach, T.G., White, C.L., Hamilton, R.L., Duda, J.E., Iwatsubo, T., Dickson, D.W., Leverenz, J.B., Roncaroli, F., Buttini, M., Hladik, C.L., *et al.* (2008). Evaluation of α-synuclein immunohistochemical methods used by invited experts. Acta Neuropathol *116*, 277-288.

Beal, M.F. (2001). Experimental models of Parkinson's disease. Nat Rev Neurosci *2*, 325-334.

Beekes, M., McBride, P.A., and Baldauf, E. (1998). Cerebral targeting indicates vagal spread of infection in hamsters fed with scrapie. J Gen Virol *79 (Pt 3)*, 601-607.

Bence, N.F., Sampat, R.M., and Kopito, R.R. (2001). Impairment of the ubiquitin-proteasome system by protein aggregation. Science *292*, 1552-1555.

Bendor, J.T., Logan, T.P., and Edwards, R.H. (2013). The function of α-synuclein. Neuron *79*, 1044-1066.

Bernis, M.E., Babila, J.T., Breid, S., Wusten, K.A., Wullner, U., and Tamgüney, G. (2015). Prion-like propagation of human brain-derived α-synuclein in transgenic mice expressing human wild-type α-synuclein. Acta Neuropathol Commun *3*, 75.

Bessen, R.A., Shearin, H., Martinka, S., Boharski, R., Lowe, D., Wilham, J.M., Caughey, B., and Wiley, J.A. (2010). Prion shedding from olfactory neurons into nasal secretions. PLoS Pathog *6*, e1000837.

Betarbet, R., Sherer, T.B., MacKenzie, G., Garcia-Osuna, M., Panov, A.V., and Greenamyre, J.T. (2000). Chronic systemic pesticide exposure reproduces features of Parkinson's disease. Nat Neurosci *3*, 1301-1306.

Betemps, D., Verchere, J., Brot, S., Morignat, E., Bousset, L., Gaillard, D., Lakhdar, L., Melki, R., and Baron, T. (2014). A-synuclein spreading in M83 mice brain revealed by detection of pathological α-synuclein by enhanced ELISA. Acta Neuropathol Commun *2*, 29.

Bosque, P.J., Ryou, C., Telling, G., Peretz, D., Legname, G., DeArmond, S.J., and Prusiner, S.B. (2002). Prions in skeletal muscle. Proc Natl Acad Sci U S A *99*, 3812-3817.

Bousset, L., Pieri, L., Ruiz-Arlandis, G., Gath, J., Jensen, P.H., Habenstein, B., Madiona, K., Olieric, V., Bockmann, A., Meier, B.H., *et al.* (2013). Structural and functional characterization of two α-synuclein strains. Nat Commun *4*, 2575.

Braak, H., and Del Tredici, K. (2004). Poor and protracted myelination as a contributory factor to neurodegenerative disorders. Neurobiol Aging *25*, 19-23.

Braak, H., Del Tredici, K., Rub, U., de Vos, R.A., Jansen Steur, E.N., and Braak, E. (2003a). Staging of brain pathology related to sporadic Parkinson's disease. Neurobiol Aging *24*, 197-211.

Braak, H., Ghebremedhin, E., Rub, U., Bratzke, H., and Del Tredici, K. (2004). Stages in the development of Parkinson's disease-related pathology. Cell Tissue Res *318*, 121-134.

Braak, H., Rub, U., Gai, W.P., and Del Tredici, K. (2003b). Idiopathic Parkinson's disease: possible routes by which vulnerable neuronal types may be subject to neuroinvasion by an unknown pathogen. J Neural Transm (Vienna) *110*, 517-536.

Breid, S., Bernis, M.E., Babila, J.T., Garca, M.C., Wille, H., and Tamgüney, G. (2016). Neuroinvasion of α-Synuclein Prionoids after Intraperitoneal and Intraglossal Inoculation. J Virol. *90*, 9182-9193.

Brown, P., Brandel, J.P., Sato, T., Nakamura, Y., MacKenzie, J., Will, R.G., Ladogana, A., Pocchiari, M., Leschek, E.W., and Schonberger, L.B. (2012). Iatrogenic Creutzfeldt-Jakob disease, final assessment. Emerg Infect Dis *18*, 901-907.

Bruce, M.E., McConnell, I., Will, R.G., and Ironside, J.W. (2001). Detection of variant Creutzfeldt-Jakob disease infectivity in extraneural tissues. Lancet *358*, 208-209.

Calderon-Garciduenas, L., Solt, A.C., Henriquez-Roldan, C., Torres-Jardon, R., Nuse, B., Herritt, L., Villarreal-Calderon, R., Osnaya, N., Stone, I., Garcia, R.*, et al.* (2008). Long-term air pollution exposure is associated with neuroinflammation, an altered innate immune response, disruption of the blood-brain barrier, ultrafine particulate deposition, and accumulation of amyloid beta-42 and α-synuclein in children and young adults. Toxicol Pathol *36*, 289-310.

Cersosimo, M.G., and Benarroch, E.E. (2012). Pathological correlates of gastrointestinal dysfunction in Parkinson's disease. Neurobiol Dis *46*, 559-564.

Cetin, A., Komai, S., Eliava, M., Seeburg, P.H., and Osten, P. (2006). Stereotaxic gene delivery in the rodent brain. Nat Protoc *1*, 3166-3173.

Clavaguera, F., Hench, J., Lavenir, I., Schweighauser, G., Frank, S., Goedert, M., and Tolnay, M. (2014). Peripheral administration of tau aggregates triggers intracerebral tauopathy in transgenic mice. Acta Neuropathol *127*, 299-301.

Cohen, F.E., Pan, K.M., Huang, Z., Baldwin, M., Fletterick, R.J., and Prusiner, S.B. (1994). Structural clues to prion replication. Science *264*, 530-531.

Collinge, J., and Clarke, A.R. (2007). A general model of prion strains and their pathogenicity. Science *318*, 930-936.

Collinge, J., Whitfield, J., McKintosh, E., Beck, J., Mead, S., Thomas, D.J., and Alpers, M.P. (2006). Kuru in the 21st century--an acquired human prion disease with very long incubation periods. Lancet *367*, 2068-2074.

Conway, K.A., Lee, S.J., Rochet, J.C., Ding, T.T., Williamson, R.E., and Lansbury, P.T., Jr. (2000). Acceleration of oligomerization, not fibrillization, is a shared property of both α-synuclein mutations linked to early-onset Parkinson's disease: implications for pathogenesis and therapy. Proc Natl Acad Sci U S A *97*, 571-576.

Cuervo, A.M., Stefanis, L., Fredenburg, R., Lansbury, P.T., and Sulzer, D. (2004). Impaired degradation of mutant α-synuclein by chaperone-mediated autophagy. Science *305*, 1292-1295.

Damier, P., Hirsch, E.C., Zhang, P., Agid, Y., and Javoy-Agid, F. (1993). Glutathione peroxidase, glial cells and Parkinson's disease. Neuroscience *52*, 1-6.

Danzer, K.M., Kranich, L.R., Ruf, W.P., Cagsal-Getkin, O., Winslow, A.R., Zhu, L., Vanderburg, C.R., and McLean, P.J. (2012). Exosomal cell-to-cell transmission of α synuclein oligomers. Mol Neurodegener *7*, 42.

Dawson, T., Mandir, A., and Lee, M. (2002). Animal models of PD: pieces of the same puzzle? Neuron *35*, 219-222.

Denkers, N.D., Seelig, D.M., Telling, G.C., and Hoover, E.A. (2010). Aerosol and nasal transmission of chronic wasting disease in cervidized mice. J Gen Virol *91*, 1651-1658.

Desplats, P., Lee, H.J., Bae, E.J., Patrick, C., Rockenstein, E., Crews, L., Spencer, B., Masliah, E., and Lee, S.J. (2009). Inclusion formation and neuronal cell death through neuron-to-neuron transmission of α-synuclein. Proc Natl Acad Sci U S A *106*, 13010-13015.

Doty, R.L. (2008). The olfactory vector hypothesis of neurodegenerative disease: is it viable? Ann Neurol *63*, 7-15.

Duda, J.E., Giasson, B.I., Chen, Q., Gur, T.L., Hurtig, H.I., Stern, M.B., Gollomp, S.M., Ischiropoulos, H., Lee, V.M., and Trojanowski, J.Q. (2000). Widespread nitration of pathological inclusions in neurodegenerative synucleinopathies. Am J Pathol *157*, 1439-1445.

Eisele, Y.S., Fritschi, S.K., Hamaguchi, T., Obermuller, U., Fuger, P., Skodras, A., Schafer, C., Odenthal, J., Heikenwalder, M., Staufenbiel, M.*, et al.* (2014). Multiple factors contribute to the peripheral induction of cerebral beta-amyloidosis. J Neurosci *34*, 10264-10273.

Eisele, Y.S., Obermuller, U., Heilbronner, G., Baumann, F., Kaeser, S.A., Wolburg, H., Walker, L.C., Staufenbiel, M., Heikenwalder, M., and Jucker, M. (2010). Peripherally applied Abeta-containing inoculates induce cerebral beta-amyloidosis. Science *330*, 980-982.

Emmanouilidou, E., Elenis, D., Papasilekas, T., Stranjalis, G., Gerozissis, K., Ioannou, P.C., and Vekrellis, K. (2011). Assessment of α-synuclein secretion in mouse and human brain parenchyma. PLoS One *6*, e22225.

Emmanouilidou, E., Melachroinou, K., Roumeliotis, T., Garbis, S.D., Ntzouni, M., Margaritis, L.H., Stefanis, L., and Vekrellis, K. (2010). Cell-produced α-synuclein is secreted in a calcium-dependent manner by exosomes and impacts neuronal survival. J Neurosci *30*, 6838-6851.

Fortin, D.L., Troyer, M.D., Nakamura, K., Kubo, S., Anthony, M.D., and Edwards, R.H. (2004). Lipid rafts mediate the synaptic localization of α-synuclein. J Neurosci *24*, 6715-6723.

Freundt, E.C., Maynard, N., Clancy, E.K., Roy, S., Bousset, L., Sourigues, Y., Covert, M., Melki, R., Kirkegaard, K., and Brahic, M. (2012). Neuron-to-neuron transmission of α-synuclein fibrils through axonal transport. Ann Neurol *72*, 517-524.

Frontzek, K., Lutz, M.I., Aguzzi, A., Kovacs, G.G., and Budka, H. (2016). Amyloid-beta pathology and cerebral amyloid angiopathy are frequent in iatrogenic Creutzfeldt-Jakob disease after dural grafting. Swiss Med Wkly *146*, w14287.

Frost, B., Jacks, R.L., and Diamond, M.I. (2009). Propagation of tau misfolding from the outside to the inside of a cell. J Biol Chem *284*, 12845-12852.

Fujiwara, H., Hasegawa, M., Dohmae, N., Kawashima, A., Masliah, E., Goldberg, M.S., Shen, J., Takio, K., and Iwatsubo, T. (2002). α-Synuclein is phosphorylated in synucleinopathy lesions. Nat Cell Biol *4*, 160-164.

Gallagher, D.A., Lees, A.J., and Schrag, A. (2010). What are the most important nonmotor symptoms in patients with Parkinson's disease and are we missing them? Mov Disord *25*, 2493-2500.

Gao, H.M., Zhang, F., Zhou, H., Kam, W., Wilson, B., and Hong, J.S. (2011). Neuroinflammation and α-synuclein dysfunction potentiate each other, driving chronic progression of neurodegeneration in a mouse model of Parkinson's disease. Environ Health Perspect *119*, 807-814.

Giasson, B.I., Duda, J.E., Murray, I.V., Chen, Q., Souza, J.M., Hurtig, H.I., Ischiropoulos, H., Trojanowski, J.Q., and Lee, V.M. (2000). Oxidative damage linked to neurodegeneration by selective α-synuclein nitration in synucleinopathy lesions. Science *290*, 985-989.

Giasson, B.I., Duda, J.E., Quinn, S.M., Zhang, B., Trojanowski, J.Q., and Lee, V.M. (2002). Neuronal α-synucleinopathy with severe movement disorder in mice expressing A53T human α-synuclein. Neuron *34*, 521-533.

Giasson, B.I., Murray, I.V., Trojanowski, J.Q., and Lee, V.M. (2001). A hydrophobic stretch of 12 amino acid residues in the middle of α-synuclein is essential for filament assembly. J Biol Chem *276*, 2380-2386.

Glass, C.K., Saijo, K., Winner, B., Marchetto, M.C., and Gage, F.H. (2010). Mechanisms underlying inflammation in neurodegeneration. Cell *140*, 918-934.

Gousset, K., Schiff, E., Langevin, C., Marijanovic, Z., Caputo, A., Browman, D.T., Chenouard, N., de Chaumont, F., Martino, A., Enninga, J.*, et al.* (2009). Prions hijack tunnelling nanotubes for intercellular spread. Nat Cell Biol *11*, 328-336.

Guo, J.L., Covell, D.J., Daniels, J.P., Iba, M., Stieber, A., Zhang, B., Riddle, D.M., Kwong, L.K., Xu, Y., Trojanowski, J.Q.*, et al.* (2013). Distinct α-synuclein strains differentially promote tau inclusions in neurons. Cell *154*, 103-117.

Guo, J.L., and Lee, V.M. (2014). Cell-to-cell transmission of pathogenic proteins in neurodegenerative diseases. Nat Med *20*, 130-138.

Hansen, C., Angot, E., Bergstrom, A.L., Steiner, J.A., Pieri, L., Paul, G., Outeiro, T.F., Melki, R., Kallunki, P., Fog, K.*, et al.* (2011). α-Synuclein propagates from mouse brain to grafted dopaminergic neurons and seeds aggregation in cultured human cells. J Clin Invest *121*, 715-725.

Hawkes, C.H., Del Tredici, K., and Braak, H. (2007). Parkinson's disease: a dual-hit hypothesis. Neuropathol Appl Neurobiol *33*, 599-614.

Hawkes, C.H., Del Tredici, K., and Braak, H. (2009). Parkinson's disease: the dual hit theory revisited. Ann N Y Acad Sci *1170*, 615-622.

He, Q., Yu, W., Wu, J., Chen, C., Lou, Z., Zhang, Q., Zhao, J., Wang, J., and Xiao, B. (2013). Intranasal LPS-mediated Parkinson's model challenges the pathogenesis of nasal cavity and environmental toxins. PLoS One *8*, e78418.

Hewitt, P.E., Llewelyn, C.A., Mackenzie, J., and Will, R.G. (2006). Creutzfeldt-Jakob disease and blood transfusion: results of the UK Transfusion Medicine Epidemiological Review study. Vox Sang *91*, 221-230.

Hill, A.F., Desbruslais, M., Joiner, S., Sidle, K.C., Gowland, I., Collinge, J., Doey, L.J., and Lantos, P. (1997). The same prion strain causes vCJD and BSE. Nature *389*, 448-450, 526.

Hilton, D., Stephens, M., Kirk, L., Edwards, P., Potter, R., Zajicek, J., Broughton, E., Hagan, H., and Carroll, C. (2014). Accumulation of α-synuclein in the bowel of patients in the pre-clinical phase of Parkinson's disease. Acta Neuropathol *127*, 235-241.

Hirsch, E., Graybiel, A.M., and Agid, Y.A. (1988). Melanized dopaminergic neurons are differentially susceptible to degeneration in Parkinson's disease. Nature *334*, 345-348.

Holmes, B.B., DeVos, S.L., Kfoury, N., Li, M., Jacks, R., Yanamandra, K., Ouidja, M.O., Brodsky, F.M., Marasa, J., Bagchi, D.P.*, et al.* (2013). Heparan sulfate proteoglycans mediate internalization and propagation of specific proteopathic seeds. Proc Natl Acad Sci U S A *110*, E3138-3147.

Holmqvist, S., Chutna, O., Bousset, L., Aldrin-Kirk, P., Li, W., Bjorklund, T., Wang, Z.Y., Roybon, L., Melki, R., and Li, J.Y. (2014). Direct evidence of Parkinson pathology spread from the gastrointestinal tract to the brain in rats. Acta Neuropathol *128*, 805-820.

Imamura, K., Hishikawa, N., Sawada, M., Nagatsu, T., Yoshida, M., and Hashizume, Y. (2003). Distribution of major histocompatibility complex class II-positive microglia and cytokine profile of Parkinson's disease brains. Acta Neuropathol *106*, 518-526.

Ischiropoulos, H., and Beckman, J.S. (2003). Oxidative stress and nitration in neurodegeneration: cause, effect, or association? J Clin Invest *111*, 163-169.

Jangula, A., and Murphy, E.J. (2013). Lipopolysaccharide-induced blood brain barrier permeability is enhanced by α-synuclein expression. Neurosci Lett *551*, 23-27.

Jaunmuktane, Z., Mead, S., Ellis, M., Wadsworth, J.D., Nicoll, A.J., Kenny, J., Launchbury, F., Linehan, J., Richard-Loendt, A., Walker, A.S., *et al.* (2015a). Erratum: Evidence for human transmission of amyloid-beta pathology and cerebral amyloid angiopathy. Nature *526*, 595.

Jaunmuktane, Z., Mead, S., Ellis, M., Wadsworth, J.D., Nicoll, A.J., Kenny, J., Launchbury, F., Linehan, J., Richard-Loendt, A., Walker, A.S., *et al.* (2015b). Evidence for human transmission of amyloid-beta pathology and cerebral amyloid angiopathy. Nature *525*, 247-250.

Jo, E., McLaurin, J., Yip, C.M., St George-Hyslop, P., and Fraser, P.E. (2000). α-Synuclein membrane interactions and lipid specificity. J Biol Chem *275*, 34328-34334.

Johansson, C.B., Momma, S., Clarke, D.L., Risling, M., Lendahl, U., and Frisen, J. (1999). Identification of a neural stem cell in the adult mammalian central nervous system. Cell *96*, 25-34.

Kalia, L.V., Kalia, S.K., McLean, P.J., Lozano, A.M., and Lang, A.E. (2013). α-Synuclein oligomers and clinical implications for Parkinson disease. Ann Neurol *73*, 155-169.

Kanazawa, T., Uchihara, T., Takahashi, A., Nakamura, A., Orimo, S., and Mizusawa, H. (2008). Three-layered structure shared between Lewy bodies and lewy neurites-three-dimensional reconstruction of triple-labeled sections. Brain Pathol *18*, 415-422.

Karpinar, D.P., Balija, M.B., Kugler, S., Opazo, F., Rezaei-Ghaleh, N., Wender, N., Kim, H.Y., Taschenberger, G., Falkenburger, B.H., Heise, H., *et al.* (2009). Pre-fibrillar α-synuclein variants with impaired beta-structure increase neurotoxicity in Parkinson's disease models. EMBO J *28*, 3256-3268.

Keith B.J. Franklin and George Paxinos (2008). The mouse brain in stereotaxic coordinates (compact third edition), Elsevier.

Kim, C., Lv, G., Lee, J.S., Jung, B.C., Masuda-Suzukake, M., Hong, C.S., Valera, E., Lee, H.J., Paik, S.R., Hasegawa, M., *et al.* (2016). Exposure to bacterial endotoxin generates a distinct strain of α-synuclein fibril. Sci Rep *6*, 30891.

Kimberlin, R.H., and Walker, C.A. (1980). Pathogenesis of mouse scrapie: evidence for neural spread of infection to the CNS. J Gen Virol *51*, 183-187.

Kimberlin, R.H., and Walker, C.A. (1986). Pathogenesis of scrapie (strain 263K) in hamsters infected intracerebrally, intraperitoneally or intraocularly. J Gen Virol *67 (Pt 2)*, 255-263.

Kincaid, A.E., and Bartz, J.C. (2007). The nasal cavity is a route for prion infection in hamsters. J Virol *81*, 4482-4491.

Klingelhoefer, L., and Reichmann, H. (2015). Pathogenesis of Parkinson disease--the gut-brain axis and environmental factors. Nat Rev Neurol *11*, 625-636.

Komatsu, M., Waguri, S., Koike, M., Sou, Y.S., Ueno, T., Hara, T., Mizushima, N., Iwata, J., Ezaki, J., Murata, S., *et al.* (2007). Homeostatic levels of p62 control cytoplasmic inclusion body formation in autophagy-deficient mice. Cell *131*, 1149-1163.

Kordower, J.H., Chu, Y., Hauser, R.A., Freeman, T.B., and Olanow, C.W. (2008). Lewy body-like pathology in long-term embryonic nigral transplants in Parkinson's disease. Nat Med *14*, 504-506.

Kruger, R., Kuhn, W., Muller, T., Woitalla, D., Graeber, M., Kosel, S., Przuntek, H., Epplen, J.T., Schols, L., and Riess, O. (1998). Ala30Pro mutation in the gene encoding α-synuclein in Parkinson's disease. Nat Genet *18*, 106-108.

Kuusisto, E., Salminen, A., and Alafuzoff, I. (2001). Ubiquitin-binding protein p62 is present in neuronal and glial inclusions in human tauopathies and synucleinopathies. Neuroreport *12*, 2085-2090.

Lashuel, H.A., Overk, C.R., Oueslati, A., and Masliah, E. (2013). The many faces of α-synuclein: from structure and toxicity to therapeutic target. Nat Rev Neurosci *14*, 38-48.

Lasmezas, C.I., Deslys, J.P., Robain, O., Jaegly, A., Beringue, V., Peyrin, J.M., Fournier, J.G., Hauw, J.J., Rossier, J., and Dormont, D. (1997). Transmission of the BSE agent to mice in the absence of detectable abnormal prion protein. Science *275*, 402-405.

Lee, H.J., Suk, J.E., Patrick, C., Bae, E.J., Cho, J.H., Rho, S., Hwang, D., Masliah, E., and Lee, S.J. (2010). Direct transfer of α-synuclein from neuron to astroglia causes inflammatory responses in synucleinopathies. J Biol Chem *285*, 9262-9272.

Lee, M.K., Stirling, W., Xu, Y., Xu, X., Qui, D., Mandir, A.S., Dawson, T.M., Copeland, N.G., Jenkins, N.A., and Price, D.L. (2002). Human α-synuclein-harboring familial Parkinson's disease-linked Ala-53 --> Thr mutation causes neurodegenerative disease with α-synuclein aggregation in transgenic mice. Proc Natl Acad Sci U S A *99*, 8968-8973.

Lesage, S., Anheim, M., Letournel, F., Bousset, L., Honore, A., Rozas, N., Pieri, L., Madiona, K., Durr, A., Melki, R., *et al.* (2013). G51D α-synuclein mutation causes a novel parkinsonian-pyramidal syndrome. Ann Neurol *73*, 459-471.

Levesque, S., Surace, M.J., McDonald, J., and Block, M.L. (2011). Air pollution & the brain: Subchronic diesel exhaust exposure causes neuroinflammation and elevates early markers of neurodegenerative disease. J Neuroinflammation *8*, 105.

Li, J.Y., Englund, E., Holton, J.L., Soulet, D., Hagell, P., Lees, A.J., Lashley, T., Quinn, N.P., Rehncrona, S., Bjorklund, A., *et al.* (2008). Lewy bodies in grafted neurons in subjects with Parkinson's disease suggest host-to-graft disease propagation. Nat Med *14*, 501-503.

Lowe, J., Blanchard, A., Morrell, K., Lennox, G., Reynolds, L., Billett, M., Landon, M., and Mayer, R.J. (1988). Ubiquitin is a common factor in intermediate filament inclusion bodies of diverse type in man, including those of Parkinson's disease, Pick's disease, and Alzheimer's disease, as well as Rosenthal fibres in cerebellar astrocytomas, cytoplasmic bodies in muscle, and mallory bodies in alcoholic liver disease. J Pathol *155*, 9-15.

Luk, K.C., Covell, D.J., Kehm, V.M., Zhang, B., Song, I.Y., Byrne, M.D., Pitkin, R.M., Decker, S.C., Trojanowski, J.Q., and Lee, V.M. (2016). Molecular and Biological Compatibility with Host A-Synuclein Influences Fibril Pathogenicity. Cell Rep *16*, 3373-3387.

Luk, K.C., Kehm, V., Carroll, J., Zhang, B., O'Brien, P., Trojanowski, J.Q., and Lee, V.M. (2012a). Pathological α-synuclein transmission initiates Parkinson-like neurodegeneration in nontransgenic mice. Science *338*, 949-953.

Luk, K.C., Kehm, V.M., Zhang, B., O'Brien, P., Trojanowski, J.Q., and Lee, V.M. (2012b). Intracerebral inoculation of pathological α-synuclein initiates a rapidly progressive neurodegenerative α-synucleinopathy in mice. J Exp Med *209*, 975-986.

Mao, X., Ou, M.T., Karuppagounder, S.S., Kam, T.I., Yin, X., Xiong, Y., Ge, P., Umanah, G.E., Brahmachari, S., Shin, J.H.*, et al.* (2016). Pathological α-synuclein transmission initiated by binding lymphocyte-activation gene 3. Science *353*.

Maragakis, N.J., and Rothstein, J.D. (2006). Mechanisms of Disease: astrocytes in neurodegenerative disease. Nat Clin Pract Neurol *2*, 679-689.

Maries, E., Dass, B., Collier, T.J., Kordower, J.H., and Steece-Collier, K. (2003). The role of α-synuclein in Parkinson's disease: insights from animal models. Nat Rev Neurosci *4*, 727-738.

Maroteaux, L., Campanelli, J.T., and Scheller, R.H. (1988). Synuclein: a neuron-specific protein localized to the nucleus and presynaptic nerve terminal. J Neurosci *8*, 2804-2815.

Masliah, E., Rockenstein, E., Veinbergs, I., Mallory, M., Hashimoto, M., Takeda, A., Sagara, Y., Sisk, A., and Mucke, L. (2000). Dopaminergic loss and inclusion body formation in α-synuclein mice: implications for neurodegenerative disorders. Science *287*, 1265-1269.

Masuda-Suzukake, M., Nonaka, T., Hosokawa, M., Oikawa, T., Arai, T., Akiyama, H., Mann, D.M., and Hasegawa, M. (2013). Prion-like spreading of pathological α-synuclein in brain. Brain *136*, 1128-1138.

Matsuoka, Y., Vila, M., Lincoln, S., McCormack, A., Picciano, M., LaFrancois, J., Yu, X., Dickson, D., Langston, W.J., McGowan, E.*, et al.* (2001). Lack of nigral pathology in transgenic mice expressing human α-synuclein driven by the tyrosine hydroxylase promoter. Neurobiol Dis *8*, 535-539.

McBride, P.A., Schulz-Schaeffer, W.J., Donaldson, M., Bruce, M., Diringer, H., Kretzschmar, H.A., and Beekes, M. (2001). Early spread of scrapie from the gastrointestinal tract to the central nervous system involves autonomic fibers of the splanchnic and vagus nerves. J Virol *75*, 9320-9327.

McClung, J.R., and Goldberg, S.J. (2000). Functional anatomy of the hypoglossal innervated muscles of the rat tongue: a model for elongation and protrusion of the mammalian tongue. Anat Rec *260*, 378-386.

McCulloch, L., Brown, K.L., Bradford, B.M., Hopkins, J., Bailey, M., Rajewsky, K., Manson, J.C., and Mabbott, N.A. (2011). Follicular dendritic cell-specific prion protein (PrP) expression alone is sufficient to sustain prion infection in the spleen. PLoS Pathog *7*, e1002402.

McGeer, P.L., and McGeer, E.G. (2008). Glial reactions in Parkinson's disease. Mov Disord *23*, 474-483.

McNaught, K.S., and Jenner, P. (2001). Proteasomal function is impaired in substantia nigra in Parkinson's disease. Neurosci Lett *297*, 191-194.

Meredith, G.E., Totterdell, S., Petroske, E., Santa Cruz, K., Callison, R.C., Jr., and Lau, Y.S. (2002). Lysosomal malfunction accompanies α-synuclein aggregation in a progressive mouse model of Parkinson's disease. Brain Res *956*, 156-165.

Mok, Y.F., and Howlett, G.J. (2006). Sedimentation velocity analysis of amyloid oligomers and fibrils. Methods Enzymol *413*, 199-217.

Mombaerts, P. (2004). Genes and ligands for odorant, vomeronasal and taste receptors. Nat Rev Neurosci *5*, 263-278.

Mulcahy, E.R., Bartz, J.C., Kincaid, A.E., and Bessen, R.A. (2004). Prion infection of skeletal muscle cells and papillae in the tongue. J Virol *78*, 6792-6798.

Munch, C., O'Brien, J., and Bertolotti, A. (2011). Prion-like propagation of mutant superoxide dismutase-1 misfolding in neuronal cells. Proc Natl Acad Sci U S A *108*, 3548-3553.

Murphy, D.D., Rueter, S.M., Trojanowski, J.Q., and Lee, V.M. (2000). Synucleins are developmentally expressed, and α-synuclein regulates the size of the presynaptic vesicular pool in primary hippocampal neurons. J Neurosci *20*, 3214-3220.

Nakamura, K., Mori, F., Tanji, K., Miki, Y., Toyoshima, Y., Kakita, A., Takahashi, H., Yamada, M., and Wakabayashi, K. (2016). α-Synuclein pathology in the cranial and spinal nerves in Lewy body disease. Neuropathology *36*, 262-269.

Oliveras-Salva, M., Van der Perren, A., Casadei, N., Stroobants, S., Nuber, S., D'Hooge, R., Van den Haute, C., and Baekelandt, V. (2013). rAAV2/7 vector-mediated overexpression of α-synuclein in mouse substantia nigra induces protein aggregation and progressive dose-dependent neurodegeneration. Mol Neurodegener *8*, 44.

Pankratz, N., and Foroud, T. (2004). Genetics of Parkinson disease. NeuroRx *1*, 235-242.

Peelaerts, W., Bousset, L., Van der Perren, A., Moskalyuk, A., Pulizzi, R., Giugliano, M., Van den Haute, C., Melki, R., and Baekelandt, V. (2015). α-Synuclein strains cause distinct synucleinopathies after local and systemic administration. Nature *522*, 340-344.

Polymeropoulos, M.H., Lavedan, C., Leroy, E., Ide, S.E., Dehejia, A., Dutra, A., Pike, B., Root, H., Rubenstein, J., Boyer, R.*, et al.* (1997). Mutation in the α-synuclein gene identified in families with Parkinson's disease. Science *276*, 2045-2047.

Prediger, R.D., Aguiar, A.S., Jr., Matheus, F.C., Walz, R., Antoury, L., Raisman-Vozari, R., and Doty, R.L. (2012). Intranasal administration of neurotoxicants in animals: support for the olfactory vector hypothesis of Parkinson's disease. Neurotox Res *21*, 90-116.

Prusiner, S.B., Woerman, A.L., Mordes, D.A., Watts, J.C., Rampersaud, R., Berry, D.B., Patel, S., Oehler, A., Lowe, J.K., Kravitz, S.N.*, et al.* (2015). Evidence for α-synuclein prions causing multiple system atrophy in humans with parkinsonism. Proc Natl Acad Sci U S A *112*, E5308-5317.

Raabe G.O., Al-Bayati M.A., Teague S.V., Rasolt A. (1998) Regional deposition of inhaled monodisperse coarse and fine aerosol particles in small laboratory animals. Ann occup. Hyg. 32, 53-63.

Recasens, A., Dehay, B., Bove, J., Carballo-Carbajal, I., Dovero, S., Perez-Villalba, A., Fernagut, P.O., Blesa, J., Parent, A., Perier, C.*, et al.* (2014). Lewy body extracts from Parkinson disease brains trigger α-synuclein pathology and neurodegeneration in mice and monkeys. Ann Neurol *75*, 351-362.

Ren, P.H., Lauckner, J.E., Kachirskaia, I., Heuser, J.E., Melki, R., and Kopito, R.R. (2009). Cytoplasmic penetration and persistent infection of mammalian cells by polyglutamine aggregates. Nat Cell Biol *11*, 219-225.

Rey, N.L., Petit, G.H., Bousset, L., Melki, R., and Brundin, P. (2013). Transfer of human α-synuclein from the olfactory bulb to interconnected brain regions in mice. Acta Neuropathol *126*, 555-573.

Reynolds, A.D., Glanzer, J.G., Kadiu, I., Ricardo-Dukelow, M., Chaudhuri, A., Ciborowski, P., Cerny, R., Gelman, B., Thomas, M.P., Mosley, R.L.*, et al.* (2008). Nitrated α-synuclein-activated microglial profiling for Parkinson's disease. J Neurochem *104*, 1504-1525.

Rivest, S. (2009). Regulation of innate immune responses in the brain. Nat Rev Immunol *9*, 429-439.

Rojo, A.I., Montero, C., Salazar, M., Close, R.M., Fernandez-Ruiz, J., Sanchez-Gonzalez, M.A., de Sagarra, M.R., Jackson-Lewis, V., Cavada, C., and Cuadrado, A. (2006). Persistent penetration of MPTP through the nasal route induces Parkinson's disease in mice. Eur J Neurosci *24*, 1874-1884.

Rubinsztein, D.C. (2006). The roles of intracellular protein-degradation pathways in neurodegeneration. Nature *443*, 780-786.

Rudge, P., Jaunmuktane, Z., Adlard, P., Bjurstrom, N., Caine, D., Lowe, J., Norsworthy, P., Hummerich, H., Druyeh, R., Wadsworth, J.D.*, et al.* (2015). Iatrogenic CJD due to pituitary-derived growth hormone with genetically determined incubation times of up to 40 years. Brain *138*, 3386-3399.

Sacino, A.N., Brooks, M., McGarvey, N.H., McKinney, A.B., Thomas, M.A., Levites, Y., Ran, Y., Golde, T.E., and Giasson, B.I. (2013). Induction of CNS α-synuclein pathology by fibrillar and non-amyloidogenic recombinant α-synuclein. Acta Neuropathol Commun *1*, 38.

Sacino, A.N., Brooks, M., Thomas, M.A., McKinney, A.B., Lee, S., Regenhardt, R.W., McGarvey, N.H., Ayers, J.I., Notterpek, L., Borchelt, D.R., *et al.* (2014a). Intramuscular injection of α-synuclein induces CNS α-synuclein pathology and a rapid-onset motor phenotype in transgenic mice. Proc Natl Acad Sci U S A *111*, 10732-10737.

Sacino, A.N., Brooks, M., Thomas, M.A., McKinney, A.B., McGarvey, N.H., Rutherford, N.J., Ceballos-Diaz, C., Robertson, J., Golde, T.E., and Giasson, B.I. (2014b). Amyloidogenic α-synuclein seeds do not invariably induce rapid, widespread pathology in mice. Acta Neuropathol *127*, 645-665.

Sanders, D.W., Kaufman, S.K., DeVos, S.L., Sharma, A.M., Mirbaha, H., Li, A., Barker, S.J., Foley, A.C., Thorpe, J.R., Serpell, L.C., *et al.* (2014). Distinct tau prion strains propagate in cells and mice and define different tauopathies. Neuron *82*, 1271-1288.

Selkoe, D.J. (2003). Folding proteins in fatal ways. Nature *426*, 900-904.

Serpell, L.C., Berriman, J., Jakes, R., Goedert, M., and Crowther, R.A. (2000). Fiber diffraction of synthetic α-synuclein filaments shows amyloid-like cross-beta conformation. Proc Natl Acad Sci U S A *97*, 4897-4902.

Singleton, A.B., Farrer, M., Johnson, J., Singleton, A., Hague, S., Kachergus, J., Hulihan, M., Peuralinna, T., Dutra, A., Nussbaum, R., *et al.* (2003). α-Synuclein locus triplication causes Parkinson's disease. Science *302*, 841.

Siso, S., Gonzalez, L., and Jeffrey, M. (2010). Neuroinvasion in prion diseases: the roles of ascending neural infection and blood dissemination. Interdiscip Perspect Infect Dis *2010*, 747892.

Sofroniew, M.V. (2009). Molecular dissection of reactive astrogliosis and glial scar formation. Trends Neurosci *32*, 638-647.

Spillantini, M.G., Crowther, R.A., Jakes, R., Hasegawa, M., and Goedert, M. (1998). α-Synuclein in filamentous inclusions of Lewy bodies from Parkinson's disease and dementia with lewy bodies. Proc Natl Acad Sci U S A *95*, 6469-6473.

Spillantini, M.G., and Goedert, M. (2000). The α-synucleinopathies: Parkinson's disease, dementia with Lewy bodies, and multiple system atrophy. Ann N Y Acad Sci *920*, 16-27.

Spillantini, M.G., Schmidt, M.L., Lee, V.M., Trojanowski, J.Q., Jakes, R., and Goedert, M. (1997). A-synuclein in Lewy bodies. Nature *388*, 839-840.

Stitz, L., and Aguzzi, A. (2011). Aerosols: an underestimated vehicle for transmission of prion diseases? Prion *5*, 138-141.

Stohr, J., Condello, C., Watts, J.C., Bloch, L., Oehler, A., Nick, M., DeArmond, S.J., Giles, K., DeGrado, W.F., and Prusiner, S.B. (2014). Distinct synthetic Abeta prion strains producing different amyloid deposits in bigenic mice. Proc Natl Acad Sci U S A *111*, 10329-10334.

Tamgüney, G., Francis, K.P., Giles, K., Lemus, A., DeArmond, S.J., and Prusiner, S.B. (2009a). Measuring prions by bioluminescence imaging. Proc Natl Acad Sci U S A *106*, 15002-15006.

Tamgüney, G., Miller, M.W., Wolfe, L.L., Sirochman, T.M., Glidden, D.V., Palmer, C., Lemus, A., DeArmond, S.J., and Prusiner, S.B. (2009b). Asymptomatic deer excrete infectious prions in faeces. Nature *461*, 529-532.

Tamgüney, G., Richt, J.A., Hamir, A.N., Greenlee, J.J., Miller, M.W., Wolfe, L.L., Sirochman, T.M., Young, A.J., Glidden, D.V., Johnson, N.L.*, et al.* (2012). Salivary prions in sheep and deer. Prion *6*, 52-61.

Tanaka, M., Chien, P., Naber, N., Cooke, R., and Weissman, J.S. (2004). Conformational variations in an infectious protein determine prion strain differences. Nature *428*, 323-328.

Theodore, S., Cao, S., McLean, P.J., and Standaert, D.G. (2008). Targeted overexpression of human α-synuclein triggers microglial activation and an adaptive immune response in a mouse model of Parkinson disease. J Neuropathol Exp Neurol *67*, 1149-1158.

Tofaris, G.K., Razzaq, A., Ghetti, B., Lilley, K.S., and Spillantini, M.G. (2003). Ubiquitination of α-synuclein in Lewy bodies is a pathological event not associated with impairment of proteasome function. J Biol Chem *278*, 44405-44411.

Tremblay, P., Bouzamondo-Bernstein, E., Heinrich, C., Prusiner, S.B., and DeArmond, S.J. (2007). Developmental expression of PrP in the post-implantation embryo. Brain Res *1139*, 60-67.

Tyedmers, J., Mogk, A., and Bukau, B. (2010). Cellular strategies for controlling protein aggregation. Nat Rev Mol Cell Biol *11*, 777-788.

Uchihara, T., and Giasson, B.I. (2016). Propagation of α-synuclein pathology: hypotheses, discoveries, and yet unresolved questions from experimental and human brain studies. Acta Neuropathol *131*, 49-73.

Ulusoy, A., Rusconi, R., Perez-Revuelta, B.I., Musgrove, R.E., Helwig, M., Winzen-Reichert, B., and Di Monte, D.A. (2013). Caudo-rostral brain spreading of α-synuclein through vagal connections. EMBO Mol Med *5*, 1051-1059.

van Dijk, K.D., Bidinosti, M., Weiss, A., Raijmakers, P., Berendse, H.W., and van de Berg, W.D. (2014). Reduced α-synuclein levels in cerebrospinal fluid in Parkinson's disease are unrelated to clinical and imaging measures of disease severity. Eur J Neurol *21*, 388-394.

Venda, L.L., Cragg, S.J., Buchman, V.L., and Wade-Martins, R. (2010). α-Synuclein and dopamine at the crossroads of Parkinson's disease. Trends Neurosci *33*, 559-568.

Vidgren, M.T., and Kublik, H. (1998). Nasal delivery systems and their effect on deposition and absorption. Adv Drug Deliv Rev *29*, 157-177.

Volpicelli-Daley, L.A., Luk, K.C., and Lee, V.M. (2014). Addition of exogenous α-synuclein preformed fibrils to primary neuronal cultures to seed recruitment of endogenous α-synuclein to Lewy body and Lewy neurite-like aggregates. Nat Protoc *9*, 2135-2146.

Volpicelli-Daley, L.A., Luk, K.C., Patel, T.P., Tanik, S.A., Riddle, D.M., Stieber, A., Meaney, D.F., Trojanowski, J.Q., and Lee, V.M. (2011). Exogenous α-synuclein fibrils induce Lewy body pathology leading to synaptic dysfunction and neuron death. Neuron *72*, 57-71.

Wang, W., Perovic, I., Chittuluru, J., Kaganovich, A., Nguyen, L.T., Liao, J., Auclair, J.R., Johnson, D., Landeru, A., Simorellis, A.K.*, et al.* (2011). A soluble α-synuclein construct forms a dynamic tetramer. Proc Natl Acad Sci U S A *108*, 17797-17802.

Watts, J.C., Condello, C., Stohr, J., Oehler, A., Lee, J., DeArmond, S.J., Lannfelt, L., Ingelsson, M., Giles, K., and Prusiner, S.B. (2014). Serial propagation of distinct strains of Abeta prions from Alzheimer's disease patients. Proc Natl Acad Sci U S A *111*, 10323-10328.

Watts, J.C., Giles, K., Oehler, A., Middleton, L., Dexter, D.T., Gentleman, S.M., DeArmond, S.J., and Prusiner, S.B. (2013). Transmission of multiple system atrophy prions to transgenic mice. Proc Natl Acad Sci U S A *110*, 19555-19560.

Webb, J.L., Ravikumar, B., Atkins, J., Skepper, J.N., and Rubinsztein, D.C. (2003). A-Synuclein is degraded by both autophagy and the proteasome. J Biol Chem *278*, 25009-25013.

Weintraub, D., Comella, C.L., and Horn, S. (2008). Parkinson's disease--Part 1: Pathophysiology, symptoms, burden, diagnosis, and assessment. Am J Manag Care *14*, S40-48.

Winner, B., Jappelli, R., Maji, S.K., Desplats, P.A., Boyer, L., Aigner, S., Hetzer, C., Loher, T., Vilar, M., Campioni, S.*, et al.* (2011). In vivo demonstration that α-synuclein oligomers are toxic. Proc Natl Acad Sci U S A *108*, 4194-4199.

Wu, J.W., Herman, M., Liu, L., Simoes, S., Acker, C.M., Figueroa, H., Steinberg, J.I., Margittai, M., Kayed, R., Zurzolo, C.*, et al.* (2013). Small misfolded Tau species are internalized via bulk endocytosis and anterogradely and retrogradely transported in neurons. J Biol Chem *288*, 1856-1870.

Wyss-Coray, T., and Mucke, L. (2002). Inflammation in neurodegenerative disease--a double-edged sword. Neuron *35*, 419-432.

Zanusso, G., Ferrari, S., Cardone, F., Zampieri, P., Gelati, M., Fiorini, M., Farinazzo, A., Gardiman, M., Cavallaro, T., Bentivoglio, M.*, et al.* (2003). Detection of pathologic prion protein in the olfactory epithelium in sporadic Creutzfeldt-Jakob disease. N Engl J Med *348*, 711-719.

Zarranz, J.J., Alegre, J., Gomez-Esteban, J.C., Lezcano, E., Ros, R., Ampuero, I., Vidal, L., Hoenicka, J., Rodriguez, O., Atares, B.*, et al.* (2004). The new mutation, E46K, of α-synuclein causes Parkinson and Lewy body dementia. Ann Neurol *55*, 164-173.

Zhang, W., Wang, T., Pei, Z., Miller, D.S., Wu, X., Block, M.L., Wilson, B., Zhang, W., Zhou, Y., Hong, J.S., *et al.* (2005). Aggregated α-synuclein activates microglia: a process leading to disease progression in Parkinson's disease. FASEB J *19*, 533-542.

Zhu, L., Ramboz, S., Hewitt, D., Boring, L., Grass, D.S., and Purchio, A.F. (2004). Non-invasive imaging of GFAP expression after neuronal damage in mice. Neurosci Lett *367*, 210-212.

9 Acknowledgements

Firstly, I would like to thank my supervisor Dr. Erdem Tamgüney who gave me the opportunity to work on this project and supported me during all these years.

I would like to thank Prof. Dr. Höhfeld, Prof. Dr. Witke and Prof. Dr. Becker for agreeing to be part of my thesis committee.

I am grateful to all collaborators and colleagues who supported and contributed to the work of the publications.

Thank you to the animal facility and the light microscopy facility for their technical assistance and experimental advices.

Thank you very much to my lab colleagues who gave me not only technical support and made work much more like fun. A special thank goes to the girls, because they are the best.

I would like to acknowledge those persons who proofread this thesis and gave me helpful comments and suggestions.

Above all, I would like to thank my family and friends for their encouragement and support all the time.